Final Technical Report

AIR BRAYTON SOLAR RECEIVER PHASE II

80-17528

December 10, 1981

Prepared by

L. E. De Anda

Approved by

M. V. Graeven
Program Manager

W. J. O'Reilly
Engineering Chief, Heat Transfer
and Cryogenic Systems

Prepared for

California Institute of Technology
Jet Propulsion Laboratory
Pasadena, California

AIRESEARCH MANUFACTURING COMPANY

FOREWORD

This final report is submitted by the AiResearch Manufacturing Company, a division of The Garrett Corporation, in fulfillment of Phase II of Contract No. NAS7-100/955136 with the Jet Propulsion Laboratory, California Institute of Technology. The report discusses the design and development of an open cycle Air Brayton Solar Receiver (ABSR).

ABSTRACT

The purpose of the Phase II project was to design and develop an Air Brayton Solar Receiver (ABSR) based on the Solar Receiver concept recommended in Phase I of the program. The ABSR consists of a cylindrical, insulated, offset plate fin heat exchanger which is mounted at the focal plane of a fully tracking parabolic solar collector. The receiver transfers heat from the concentrated solar radiation (which impinges on the inside walls of the heat exchanger) to the working fluid i.e., air. The hot air would then be used to drive a small Brayton cycle heat engine. The engine in turn drives a generator which produces electrical energy.

The cavity size of the receiver is 28-in. long by 20-in. in diameter. The ABSR core is constructed of two metallic parallel plate-fin flow passages. The plate and fin material is Inconel 625. The core is insulated with a 4.5-in. layer of Cerawool blanket wrapped around the outer wall. The aperture end and the reflector back plate at the closed end section are made of silicon carbide. The ABSR accepts 85 kwth and has a design life of 10,000 hours and 1500 cycles, under operating conditions of 1500°F, 36.75 psia and airflow of 0.57 pounds per second.

The analysis of the ABSR includes symmetrical and asymmetrical solar power input into the receiver. The symmetrical cases involve the baseline incident flux and the axially shifted incident fluxes. The asymmetrical cases correspond to the solar fluxes that are obtained by reduced solar input from one half of the concentrator or by receiver offset of ± 1 inch from the concentrator optical axis.

TABLE OF CONTENTS

ILLUSTRATIONS

ILLUSTRATIONS (Continued)

TABLES

1. INTRODUCTION

This report documents the work completed during Phase II of the Air Brayton Solar Receiver (ABSR) development program. The work was performed by AiResearch for the Jet Propulsion Laboratory, under contract no. NAS7-100/955136. Phase I of the ABSR program arrived at the basic design of the receiver for use in a point-focus, 85 KWth Brayton power system. Figure 1-1 shows the parabolic concentrator that serves as the solar energy focusing device. The concentrator characteristics are summarized on Table 1-1. Figure 1-2 represents the Air Brayton System schematic. The receiver transfers heat from the concentrated solar radiation incident (on the heat exchanger walls of the interior cavity) to the working fluid i.e., air. Phase I consisted of a parametric study that analyzed a wide range of receiver designs under varying conditions and then recommended a final design for Phase II detail study. The model presented from Phase I consisted of an offset plate fin matrix in a cylindrically shaped cavity heat exchanger section, fabricated from Haynes 188 steel. A flat ceramic plate, made from silicon carbide, was in the closed end of the receiver. The aperture end of the receiver was a conically shaped skirt, also made from silicon carbide. A mild steel housing with an aperture opening on one end enclosed the heat exchanger. Eight support spokes connect the heat exchanger to the receiver housing. Cerablanket insulation fills the annulus between the heat exchanger and the housing. Phase I also studied thermal storage devices and made a preliminary recommendation of the use of sodium chloride (NaCl) as a storage medium. It advised further study of other possible materials too. The results of Phase I are presented in AiResearch report no. 79-15677.

Phase II of the ABSR program completed design work on the receiver chosen in Phase I. Thermal analysis performed during Phase II concentrated on: (a) optical modeling of the concentrator-receiver system; (b) verification of the receiver performance after final design iterations; and (c) evaluation of the final design performance under off-design point conditions. Stress analysis concentrated on determining the design loads on the receiver and the expected operational life. Design iterations concluded with an Inconnel brazed, annular heat transfer matrix replacing the Haynes 188 Phase I design. Two prototype units were then fabricated, and they underwent acceptance tests. The thermal energy storage device was excluded from further study. The remainder of this report documents the work performed by AiResearch during Phase II of the ABSR program.

1.1 SUMMARY

At the initiation of Phase II, AiResearch received a problem statement specifying the final design conditions that the ABSR should meet. See Table 1-2. That problem statement was similar to the final Phase I work statement. The receiver concept also remained similar, but incorporated some new features: The mounting system for the heat exchanger changed to a non-fixed 8 point

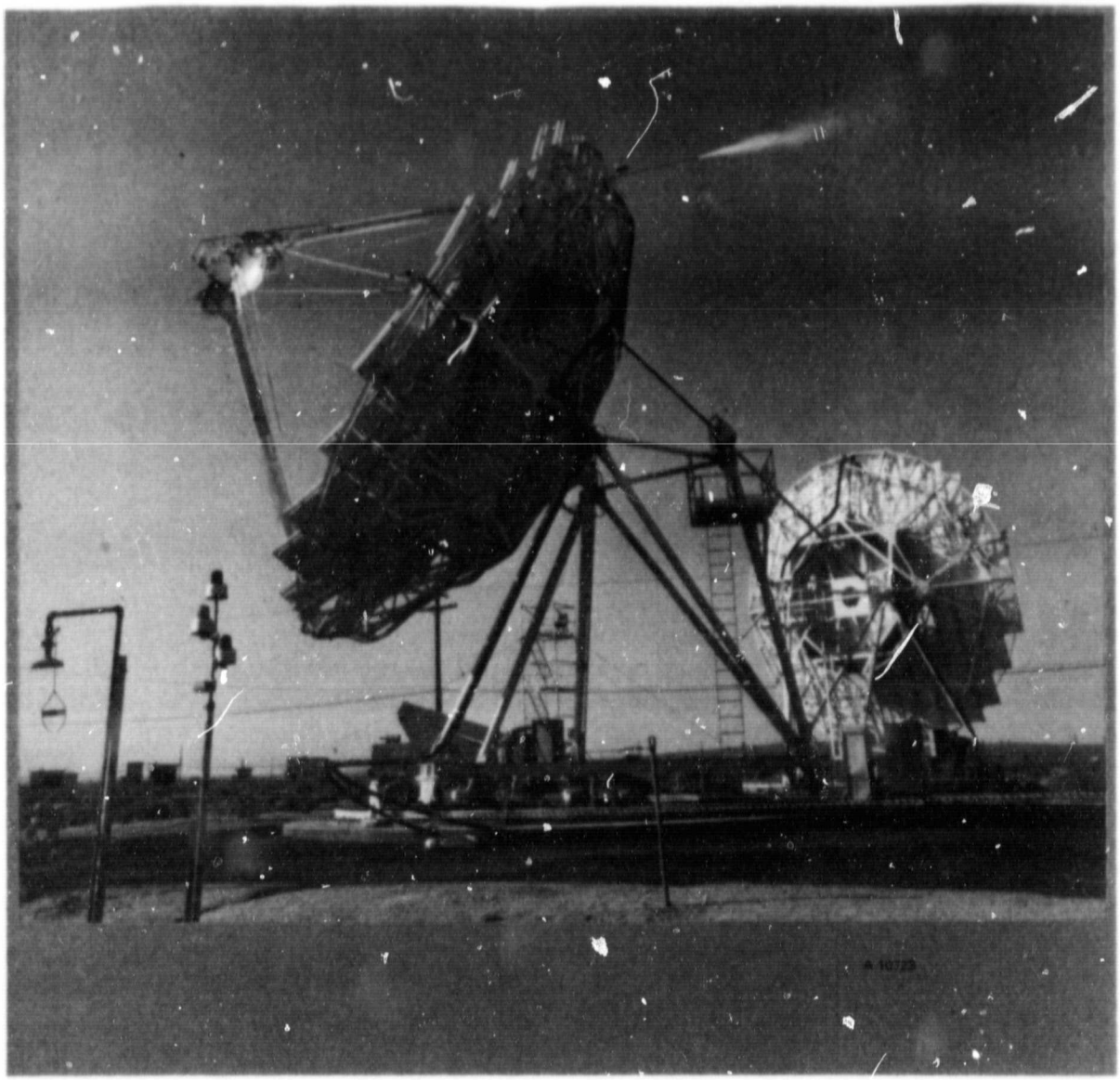

Figure 1-1. Parabolic Solar Concentrator

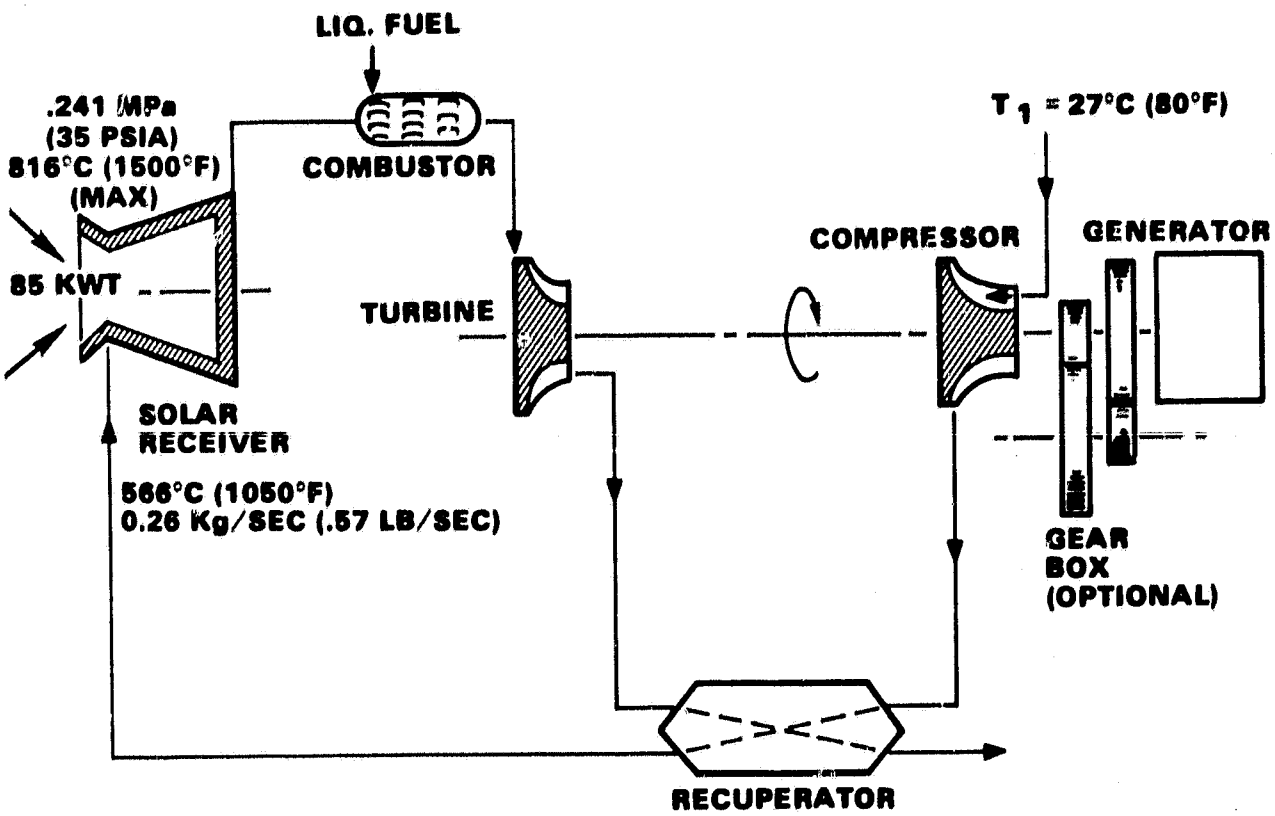

Figure 1-2. Air Brayton System Schematics

TABLE 1-1

SOLAR CONCENTRATOR CHARACTERISTICS

Type:	two axis, tracking, faceted parabolic dish
Size:	11-meter aperture
Reflectivity:	0.86 to 0.94 (maximum)
Peak thermal energy at focus:	85 kwt
Tracking error:	0.1 deg
Tracking system:	evaluation/azimuth
Slew rates:	elevation 400 deg/hr approximate azimuth 150 deg/hr approximate
Focal length:	0.6 diameter
Slope error:	1 to 2 milliradians (0.1 deg nominal)

support system. The aperture assembly was switched from a one piece ceramic component to a ceramic outer skirt and a RA-330 inner skirt. Material chosen for the heat exchanger was changed to Inconel 625 from Haynes 188. The diameter was slightly reduced and the length increased in the heat exchanger core.

This ABSR design underwent extensive thermal analysis. The receiver was designed to accept 85 KWth to the working fluid with a receiver thermal efficiency of 90.7%. The predicted pressure drop was 2.5%. Table 1.3 summarizes the predicted ABSR thermal performance. Considerable work was done to establish that the ABSR could accept various flux irregularities due to unknown concentrator characteristics. Optical inputs resulting from mirror or mounting irregularities were investigated.

A stress analysis of the ABSR looked at the pressure, thermal, and inertial loads on the receiver, adjusted the design where necessary, and predicted a prototype life for the receiver of two years of continuous operation, (10,000 hours and 1500 cycles). Cycle fatigue was determined to be more restrictive to the ABSR life than creep strength limitations.

Two ABSR's were fabricated by AiResearch. The plate fin core was brazed in two stages. The manifolds and ducts were welded to the brazed core to make the heat exchanger assembly. The aperture assembly and reflector plate assembly were fabricated separately. These three assemblies were installed in the receiver housing.

TABLE 1-2

AIR BRAYTON SOLAR RECEIVER

ABSR PROBLEM STATEMENT REVIEW

DESIGN POINT CONDITIONS AND PERFORMANCE GOALS

THERMAL INPUT_____85 KW PEAK
FLUX DISTRIBUTION____FROM 1-2 MRAD MIRROR
AIR INLET_____1049°F
AIR OUTLET_____1500°F
AIRFLOW_____0.57 LB/SEC (86% EFFICIENCY)
INLET PRESSURE_____36.75 PSIA

PRESSURE DROP GOAL__2%

TABLE 1-3

ABSR THERMAL PERFORMANCE SUMMARY

Q OFF CONCENTRATOR	85.0 KW
ASSUMED APERTURE LOSSES (SPILLAGE AND CONVECTION)	3.0
INSULATION LOSSES	1.1
APERTURE RADIATION LOSS (10-INCH APERTURE)	3.8
Q TO FLUID	77.1
TOTAL	85.0
Q TO FLUID FROM COMPUTER MODEL	77.1
PROBLEM STATEMENT GOAL	73.1
MARGIN	4.0
CORE FRICTION PRESSURE DROP	2.1%
ESTIMATED TOTAL PRESSURE DROP	2.5%

9-42351

The heat exchangers of the two solar receivers fabricated by AiResearch underwent acceptance tests. They consisted of leakage, proof pressure and pressure drop tests. The first unit tested had a leakage rate at the design condition of 3.5%. The unit underwent a proof pressure of 50 psig with no visible permanent deformation. The pressure drop test indicated a 2.9 psi pressure drop at room temperature at 0.57 lbm/sec, the design point flowrate. The second ABSR fabricated, incorporating new manufacturing procedures, had a leakage rate of 0.2% at the design point condition. It also passed the 50 psig proof pressure test. The pressure drop was measured at 3.5 psi for room temperature conditions and 0.57 lbm/sec flowrate.

2. AIR BRAYTON SOLAR RECEIVER (ABSR) DESCRIPTION

The cutaway drawing of the ABSR is shown in Figure 2-1. The main components of the 85 KWth ABSR are a cylindrical core assembly, an adjustable aperture assembly, and a rear plate assembly.

The cylindrical core martix consists of 16 identical panels. Each panel is constructed of two metallic parallel plate-fin flow passages. The panels are distributed among three 120° panel segments. These segments were brazed individually and then brazed together to form the core. The panels have transverse openings on the outer wall near the ends. This is to allow the working fluid to flow from the inlet to the outlet ducts.

A high performance offset fin matrix was used in the construction of the panels. The schematic of the fin type used is shown in Figure 2-2. The fins and the plates used were made of Inconel 625.

The aperture assembly consists of a Silicon Carbide (SIC) ceramic plate, 0.28-in. thick, an RA-330 stainless steel aperture support skirt, an Inconel 625 aperture mount plate, and a Corrosion Resistant Steel (CRES) type 347 aperture support ring assembly. The assembly has the option of incorporating two different ceramic aperture plates. One has an 8-in. diameter opening, and the other a 10-in. diameter opening. When changing the size of the aperture plate, the RA-330 support changes accordingly. All the other parts in the assembly remain the same however, since they are independent of the choice of aperture plates. The aperture plate also serves to reflect the re-radiated energy back into the receiver cavity.

The rear plate originally was fabricated from 0.28-in. thick, SIC plate. The rear plate assembly consists of an Inconel 625 support structure, and a mild steel rear outer shell. The shell has two ports in it, which allow the inlet and outlet ducts to pass through to the outside.

There is also an Inconel 625 toroidal manifold in both the inlet and outlet sections of the cylindrical core.

The cylindrical core is insulated with 4.5-in. of Cerablanket insulation wrapped around the core outside wall, surrounded by a 0.118-in. thick, carbon steel case.

The design weight of the ABSR was determined to 480 lbs.

A summary of the geometrical characteristics for the ABSR are presented in Table 2-1.

Detailed design drawings of the entire unit are provided in Appendix A at the end of this report.

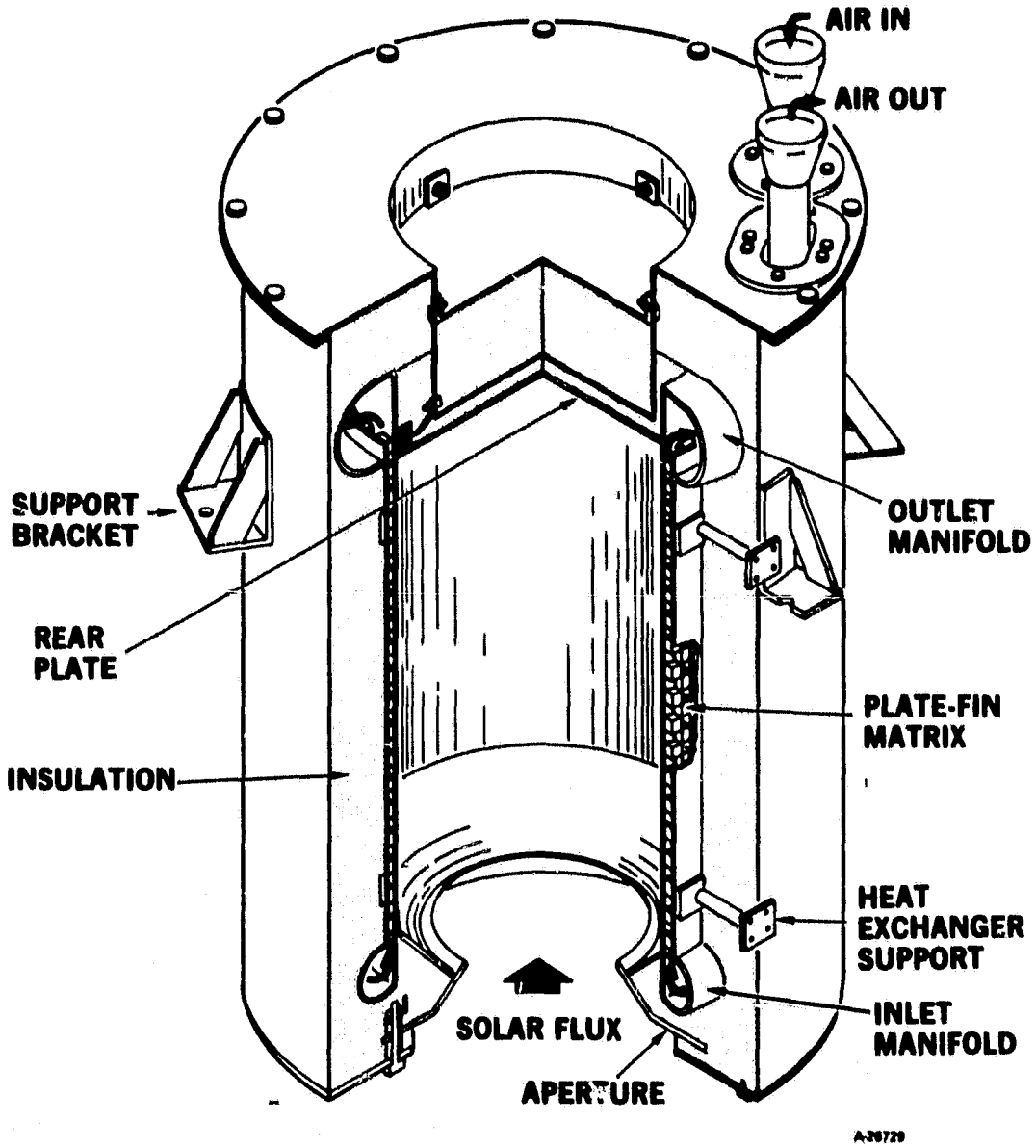

Figure 2-1. Air Brayton Solar Receiver (Cutaway)

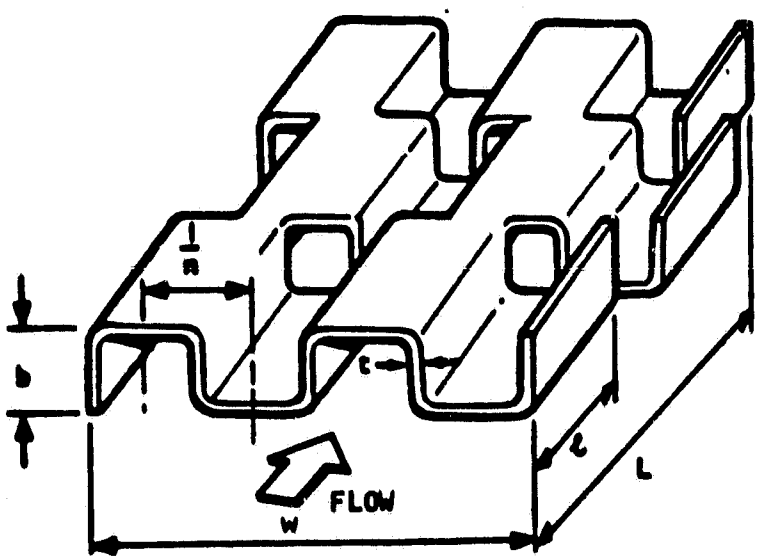

DESIGNATION: n_R - b - ℓ - t

12R-.25-.50-.005

Figure 2-2. Rectangular Offset Plate Fin

TABLE 2-1

85-KWt ABSR GEOMETRICAL CHARACTERISTICS

Geometrical Characteristics	Phase II	
Cavity dimensions, internal, ft (in)		
Overall height	2.75	(33.0)
Length of cylindrical section	2.33	(28.0)
Diameter of cylindrical cavity section	1.665	(20.0)
Diameter of aperture opening	0.666 0.833	(8.0) (10.0)
Other dimensions		
Insulation thickness on cylindrical wall, in.	4.5	
Overall outside diamter, ft (in)	2.5	(30.0)

3. ABSR ANALYSIS

Analysis of the Air Brayton Solar Receiver (ABSR) included both thermal analysis of the ABSR, in order to ensure the adequacy of its thermal performance characteristics, and structural analysis, in order to ensure that the desired lifetime of the receiver is reached.

3.1 THERMAL ANALYSIS

Thermal analysis performed by AiResearch during Phase II of the ABSR program consisted of three major efforts. Optical models of the concentrator-receiver system were created to determine the thermal inputs to the receiver for concentrators with different characteristics. The calculated receiver performance was confirmed after final design iterations. The ABSR performance was evaluated under various off-design conditions.

The calculated thermal and pressure-drop performance of the receiver under design conditions is summarized in Table 1-3. The thermal margin allows for miscellaneous heat loss paths not accounted for in the computer program. The slightly higher than goal pressure drop results from the trade-off between the low pressure drop desired for overall system efficiency and the low-cavity temperatures and temperature gradients dictated by receiver operating life requirements.

3.1.1 Optical Modeling

The total design power directed toward the receiver by the concentrator was defined as 85 KWth. An estimated distribution of the normal heat flux on planes parallel to the focal plane was provided by JPL from two different concentrators. The concentrators had slope errors of 1 and 2-milliradians (mrad). An additional vertical distribution was provided for the 2-mrad concentrator.

In order to accurately evaluate the performance of a receiver design of Phase II, not only the total incident flux must be known, but also its distribution over the interior surfaces of the cavity. This flux distribution depends on a number of factors, including: (a) the characterization of the optical source; (b) the overall geometry of the concentrator (surface shape and speed i.e., the smaller the angular size of the source, the slower the optical system). AiResearch had the availability of a mathematical solar simulator program developed by Dr. George Schrenk and supplied through Scientific Time Sharing Corporation (STSC). This program properly treats the sun as a source of finite angular dimensions and uses an efficient cone-optics method of evaluating the incident concentrated flux, rather than using a ray-trace technique (which is used in analyzing image producing optical systems). The effects of radiation due to atmospheric scattering and of concentrator slope errors are taken into account by specifying an effective sum half-angle (αeff) larger than the actual half-angle (α).

A simple but effective model was used to determine the receiver heat inputs for the parametric study of Phase I of the program. The results from this model were seen to be essentially indistinguishable from those obtained via the STSC program.

Figure 3-1 illustrates the optical differences between a very distant point source (resulting in parallel incident rays) and a source of finite angular dimensions. The paraboloidal concentrator shown has an f/D ratio of 0.6. On the right hand side of the figure, the paths of the incident and reflected rays from a finite source are shown being reflected from selected points on the reflecting surface. Similarly, the left hand side shows the results for flux incident from a distant point source. The drawing is to scale and the paths of the reflected rays were determined by an exact ray trace program. Two observations can be made:

(1) For a distant point source on the optical axis, a paraboloid of revolution focuses all the incident rays through the prime focus. Thus, the aperture flux distribution is a poor approximation to the actual flux distribution from an extended source.

(2) For regions away from the focal plane, the character of the flux field produced by the distant point source is not substantially different from that for an extended source.

By adopting the distant point source approximation (simple model), the flux in the cavity can now be represented by a simple vector field. The flux vector $\vec{F}$, is fully described once its magnitude F and polar angle θ are specified (there being azimuthal symmetry). At a location (r, z) in the cavity, F and θ are given by

$$F(r, z) = \frac{\rho S R H \cos\left[\arctan (R/2f)\right]}{\cos\left[\arctan (r/z) - \arctan (R/2f)\right] r \sqrt{r^2 + z^2}} \qquad (3\text{-}1)$$

where

$$H = \sqrt{R^2 + (f - R^2/4f)^2} \qquad (3\text{-}2)$$

and

$$R = \left[2f/(r/z)\right] \left(\sqrt{1 + r^2/z^2} - 1\right), \quad r/z > 0, \qquad (3\text{-}3)$$

$$= 0, \quad r/z = 0, \qquad (3\text{-}4)$$

and

$$\theta\ (r/z) = \arctan (r/z). \qquad (3\text{-}5)$$

The geometric quantities r, z, R, H, and f are defined in Figure 3-2. The physical quantities ρ and S are the concentrator reflectivity and the direct normal incident solar radiation, respectively. F will have the same units as S (e.g., kW/m^2) if all the geometric quantities use the same linear unit (e.g., meters).

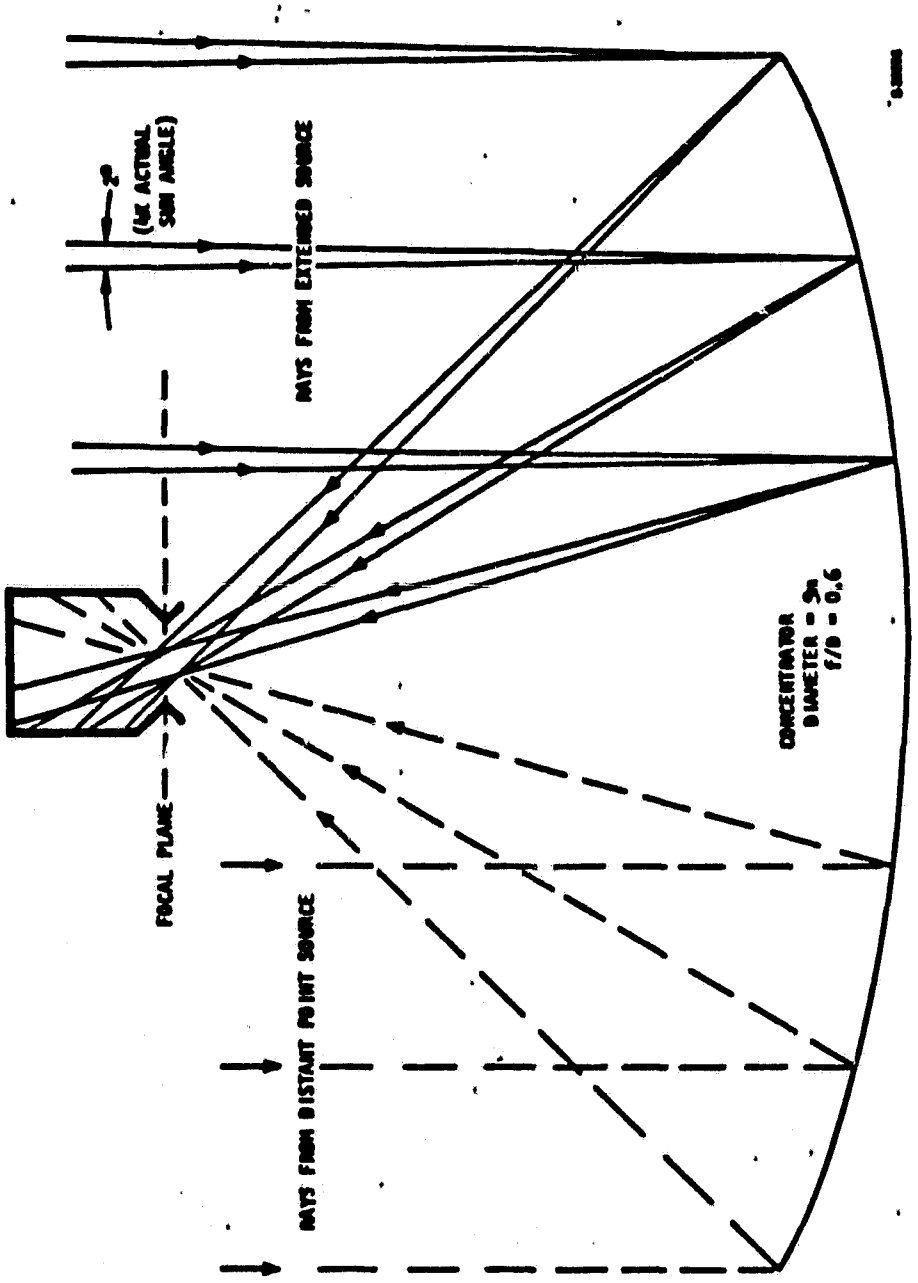

Figure 3-1. Concentrator and Receiver Optics

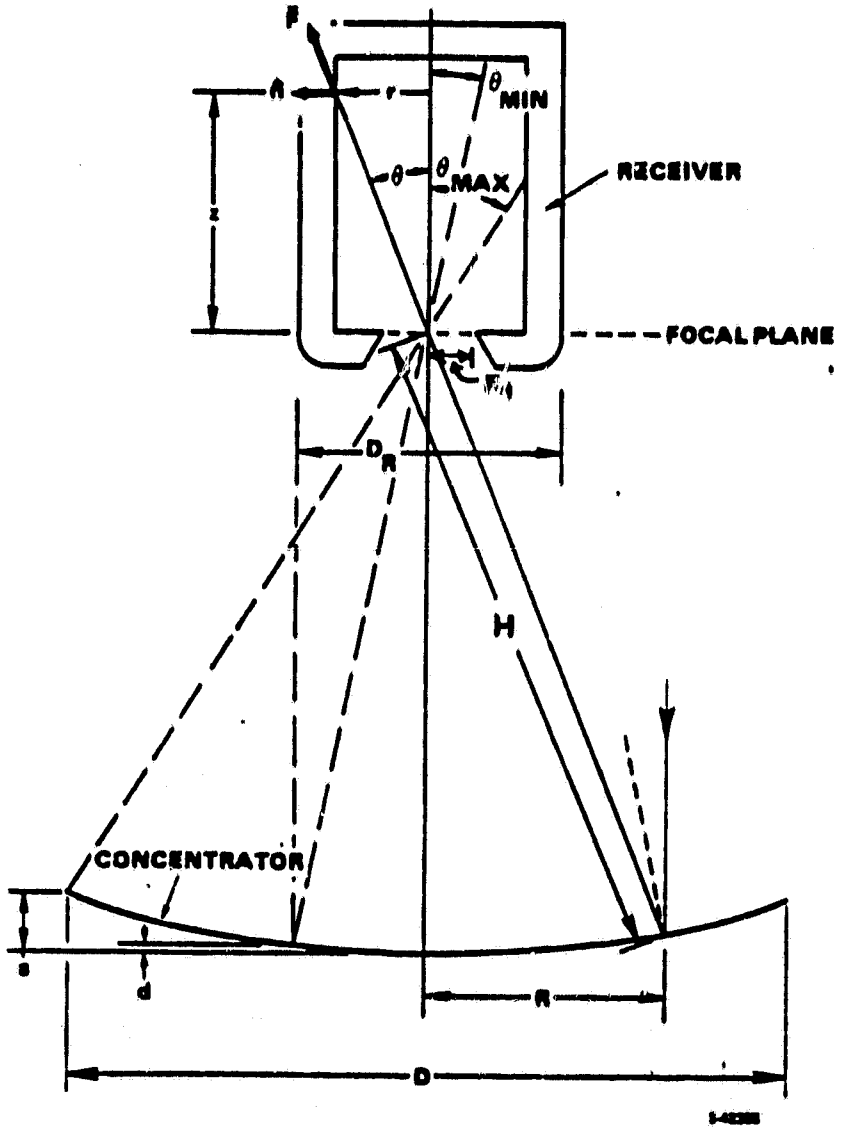

Figure 3-2. Optical Flux Parameters

The effect of the concentrator diameter, D, is applied through the additional constraint

$$F = 0 \text{ if } \theta > \theta_{max} \tag{3-6}$$

where

$$\theta_{max} = \arctan \frac{D/2}{f-s} \tag{3-7}$$

and

$$s = \frac{1}{4f}(D/2)^2 \tag{3-8}$$

Also, shadowing by the receiver itself results in the constraint

$$F = 0 \text{ if } \theta < \theta_{min} \tag{3-9}$$

where

$$\theta_{min} = \arctan \frac{D_R/2}{f - d} \tag{3-10}$$

and

$$d = \frac{1}{4f}(D_R/2)^2 \tag{3-11}$$

Finally, the incident energy per unit area of cavity wall, q, is

$$q(r,z) = \vec{F}(r,z) \cdot \vec{n}(r,z) \tag{3-12}$$

where $\vec{n}$ is the outward directed unit vector normal to the cavity wall at the point of interest.

A comparison of q determined by both the STSC program and this simple approximation is shown in the upper portion of Figure 3-3. The results shown are for the typical cavity shown in the insert at the lower portion of the figure. The simple model's sharp cutoff occurs at $\theta = \theta_{max}$. The fact that the peak value of the simple model curve is quite a bit higher than the STSC curve is really of little concern. What is of importance here is not the instantaneous value of q (z,r), but the integral of this quantity over the finite area of a wall element (the cavity is divided into six finite elements). The lower portion of Figure 3-3 shows two superimposed histograms giving the total energy incident upon each element using both the STSC program (solid line) and the distant point source model (dashed line). The difference between the two is seen to be rather small, with a maximum difference of 12.0 percent. Because of radiation effects, the abosrbed power curve is more smeared out than the incident power curve. This serves to further reduce the importance of choosing the more exact flux model. The final and most important result is that the wall temperature distribution and peak temperature value is not significantly influenced by using the simpler flux model.

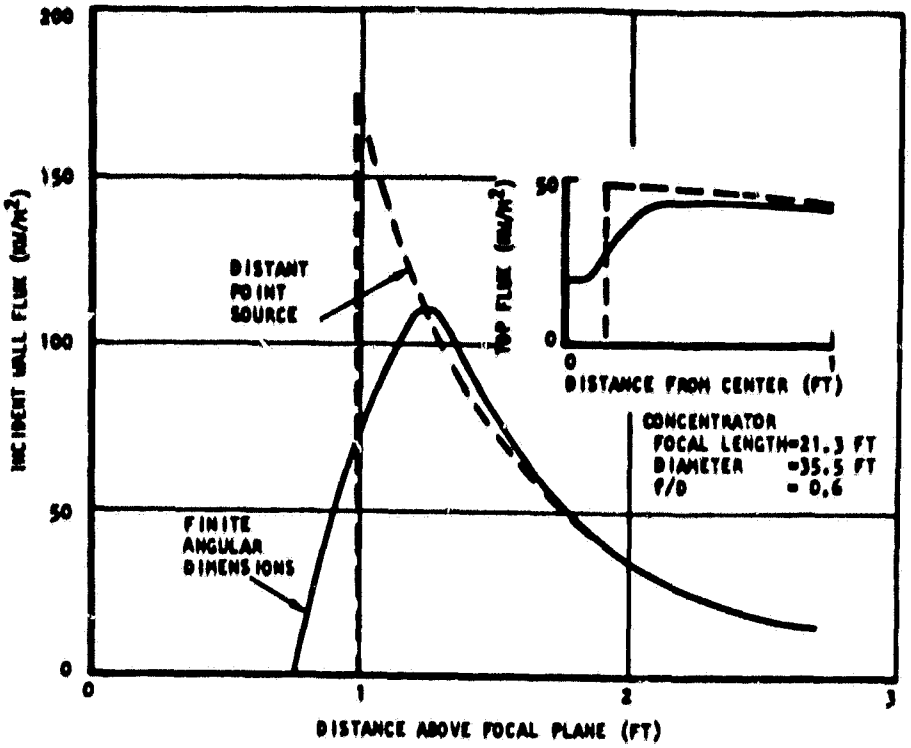

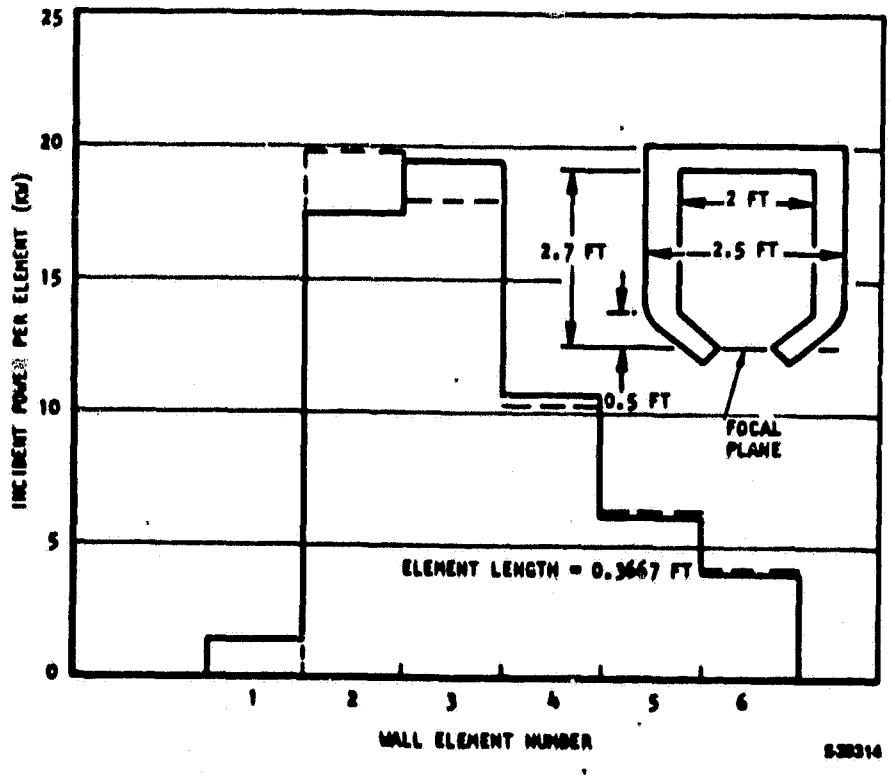

Figure 3-3. Comparison of Parallel Ray and Cone Optics Models

The effect of the concentrator imperfections is to apply a smoothing function to the distribution that would otherwise result from reflection from a perfect mirror. Thus, the simple model histograph can be improved by applying a smoothing technique which employs two empirically determined parameters, N and S_1. N is the number of times the smoothing is applied to the histogram, while S_1 measures the amount of smoothing per pass. The optical input for the thermal analysis of the receiver under development was obtained using a distant point source model and the smoothing function.

Figure 3-4 compares the vertical flux distribution given in Exhibit II of the JPL work statement with a histogram obtained in the described manner. The excellent agreement far from the aperture is as expected; near the aperture, the Exhibit II curve seems to be deficient in integrated power.

Knowledge of the flux distribution across the focal plane is necessary in order to establish the receiver aperture size. Figure 3-5 is a collection of aperture flux plots presented as concentration ratio vs the radius R_1. The plots on the right side of the figure are a continuation of the plots on the left side on a greatly expanded scale. The rectangular "simple optics" plot ignores all optical aberrations that accompany non-paraxial rays and fast optical systems. It does, however, provide a convenient datum against which all others can be compared. The "Schrenk" plot was generated by the STSC program. The 1.7 factor was chosen to give reasonable agreement with the "1.75 mrad" curve, which was supplied by JPL for the Phase I proposal effort. The curves labeled "1 mrad" and "2 mrad" are from the Exhibit II supplied in Phase II; interpolation between these two gives the "1.75 interpolated" curve for the specified nominal value of 1.75 mrad.

The new curves clearly are in disagreement with the older 1.75 mrad curve and, especially for the 1 mrad case, exhibit unusual behavior for small R_1. Based on these considerations, a conservative value of R_1 = 5-in. was chosen for the baseline aperture size for the analysis, but the actual receiver was provided with aperture size adjusting features.

3.1.2 Final Design

The ABSR was designed with several objectives in mind. The maximum cavity efficiency was desired. The metal temperatures had to be kept under certain limits for acceptable receiver life. The pressure drop was intended to be below a certain value so that system performance would not be significantly affected. The weight of the unit was kept to a minimum to keep the receiver support system simple. The basic parametric analysis of the receiver involving these variables was performed during Phase I.

Phase II interface specifications required changes in the dimensions of the recommended Phase I receiver. The parametric study guided the alterations. Once the final design was determined, conduction, radiation, and convection losses were calculated for the receiver to assure adequate performance.

The changes required by the new interface restrictions forced the reduction of the heat exchanger diameter from 24-in. to 20-in. The parametric curves from Phase I used in the adjustment are shown in Figure 3-6. The maximum wall

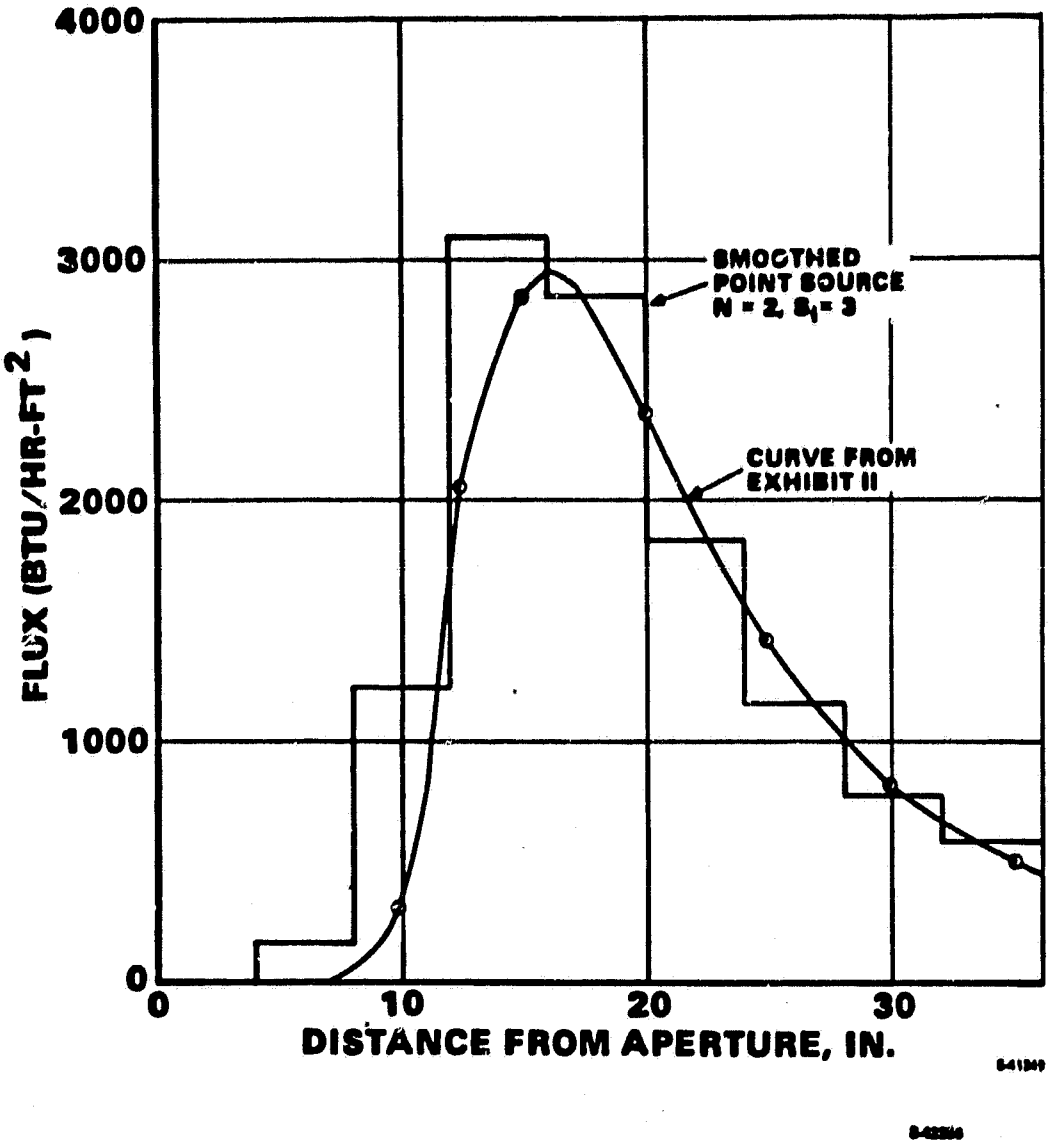

Figure 3-4. Comparison of AiResearch and JPL Flux Plots for a 12-In. Radius Cylinder

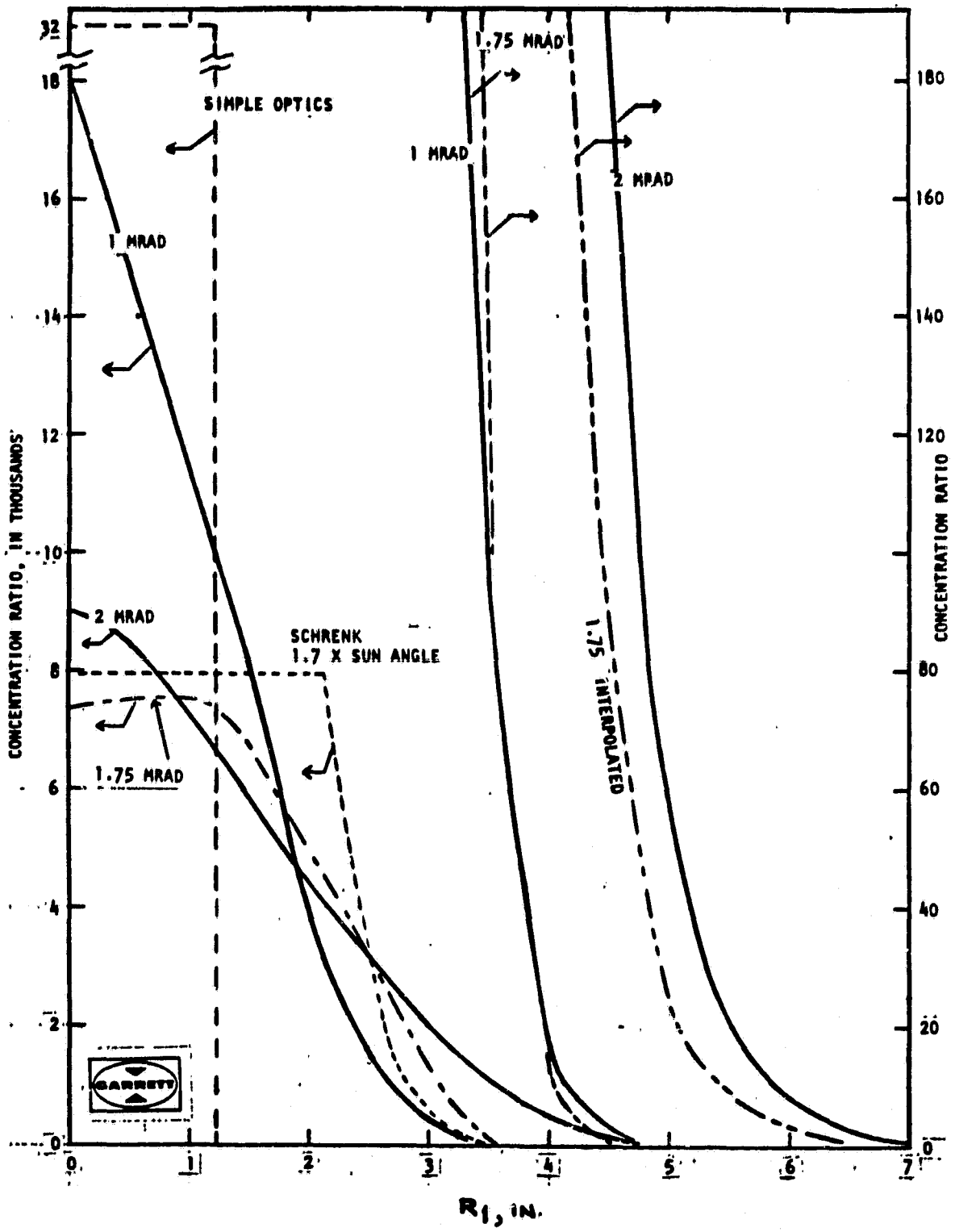

Figure 3-5. Aperture Flux Plots. Concentration Ratio vs. Radius of Receiver Opening

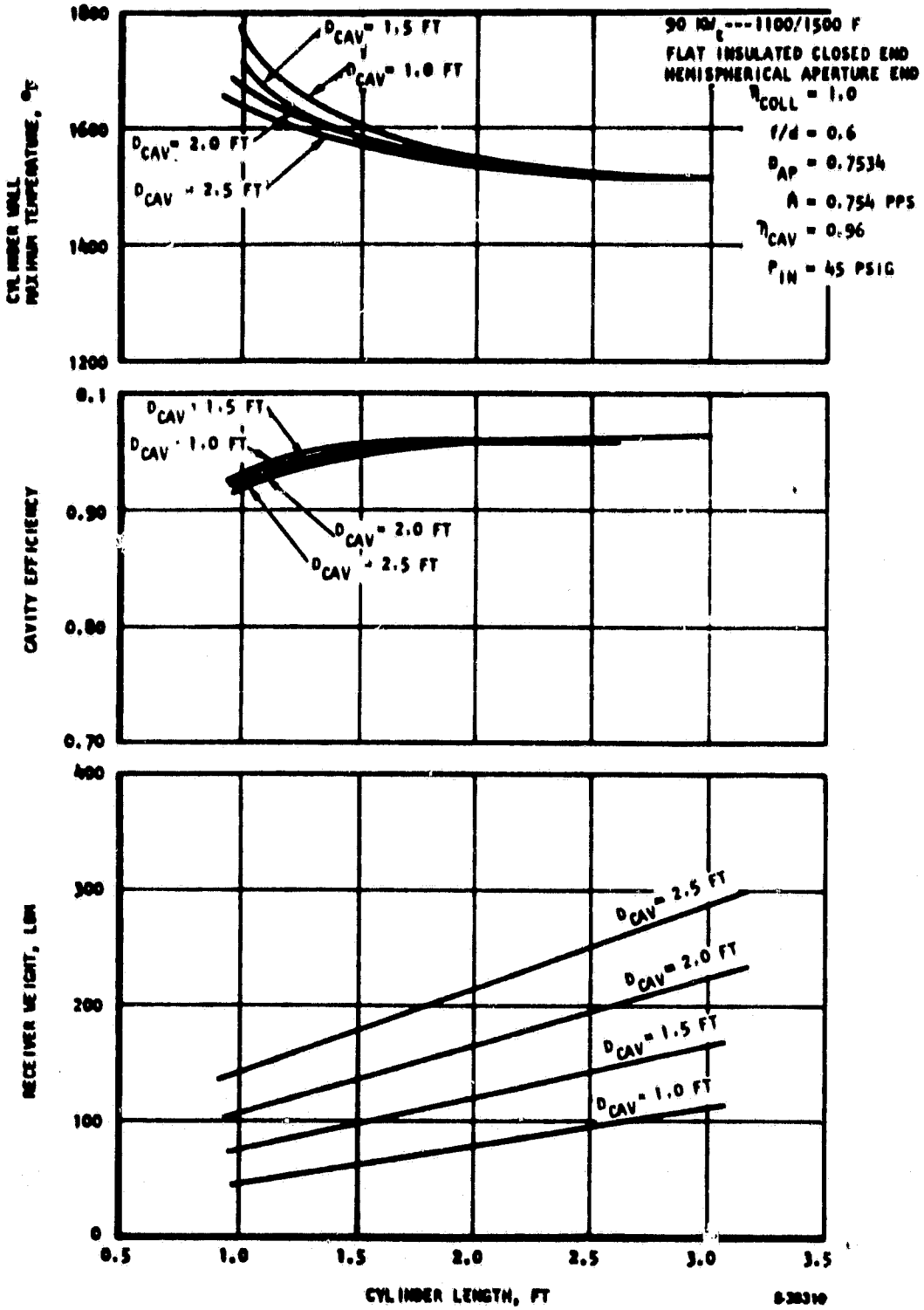

Figure 3-6. Brayton Cycle Plate-Fin Receiver Weight, Cavity Efficiency, and Maximum Cylinder Wall Temperature as a Function of Cavity Diameter and Cylindrical Length - 90 KWt and 1100/1500°F. Aperture Convection Losses Not Included.

temperature plot showed no significant advantage for cylinder lengths greater than 30-in. Cavity efficiency levels out beyond a 24-in. long cylinder, while the receiver weight increases linearly with cavity length. Pressure drop also increases with increasing cavity length. A cavity length of 28-in. was decided upon as the best compliment to the cavity diameter of 20-in. Figure 3-7 shows the basic dimensions of the final ABSA. Heat losses from the receiver were based on this final size.

Conduction, convection, and radiation losses were calculated. Conduction losses outward through the insulation were calculated to total approximately 1.1 kw. Convection losses from the cavity walls to the ambient air were estimated at 3.0 kw. Radiation losses from the cavity through a 10 inch diameter aperture were approximated at 3.8 kw. These numbers were based on a 85 kw input from the concentrator and resulted in an estimated 90.7% of the concentrator heat input being transferred to the working fluid.

Incident solar flux on the inner surfaces of the receiver was computed. The underlying assumption is that parallel rays emanating from the sun (point source) are being reflected from a perfect parabolic concentrator. The resulting flux profile was smoothed out (Section 3.1.1 Optical Modeling) and represented in a histogram input to the computer program. This allowed computation of the radiation interchange, fluid heat transfer, and pressure drop.

The Solar Receiver thermal Performance program (RECMDL) is used to analyze the thermal performance of plate-fin or tubular solar receivers. RECMDL uses a finite-element model. The output provides a complete nodal temperature map, absorbed heat inputs, heat losses, and fluid conditions. The flow chart for the program is presented in Figure 3-8.

The model generation portion of the program consists of three subroutines which consider the aperture end, cylindrical heat transfer section, and the closed end. The end sections can be either hemispherical or flat, and the cylindrical section may have either plate-fins or tubes as the heat transfer surface. The primary output information from the modeling routines consists of the thermal resistances associated with the finite elements and the material weights.

From the input information and the model generation calculations, the Geometrical Radiation View Factor routine calculates the view factors for the inner cavity from a set of exact closed form equations. The basis for the view factor analysis comes from the closed form equation for parallel concentric disks and view factor algebra. The results are exact for smooth wall cavities (as in the plate-fin case). However, the results are only approximate for rough surfaces (tubular concept).

The program performs transient and steady-state calculations. The steady-state thermal analysis routine utilizes a Newton-Raphson iteration technique to converge on a specified temperature and heat balance condition.

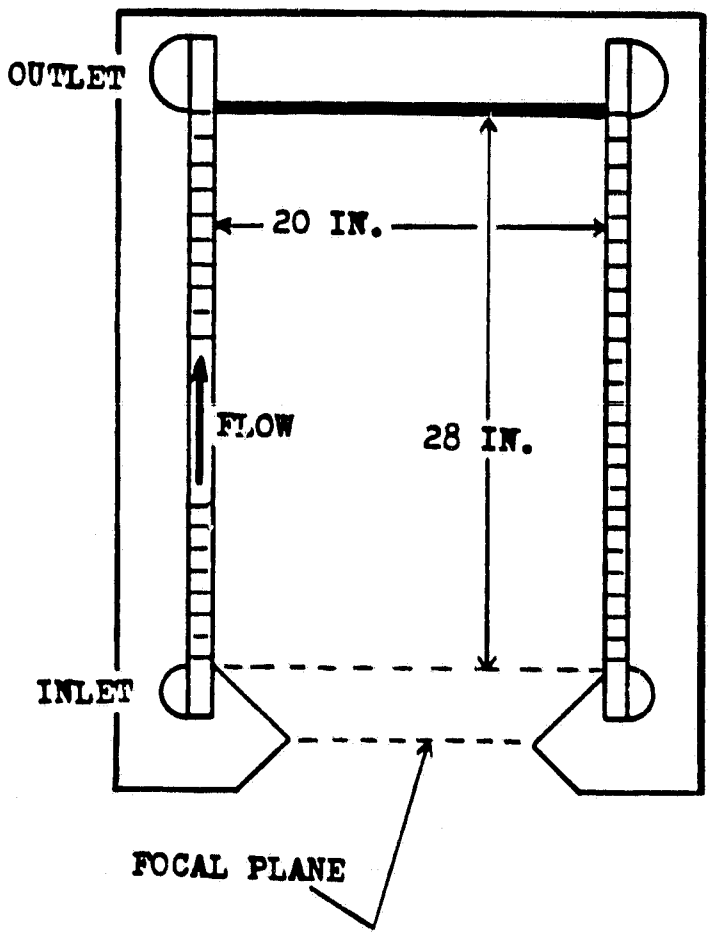

Figure 3-7. ABSR Basic Dimensions

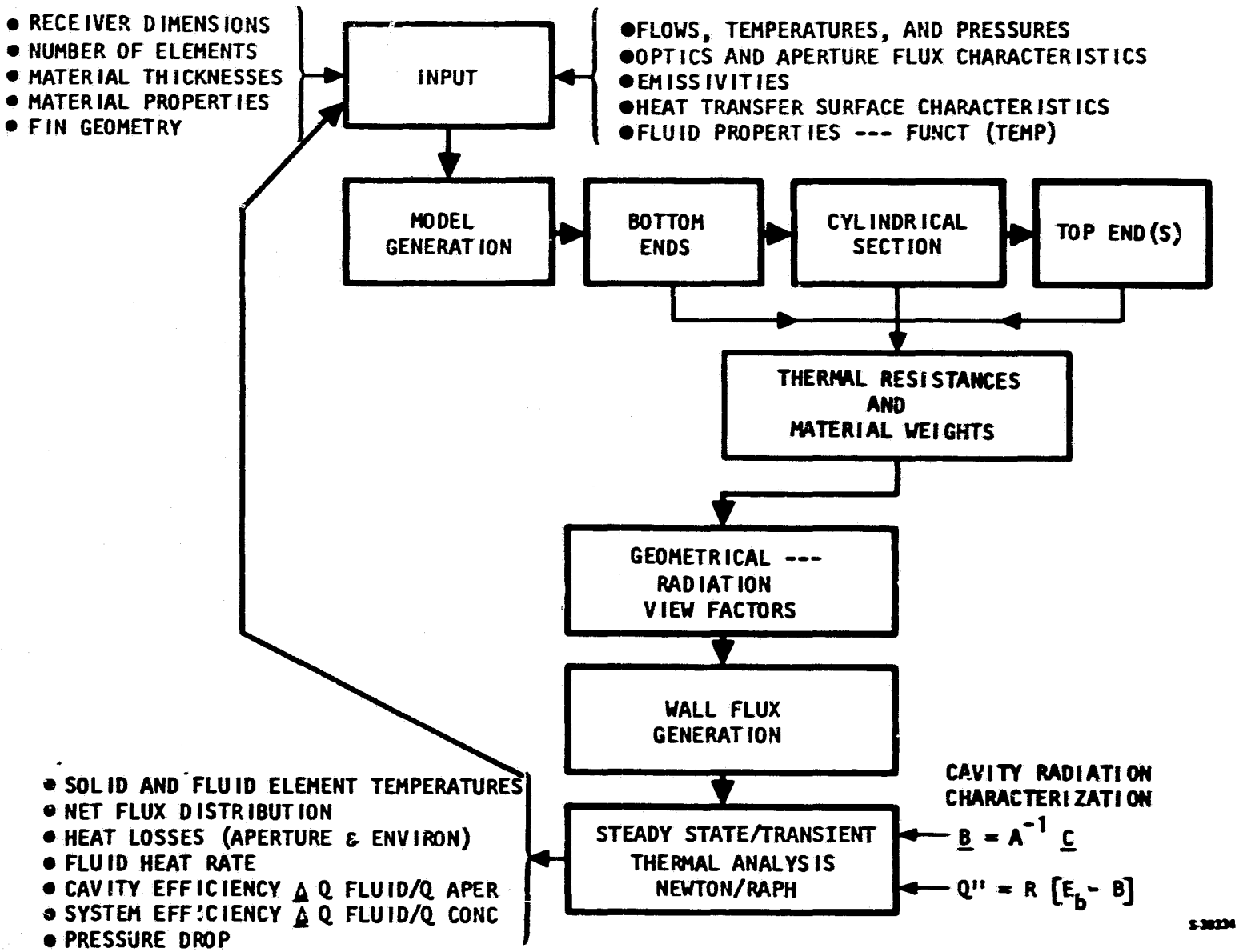

Figure 3-8. Flow Chart for Solar Receiver Computer Code--Plate-Fin/Tubular

Reflected and emitted energy within the cavity was included in the analysis by the following equation

$$\underline{B} = A^{-1}\,\underline{C} = \text{reflected energy} + \text{emitted energy}$$

where $\underline{B}$ is the radiosity column matrix, A is an NxN characteristic matrix, and $\underline{C}$ is a temperature dependent column matrix. This equation assumes a gray body and diffuse emittance and reflections.

During Phase II, RECMDL was primarily used to determine the sensitivity of the receiver to various off-design heat flux inputs from the concentrator.

The manifold flow characteristics of the unit were also analyzed to ensure uniform flow. Uniform flow distribution is essential in high-flux solar receivers in order to minimize the possibility of localized hot spots and possible burnouts. Also, to maintain a high cavity efficiency, flow maldistribution must be minimized. The inlet and outlet manifolds are toroidal in shape. A flow maldistribution of about 3 percent was calculated, which is negligibly small in terms of performance degradation.

3.1.3 Heat Flux Sensitivity Analysis

The ABSR was analyzed under various heat flux inputs to determine its sensitivity to off-design conditions. This analysis examined the effect of both symmetric (flux profiles which vary in the axial direction only) and assymetric incident solar fluxes on the receiver. The symmetric incident fluxes include the baseline flux (the smoothed incident flux profile described in Section 3.1.2-Final Design), and axially shifted flux profiles with reduced peak flux patterns. The asymmetric flux patterns, in one case, offset the receiver 1-inch, and in another case reduced the input (10% less total power) from one-half of the concentrator.

A heat flux sensitivity analysis based on three assumed symmetrical incident heat flux profiles was performed on the receiver. For the analysis, the receiver cavity was longitudinally divided into seven nodes. It includes the cylindrical section only, as no ends are involved. The three cases considered were the baseline heat flux distribution, and a 3-in. and a 6-in. axially shifted fluxes. Figure 3-9 shows the corresponding flux patterns. The total power input in each case is the same (85 kwth). The heat peak values for the axially shifted cases are equal to the peak value of the baseline case.

The behavior of the heat flux distribution for the three cases is very similar. The discrepancy is due to the fact that each node in the receiver cavity receives different solar input in each case. It is also due to the fact that the system optics would have to be different in order to allow a shift of the heat patterns.

A node by node summary of the changes of the power input in the cavity of the ABSR is presented in Table 3-1. The table shows a comparison of the integrated nodal power inputs for each case. For the baseline case, the peak flux lies on node No. 3 at an approximate distance of 9-in. from the opened end of the cavity. For the 3-in. shifted solar influx, the peak occurrence

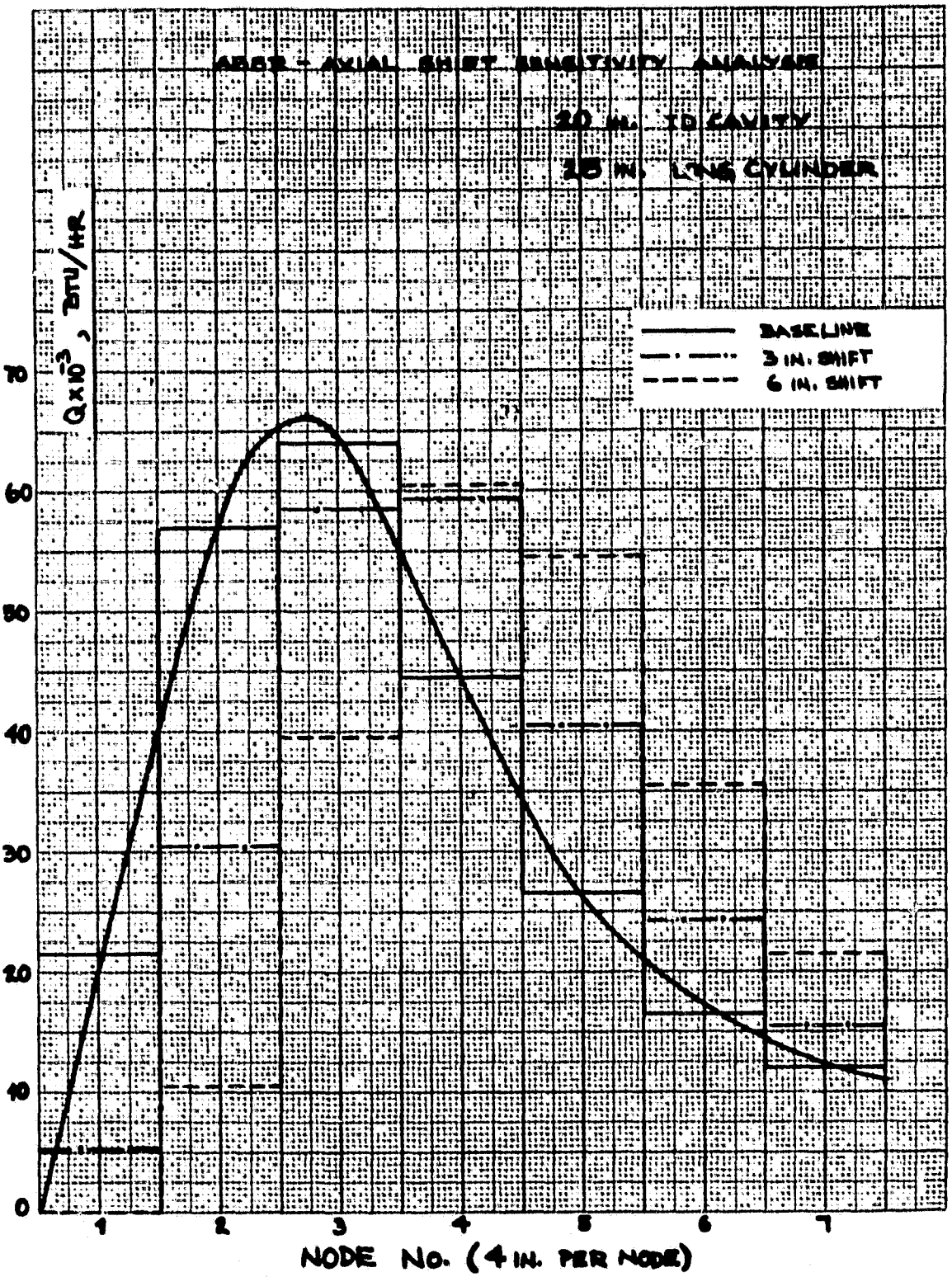

Figure 3-9. ABSR Symmetrical Incident Heat Fluxes

TABLE 3-1

INTEGRATED POWER INPUTS-SYMMETRICAL CASES

Node No.	Baseline (btu/hr) x 10^3	3-inch Shifted (btu/hr) x 10^3	6-inch Shifted (btu/hr) x 10^3
1	21.5	5.3	0.0
2	57.0	30.5	10.8
3	64.0	58.5	39.4
4	44.5	59.2	60.6
5	26.8	40.3	54.2
6	16.8	24.3	35.7
7	12.2	15.7	21.8

is between nodes No. 3 and No. 4, at 12-in. from the opened end of the cavity. The 6-in. shifted distribution shows that the peak takes place on node No. 4, 15-in. from the same reference point.

The temperature distributions of the cavity wall and fluid for the three related cases are given in Figure 3-10. The cavity wall temperature profiles have a steep region, followed by a moderate or less steep region. The transition of regions occurs near the location of maximum temperature difference (T_{max}) between the wall and the fluid temperatures. This is true for all three cases presented. The T_{max} falls in a range of 230°F to 280°F for each case. This temperature difference is found to be located at a distance of 8-in. from the opened end of the cavity. It is at a distance of approximately 12-in. and 14-in. for the 3-in. and 6-in. shifted flux cases, respectively. There is a close correspondence between the locations of the heat flux peak and T_{max} in every case.

It is also noted that while the wall temperature profiles intersect each other, this is not the case for the fluid temperatures. This is related to the difference in temperature response that these two system elements have. The cavity wall responds faster than the fluid to changes in the heat input. As a result of the flux shifts, the peak metal temperature increases by approximately 20°F to 40°F at the rear end of the receiver. These temperature increases are significant due to the normally high operating temperatures.

Asymmetric heat flux inputs analyzed consisted of offsetting the receiver 1-inch, and secondly, reducing the input from one-half of the concentrator. Figure 3-11 shows the offset cavity geometry. The cavity wall was divided into

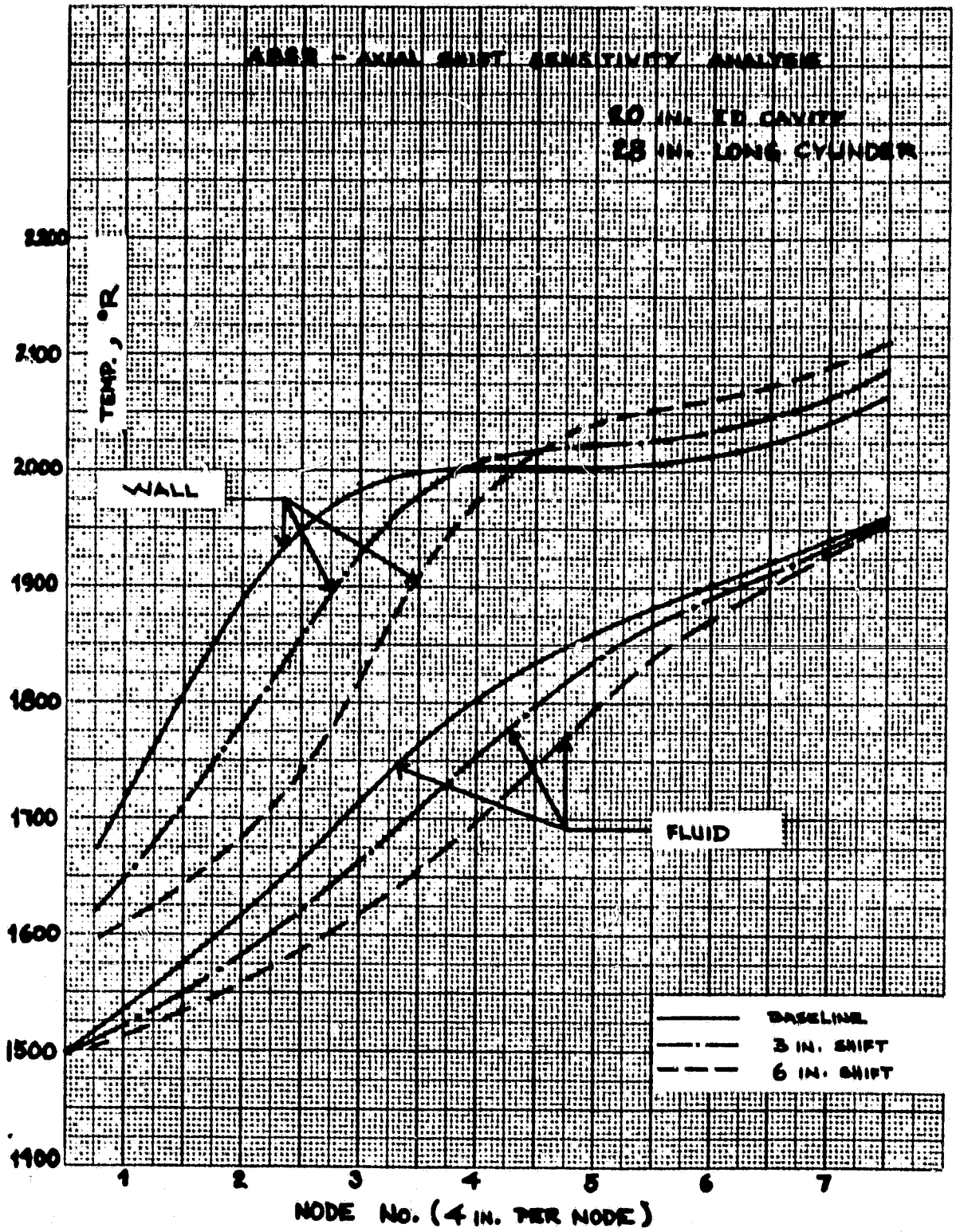

Figure 3-10. Temperature Distribution for the Symmetrical Heat Fluxes

OF POOR QUALITY

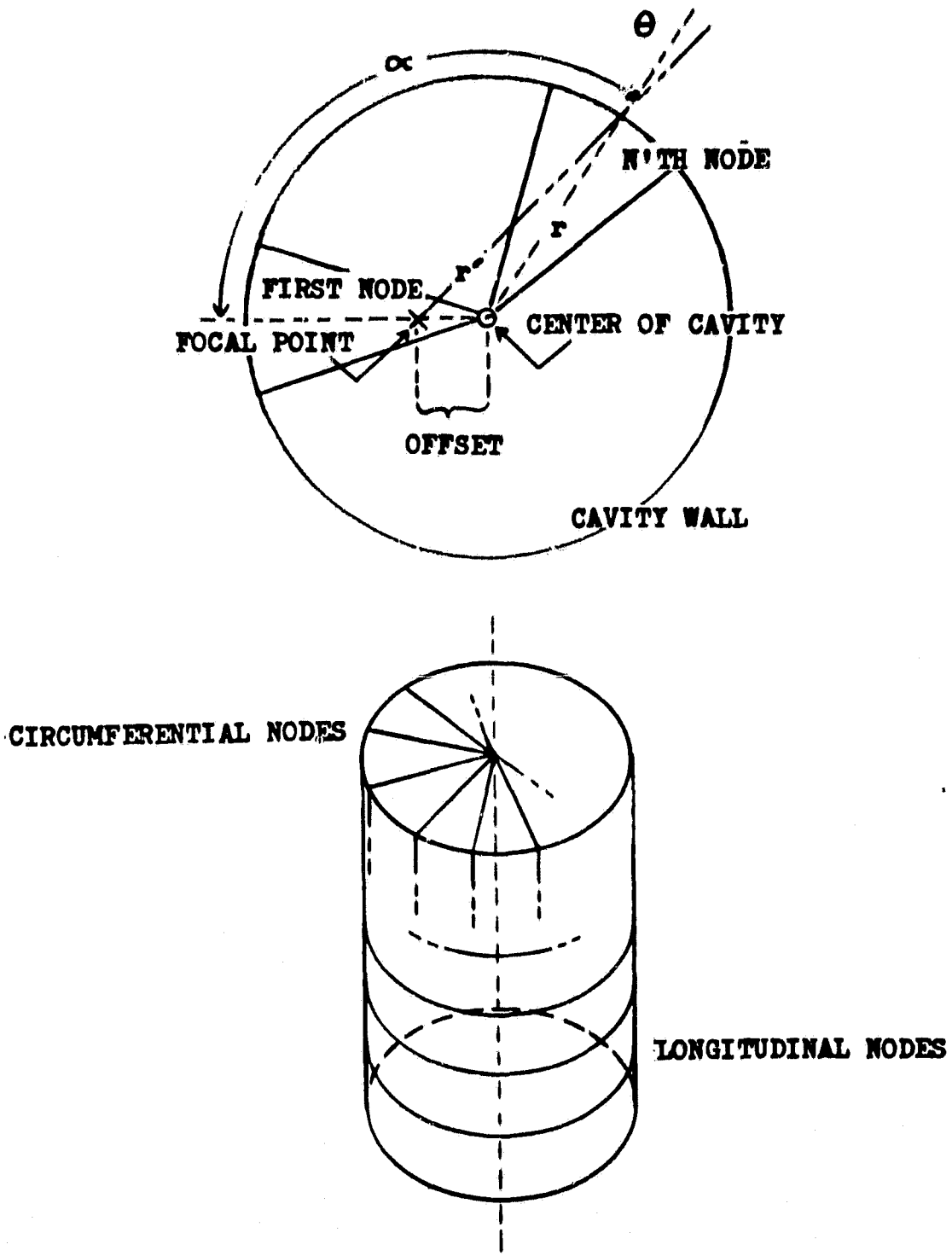

Figure 3-11. Offset Cavity Geometry

12 longitudinal nodes of equal length and into 12 equal circumferential nodes. The first circumferential node is the closest to the focal point. Offsetting the receiver resulted in a metal wall temperature increase of approximately 20°F. This occurs at the rear end of the cavity on the side closest to the focal point. The maximum flux increases by 11% in this configuration with respect to the corresponding baseline value. The flux changes are illustrated in Figures 3-12 and 3-13.

Figure 3-12 shows the incident power along the cavity wall of the receiver. It presents the integrated longitudinal heat distribution for two circumferential nodes only i.e., the closest and the farthest nodes with respect to the focal point. The near side shows more drastic changes in the heat flux distribution than the far side. At the rear end of the cavity, the changes in incident power with resepct to the baseline are minor in both cases. However, at the front half of the receiver (including longitudinal nodes 1 to 6), these changes are substantial.

Figure 3-13 presents the power absorbed by the cavity as a function of the circumferential nodes. For each node, the heat input over the total length of the cavity is considered. It shows a circumferential power fluctuation of about $\pm$2.6% with respect to the baseline heat input (no-offset condition). The peak power correpsonds to the circumferential node closest to the focal point (node No. 1). The minimum absorbed power corresponds to the node diametrically opposed to node No. 1. This flux pattern has less adverse effect than the second asymmetric flux pattern analyzed. The second pattern had a reduction in flux from one half the concentrator resulting in a 10% reduction in the total power input. See Figure 3-14. This reduction in power input causes the air flow rate to decrease accordingly in order that the average fluid outlet temperature remains constant. Therefore, the half of the receiver where the maximum flux remains, functions with the reduced flowrate. An approximate 58°F increase occurs on this side of the receiver at the closed end. Table 3-2 summarizes the flux sensitivity study performed on the ABSR. These flux variations result in various reductions in receiver life.

3.1.4 Process Heat Investigation

Operation of the ABSR for process heat applications was investigated. It appears that the receiver can be used for the cases analyzed without adversely affecting receiver life. The acceptable conditions investigated had air inlet conditions of 100°F, 36.75 psia, and a flowrate varying from 0.4 to 1.0 lbm/sec. Flowrates below 0.4 lbm/sec begin to impose significant thermal gradients on the core that would affect receiver life. Full power was input with the baseline flux profile.

3.1.5 Pressure Drop

The predicted pressure drop for the ABSR at the design point was 0.92 psi or 2.5% of the inlet pressure 36.75 psia. After the unit was fabricated and tested, the actual pressure drop of the unit at the design point was determined to be 3.5 psi or 10.3% of the inlet pressure. The reason for the discrepancy was determined to be primarily due to restrictions in the inlet duct. The inlet duct was downsized from a 3 to 2-in. diameter tube to meet interface

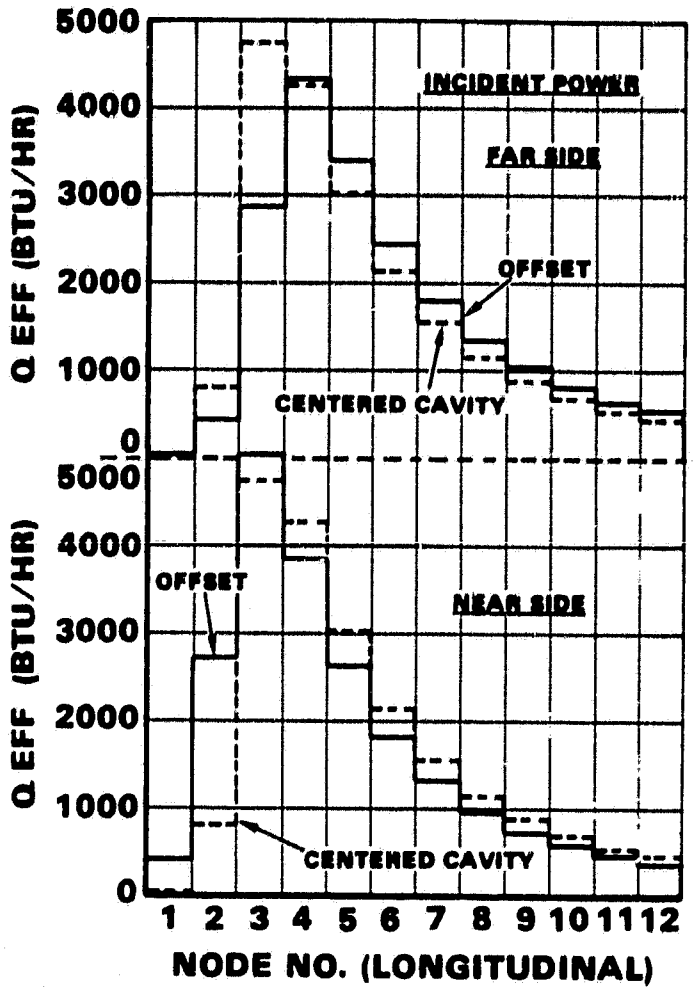

S-42364

Figure 3-12. Incident Flux vs. Longitudinal Nodes, for the ABSR 1-inch Cavity Offset

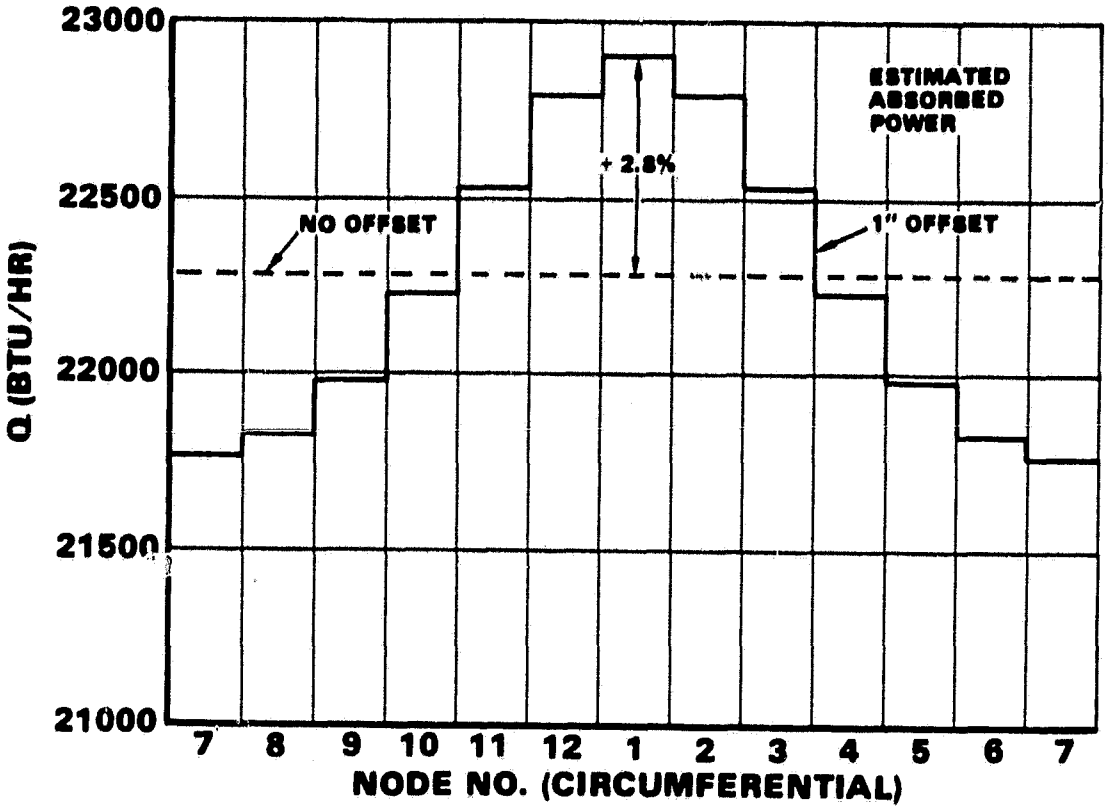

Figure 3-13. ABSR-Absorbed Power vs. Circumferential Nodes

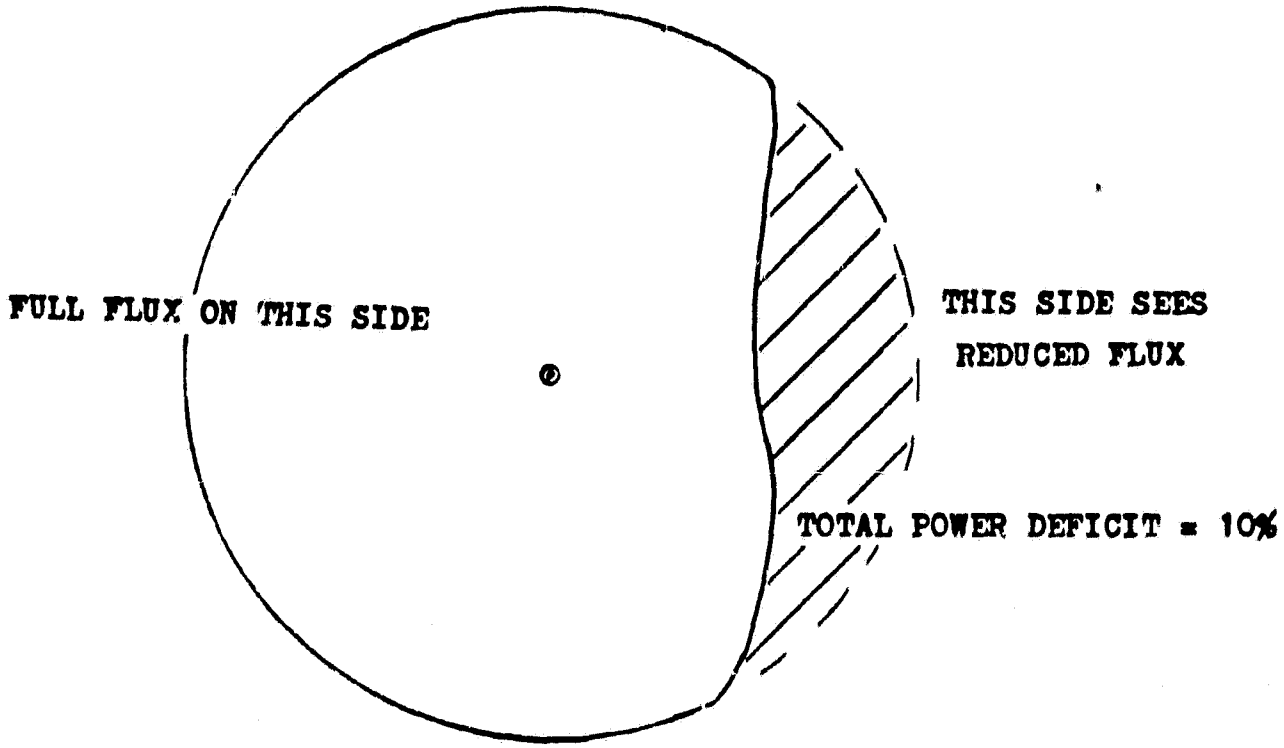

FLUX POLAR PLOT

Figure 3-14. Reduced Input from One-Half of Concentrator

TABLE 3-2

ABSR FLUX DISTRIBUTION VARIATION SENSITIVITY STUDY

TYPE OF FLUX VARIATION	CHANGE IN MAX. T_{WALL} (°F)	POSITION OF MAX. T_{WALL}	POSITION OF MAX. FLUX (IN. UP CYL.)	% INCREASE OF MAX. FLUX
BASELINE	0	TOP	9	0
AXIAL SHIFT 3"	20	TOP	12	0
AXIAL SHIFT 6"	47		15	
1 INCH RADIAL OFFSET	20	TOP, SIDE CLOSEST TO FOCAL PT.	8 SIDE CLOSEST TO FOCAL PT.	11
DISTORTED FLUX 10% POWER LOSS	58	TOP, SIDE WITH NO FLUX DECREASE	9 SIDE WITH NO FLUX DECREASE	0

S-42348

requirements for the outer diameter of the receiver housing. However, it has been determined that the inlet duct can be redesigned to substantially reduce the pressure loss, and still meet the interface requirements.

3.2 STRUCTURAL ANALYSIS

The structural analysis of the ABSR during Phase II studied pressure, thermal, and inertial loads on the receiver and predicted the life of the unit. The solar receiver unit was designed to withstand normal operational test pressures, temperatures, and environmental conditions. The specifications in design requirements are outlined in Exhibit II of the Phase II contract. Normal operational conditions include wind conditions of 30-mph steady-state, with 20-percent gust factor; temperature and humidity extremes (0° to 125°F and 0 to 100 percent, respectively); blowing dust; and altitude conditions of 0 to 6000 ft. In addition, survival environmental conditions such as 100-mph winds, seismic lateral loads, and snow and ice loads were considered. Codes and standards such as the ASME Boiler and Pressure Vessel Code as well as the Safety Regulations of the California Occupational Safety and Health Administration are also recognized. Positive margins of safety were calulcated for short-term internal pressure stress only. The primary loads analyzed were the internal pressure load of 23 psig, the thermal load associated with the 85 kwth input, and the non-operating inertial load of 3 g's. Realistic combinations of the first two load conditions were made to determine the stresses that would cause cumulative fatigue and creep damage to the unit in operation. In actual service, the unit must withstand both steady-state and transient thermal-pressure loadings, combined with the environmental loads under normal and surviving conditions. The predicted prototype life of the ABSR under those conditions was predicted to be 10,000 hours of operation, approximately 2 years, and 1500 cycles. Table 3-3 summarizes the structural analysis performed by AiResearch on the ABSR. Cycle fatigue was determined to be more restrictive to the ABSR life than creep strength limitations.

3.2.1 Internal Pressure and Thermal Load Analysis

Several computer models were used throughout the structural analysis of the ABSR. A small computer model was set up to determine pressure stresses in the components of the heat exchanger part of the unit, the outer skin, the intermittent inner skin, the fins and the longitudinal closing channels. The model included a 10° arc of the unit, 1-in. long in the axial direction. The finite element, structural computer program STRUDL was used in the analysis. Further, a detailed hand analysis was performed on the manifold and the pressure bearing structure around it. Margins of safety for all pressure stresses were calculated and found positive both for operating and proof conditions. Figure 3-15 shows the model of the cross section analyzed, and the corresponding local stresses due to internal pressure. This model is a beam construction simulating the fin and shell configuration of the receiver core. The stresses correspond to direct, bending and maximum stresses. In order to determine the effects of the thermal input, a large computer model was set up. The model included a 10° arc of the unit, and the entire length from manifold to manifold. The three dimensional, finite element, structural computer program ANSYS was used in the analysis. Steady state temperatures as shown on Figure 3-16 were input as thermal loads. Transient temperatures, expected to be less severe on

TABLE 3-3

ABSR FINAL STRUCTURAL EVALUATION AND ANALYSIS

• **INTERNAL PRESSURE LOAD ANALYSIS:**	**FIN AND SHELL (STRUDL)** **MANIFOLD (OUTLET)** **MANIFOLD SHELL INTERFACE** **STRUCTURE UNDER MANIFOLD**
• **THERMAL LOAD ANALYSIS:**	**LARGE COMPUTER MODEL, 10° ARC OF CORE (ANSYS)** **LCF (AIRESEARCH x0875)**
• **INERTIA LOAD ANALYSIS:**	**CORE AND SUPPORT TUBE INTERFACE** **CASING**

8-4240b

INTERNAL PRESSURE ANALYSIS (23 PSIG)

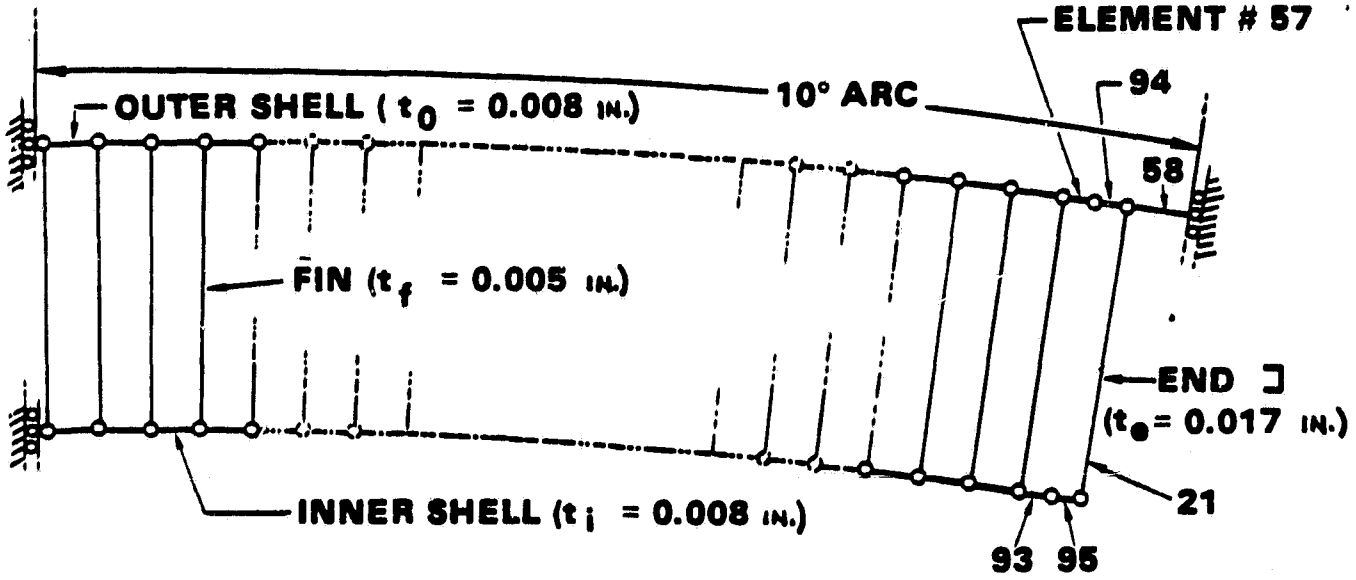

ELEMENT	DIRECT STRESS (KSI)	BENDING STRESS (KSI)	MAX. STRESS (KSI)
57	0.72	11.62	12.33
94	0.20	3.20	3.40
93	0.45	4.87	5.32
95	0.20	3.17	3.37
21	0.28	9.43	9.72
58	0	0.62	0.62

S-42614

Figure 3-15. Computer Model of Solar Receiver Core Section

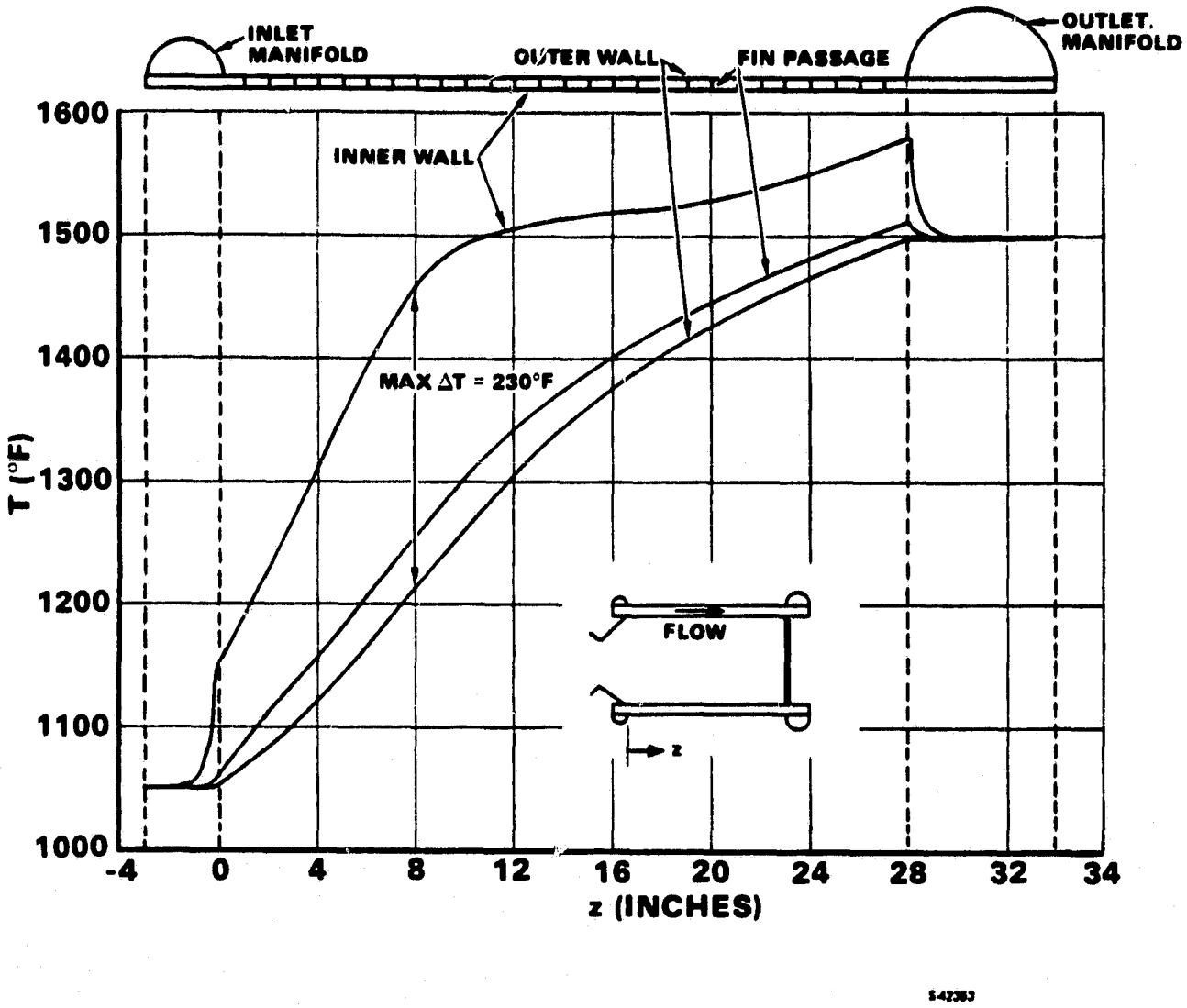

Figure 3-16. Baseline Temperature Distribution

the unit, were therefore not examined any further. Computer output shows the highest stresses at the location where the largest ΔT occurs between the inner and outer skin.

Figure 3-17 represents the finite element computer model of the solar receiver core, and Figure 3-18 shows a closeup of a core detail.

The thermal stresses were combined with the pressure stresses in order to determine the overall stress levels in the receiver due to thermal and pressure loads. The resultant Von Mises stresses were found to be 27.12 ksi at 1460°F on the inner skin, near the longitudinal segment enclosure channel. The major component of this stress is compression in the axial direction, 20.73 ksi. Although the resultant stress is lower than the elastic limit of the material, a low cycle fatigue analysis was performed because of potential creep due to the high temperatures. Results show that the major damage (life consumption) occurs during the initial creep relaxation in the first few cycles. The expected life of the unit is in excess of 6000 cycles, which is much higher than the requirement of 1500 cycles. Thermal stresses are much lower toward both ends of the heat exchanger, and temperatures rise to approximately 1500°F toward the exit manifold. Pressure induced stresses at this location are 12.33 ksi in the outer skin. If the shape of the outer skin remains circular, creep damage may cause the unit to fall short of its life requirement. However a slight bulging will relieve the 12.33 ksi stress to a much lower stress level and thus the life is expected to meet the requirement.

3.2.2 Life Prediction

In the areas where the calculated transient stresses obtained with an elastic stress analysis exceed the yield strength of the material, fatigue life must be predicted. AiResearch uses the latest, state-of-the-art, elastic-plastic analysis to make these calculations. The Wetzel-Morrow method, employing Neuber hyperbolas, is used to establish the stabilized total cyclic strain range; this strain range is input to the Manson-Coffin equation to predict the cyclic life. Some of the details involved in this method, computerized and thoroughly checked out by AiResearch (digital program X0870), are shown in Figure 3-19.

To ascertain the effects of cumulative fatigue and creep damage, the intensity, duration, and frequency of the various imposed loadings are established. The number of cycles to failure and the time to failure at a given stress condition are calculated; the two effects are then combined for any number of load conditions by using a linear damage function law (such as the Miner-Palmgren rule) where

$$\sum_{i=1}^{n} = \frac{N_i \text{ actual}}{N_i \text{ predicted}} + \frac{T_i \text{ actual}}{T_i \text{ predicted, creep}} \leq 1.0$$

Initiation of a crack is imminent when this sum approaches unity. It should be noted that initiation of a crack does not necessarily mean failure, but it could cause some leakage. This would most probably be a small percentage of the total mass flow.

10° ARC

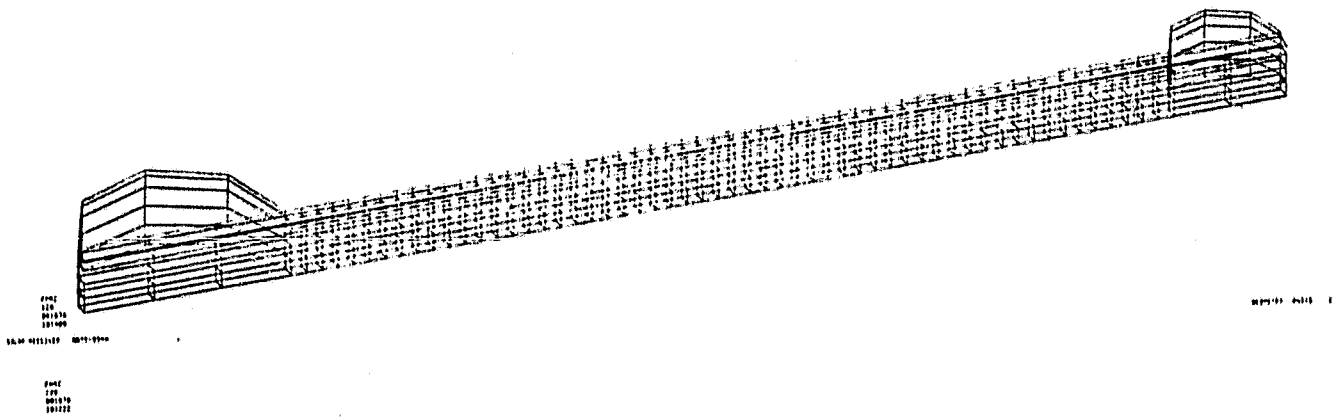

S-42405-A

Figure 3-17. Finite Element Computer Model of Solar Receiver Core

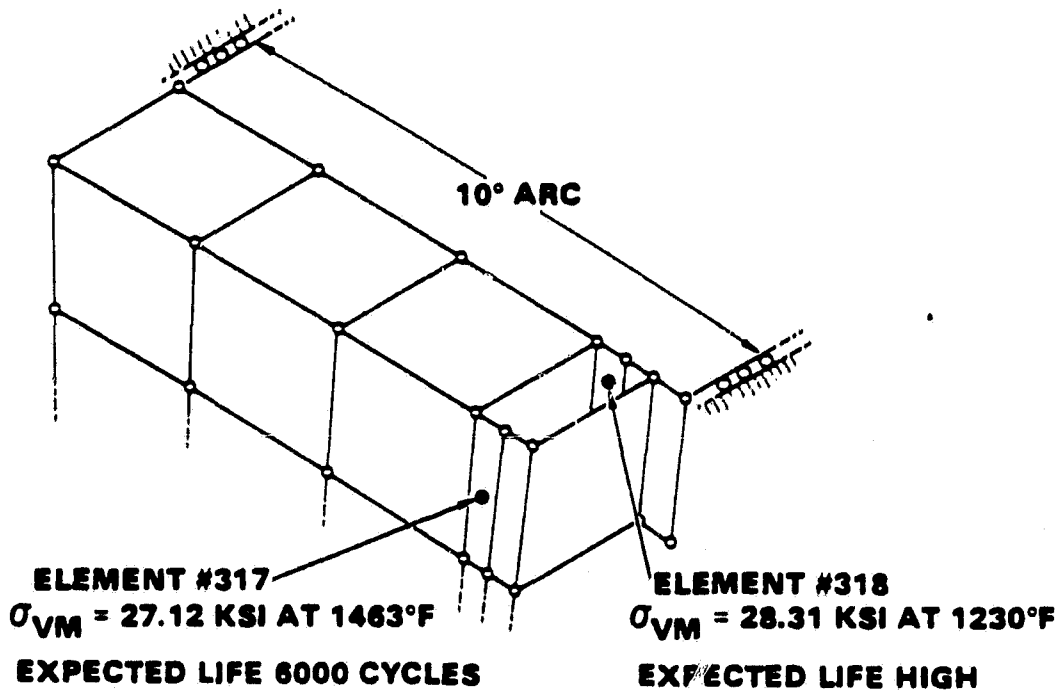

Figure 3-18. Computer Model Detail

PREDICTION OF UNIT LIFE FROM LEVELS OF APPARENT ELASTIC STRESS REACHED DURING TRANSIENT LOADINGS (AIRESEARCH COMPUTER PROGRAM X0870)

- WETZEL-MORROW ELASTIC-PLASTIC ANALYSIS USING NEUBER HYPERBOLAS TO OBTAIN STABILIZED CYCLIC STRAIN RANGE.
- NUMBER OF CYCLES TO CRACK INITIATION OBTAINED USING MANSON-HIRSCHBERG EQUATION OR MODIFIED MANSON-COFFIN EQUATION.

$$\epsilon_{TOT} = 3.5 \frac{\sigma'_f}{E N_f^{0.12}} + \frac{(\epsilon'_f)^{0.6}}{N_f^{0.6}} \quad \cdots$$

WHERE σ'_{f_1} = TRUE ULT. FAILURE STRESS

ϵ'_{f_1} = FAILURE STRAIN

} FROM PULL TEST

n = STRAIN HARDENING EXPONENT

- ACCUMULATIVE FATIGUE DAMAGE. (MINER-PALMGREN RULE)

$$\sum_{i=1}^{p} = \frac{N_i \text{ ACTUAL}}{N_i \text{ PREDICTED, FATIGUE}} \leq 1.0$$

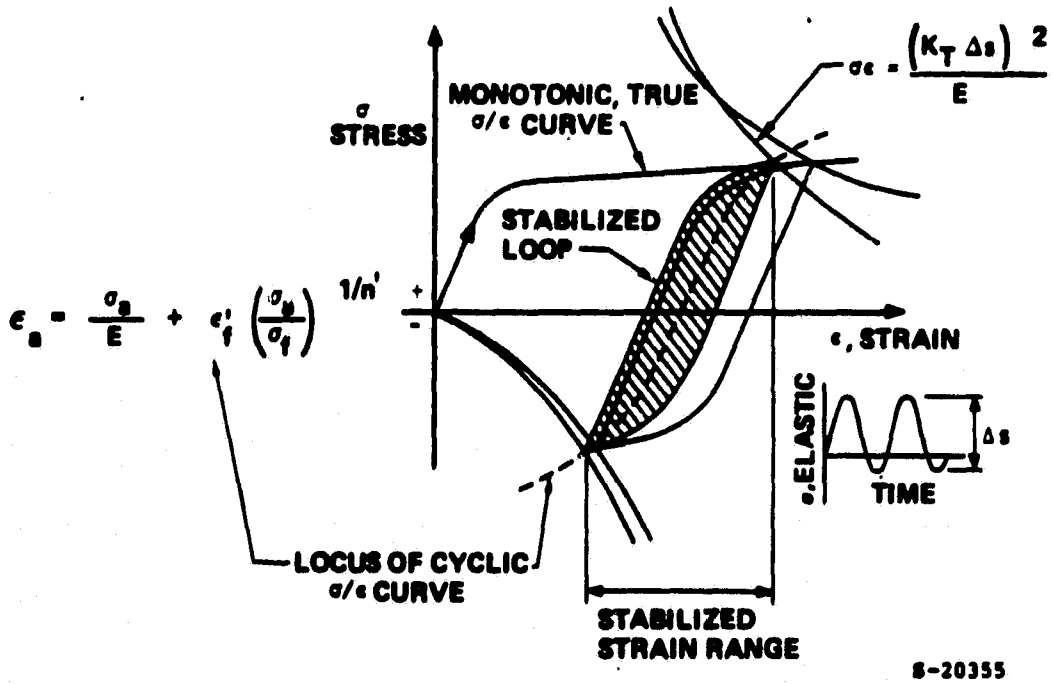

Figure 3-19. Low-Cycle Fatigue Analysis

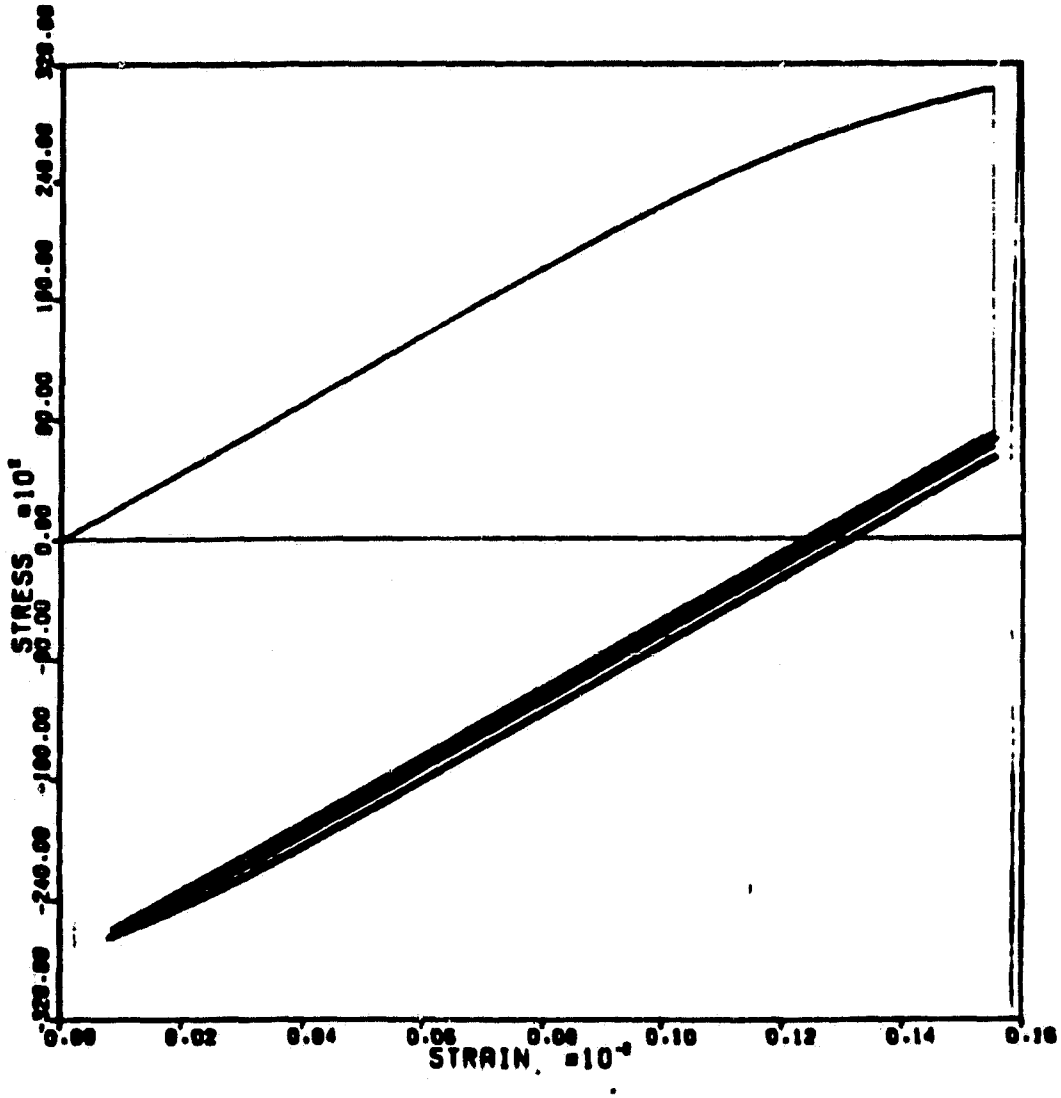

Figure 3-20. Life Cycle Fatigue Analysis Plot for the ABSR

The life cycle fatigue plot for the ABSR is shown in Figure 3-20. The expected life of the receiver is approximately 2 years, 10,000 hours and 1500 cycles.

3.2.3 Inertial Load Analysis

Analysis of the solar receiver housing assembly, including the core mounting structure, consisted of studying a 3 g shock load condition. Hot section rings and longitudinal stiffeners were added to the outer cylindrical shell to resist potential buckling at areas of concentrated loads. The interface between the support tubes and the heat exchanger (core support cross key) was analyzed in detail. A 5 g static loading was applied to account for the response in the 3 g input shock testing. Positive margins of safety were calculated for all components at this interface. Figure 2-21 shows the margins of safety for the major load points of the assembly. The margins of safety are good and indicate that the ABSR will have an acceptable tolerance for mechanical loads.

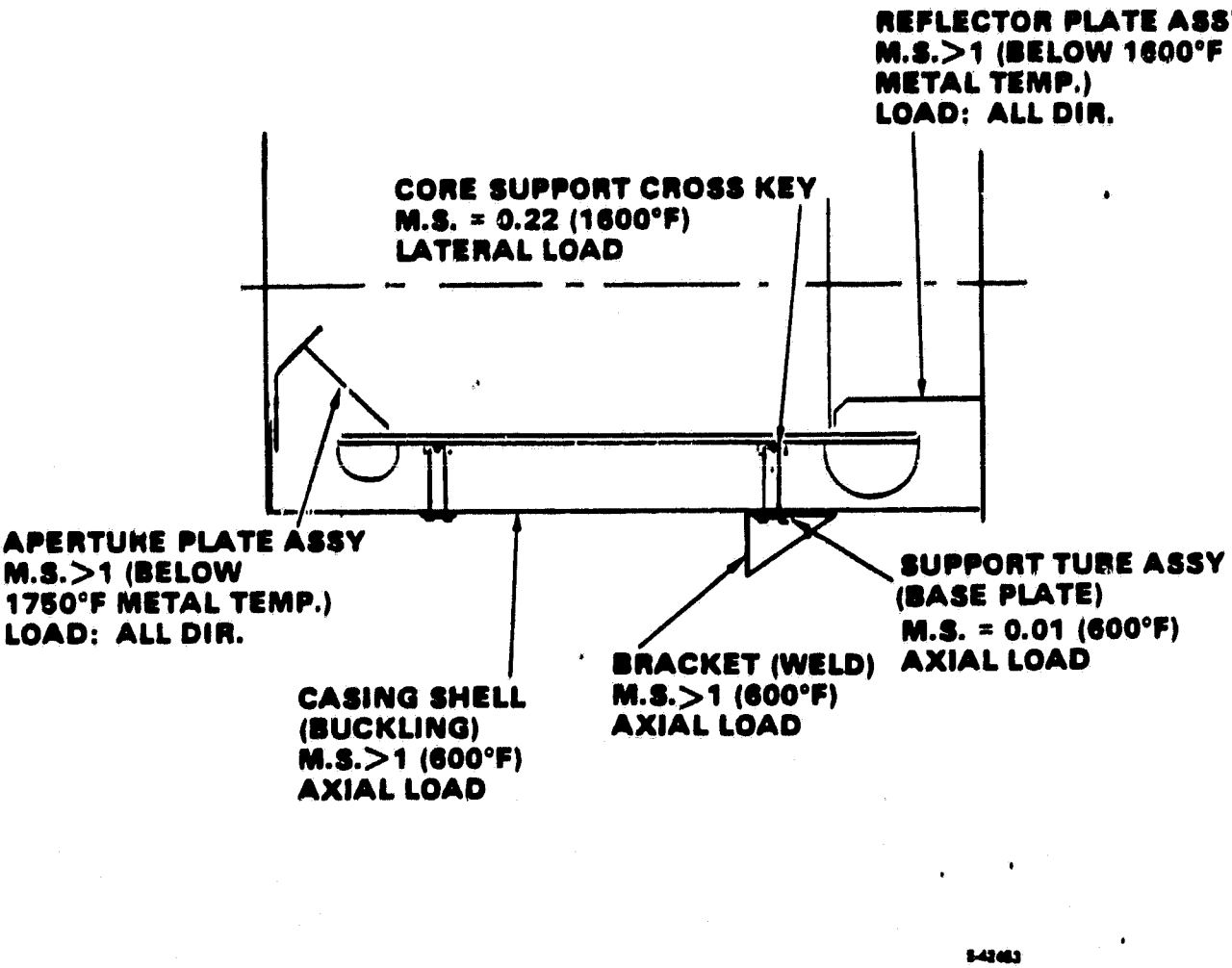

Figure 3-21. ABSR Inertia Load Analysis

4. ABSR FABRICATION

Fabrication efforts on the Air Brayton Solar Receiver commenced once the final design was completed. Two complete units were fabricated. The three sub-assemblies of the receiver (the brazed core, the aperture assembly, and the reflector plate assembly) bolt individually onto the outer housing. Since these sub-assemblies are not connected to each other, the individual assemblies can grow at different rates without interference. This also allows greater accessibility to the aperture and reflector plate components.

In order to form the heat exchanger, toroidal inlet and outlet manifolds and ducts had to be welded to the cylindrical core assembly.

Final assembly of the ABSR occurs in three stages.

(a) The complete heat exchanger assembly is wrapped in insulation, slipped inside of, and attached to, the outer housing. This is done via eight radial tubular supports. The tubes are fixed to the receiver enclosure, extend radially inwards toward the receiver core, and are slotted at the other end. Longitudinal and intersecting (in the form of cross) keys are located on the receiver core and mate the slot at the support tube end. The longitudinal keys allow for radial and longitudinal growth of the receiver. The intersecting keys restrain the core from longitudinal and lateral motion while allowing radial growth.

(b) The aperture plate assembly is bolted to the aperture end of the outer shell.

(c) The reflector plate assembly is bolted to the other end of the outer shell. The inlet and outlet ducts are guided through holes in the rear outer shell of the reflector plate assembly.

Insulation was filled in all gaps in the receiver as the final assembly progressed.

Connection to the solar concentrator is made by means of a mounting ring with six mount points.

Figure 4-1 through 4-4 show the various stages of fabrication, and Figure 4-5 represents the ABSR final assembly.

The materials used in the fabrication of the ABSR, as well as the general dimensions and parts that constitute the unit, are referred to in Section 2 of this report (ABSR description) and in the detailed drawings of Appendix A.

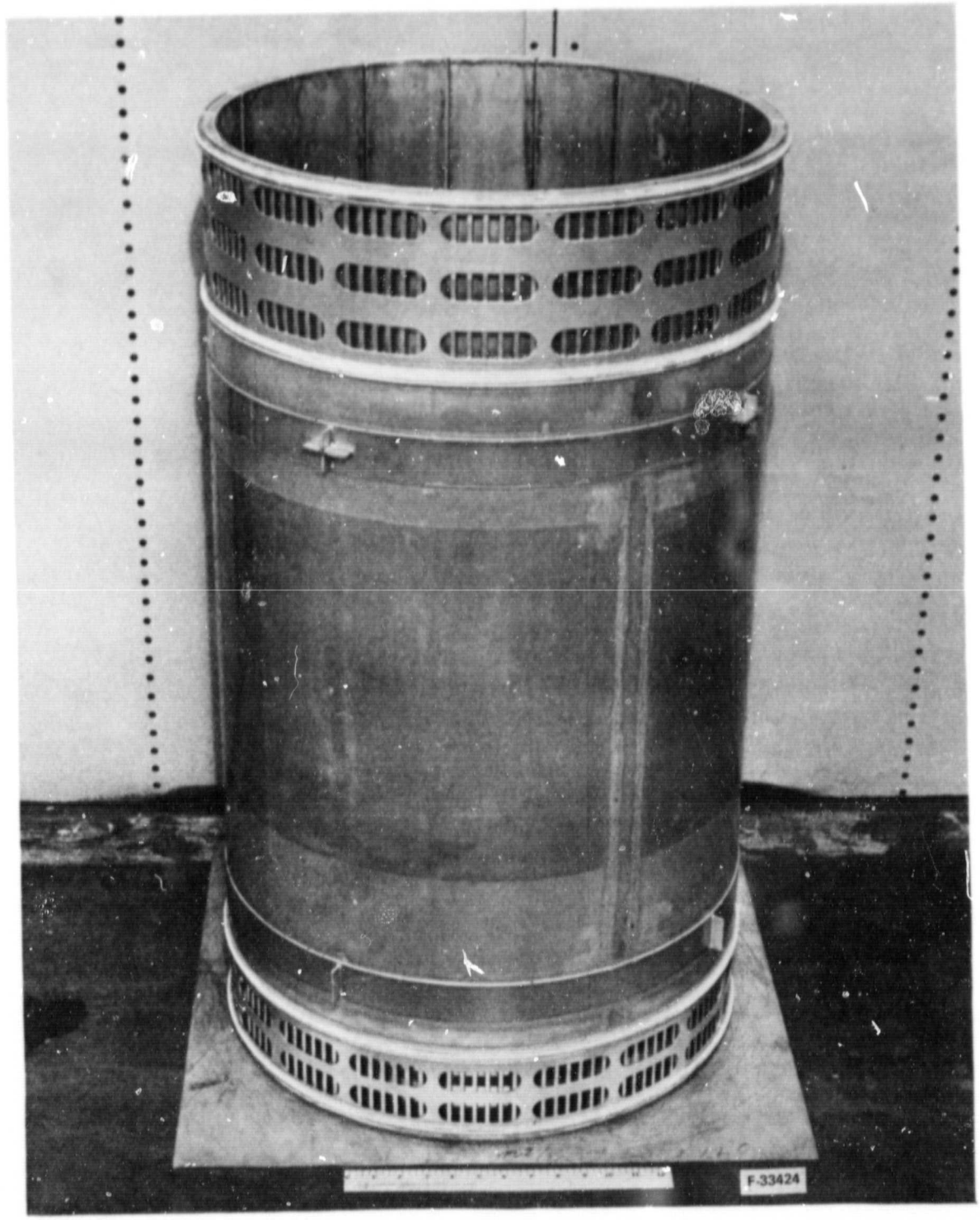

Figure 4-1. Brazed Cylindrical Core

Figure 4-2. Heat Exchanger Assembly

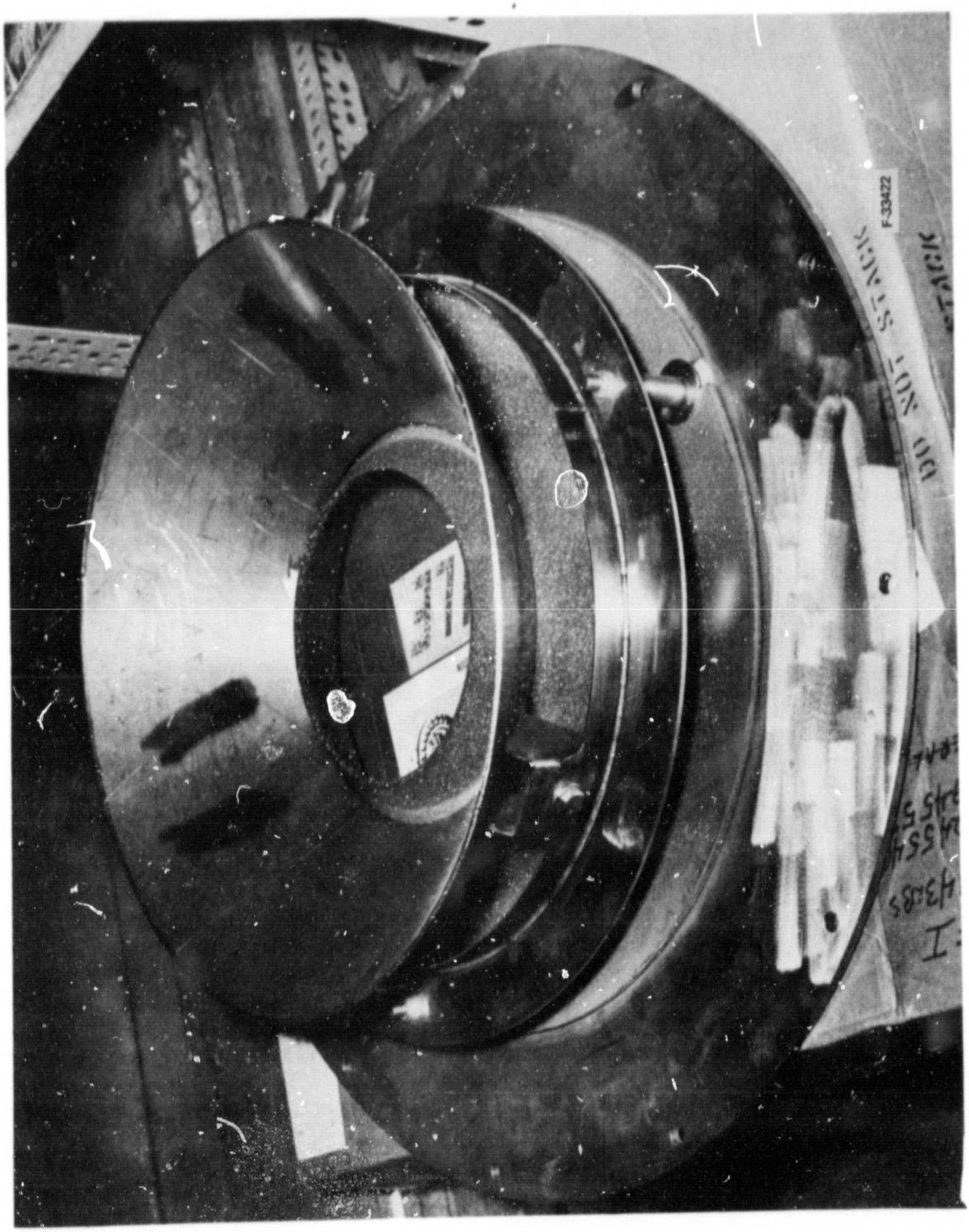

Figure 4-3. Aperture Assembly

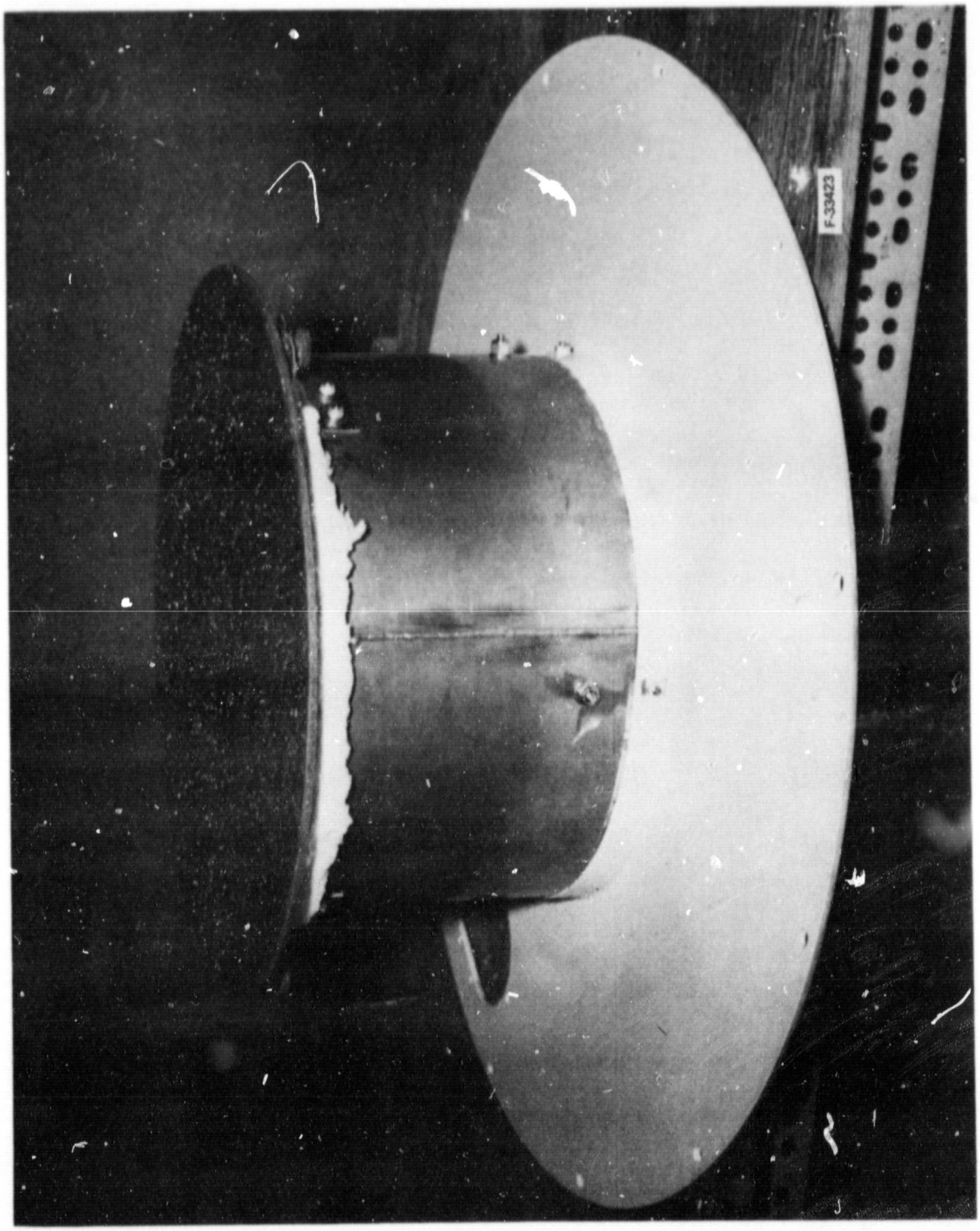

Figure 4-4. Reflector Plate Assembly

ORIGINAL PAGE
BLACK AND WHITE PHOTOGRAPH

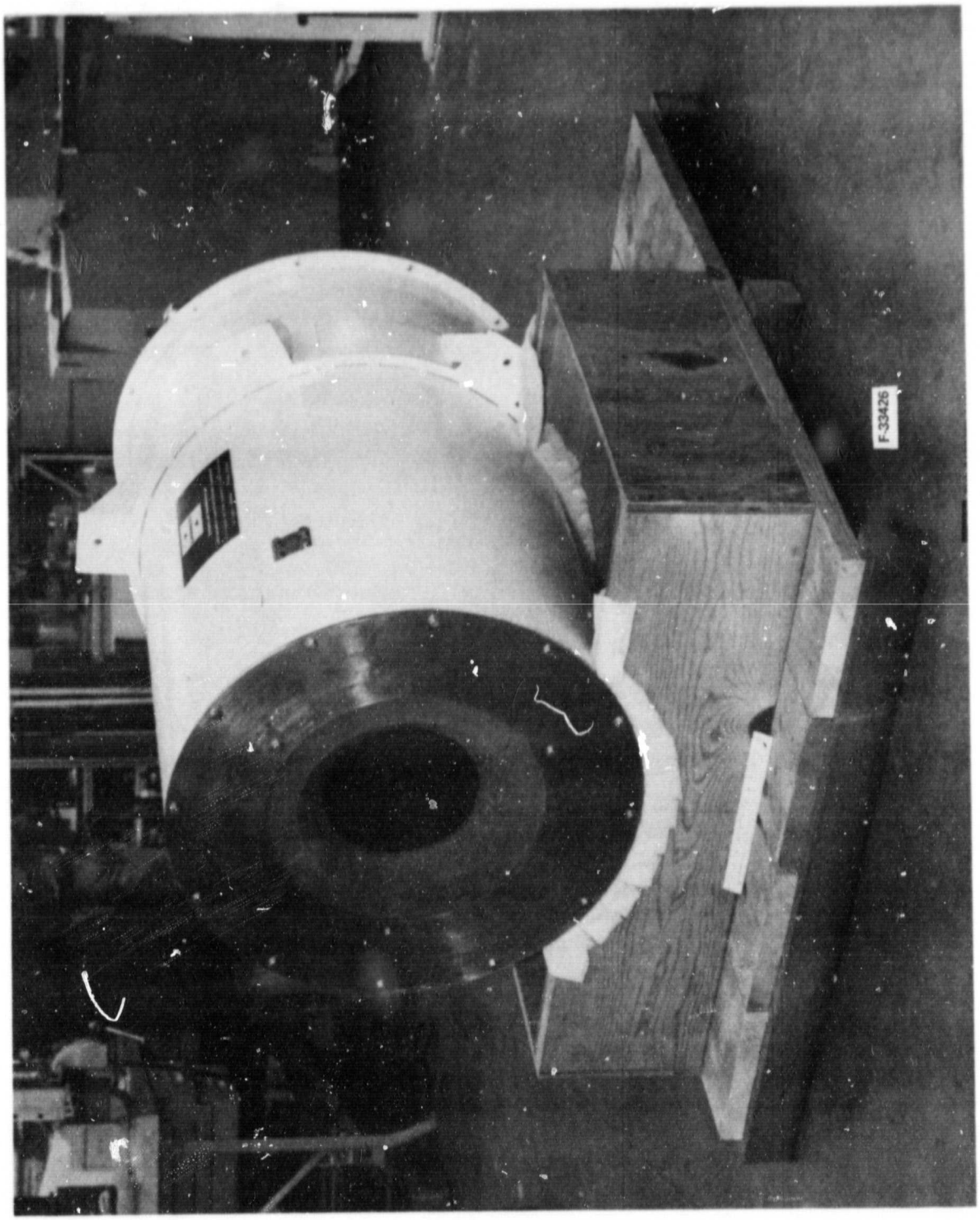

Figure 4-5. ABSR Final Assembly

5. ABSR TESTING PROCEDURES AND RESULTS

Acceptance tests were performed on the heat exchangers of the two Air Brayton Solar Receiver units. Tests were included for proof pressure, leakage, and pressure drop.

5.1 PROOF PRESSURE TEST

The proof pressure test consisted of applying a pneumatic pressure of 50 psig to the heat exchanger. To compensate for testing at room temperature, the pressure is higher than the design point pressure of 22 psig. The pressure in the system was held for 5 minutes. The units were observed at pressure for deformation. No permanent deformation was observed in either of the tested units.

5.2 LEAKAGE TEST

The leakage test measured the air mass flow rate leaking through the heat exchanger at various pressures. The first unit tested had a leakage rate of 5.73 lbm/min at 50 psig, whereas the second unit had a leakage rate of 0.25 lbm/min at the same pressure. The pressure decay test was also a measure of the leakage rate. The unit was pressurized to 50 psig, the air supply cut off, and the times to decay to various pressures were measured. This data was reduced to give a design point leakage rate of 3.5% for the first unit, and 0.2% for the second unit. Figure 5-1 shows the test set-up.

5.3 PRESSURE DROP TEST

This consisted of an isothermal (room temperature) pressure drop test that was performed by passing air through the heat exchangers at various flow rates, while measuring the inlet pressure and pressure difference across the units. See Figure 5-2.

The test results for the two heat exchangers are described in Tables 5-1 and 5-2. The first unit (S/N 1) had a measured pressure drop of 2.9 psi at the design flow rate of 0.57 lbm/sec. The second unit (S/N 2) showed a pressure drop of 3.5 psi at the same conditions. These values were significantly larger than the anticipated value of 0.92 psi for the design point. See Figure 5-3 for pressure distribution. The reason for the discrepancy was determined to be due to restrictions in the inlet duct. Section 3.1.5 of the ABSR thermal analysis discusses this finding.

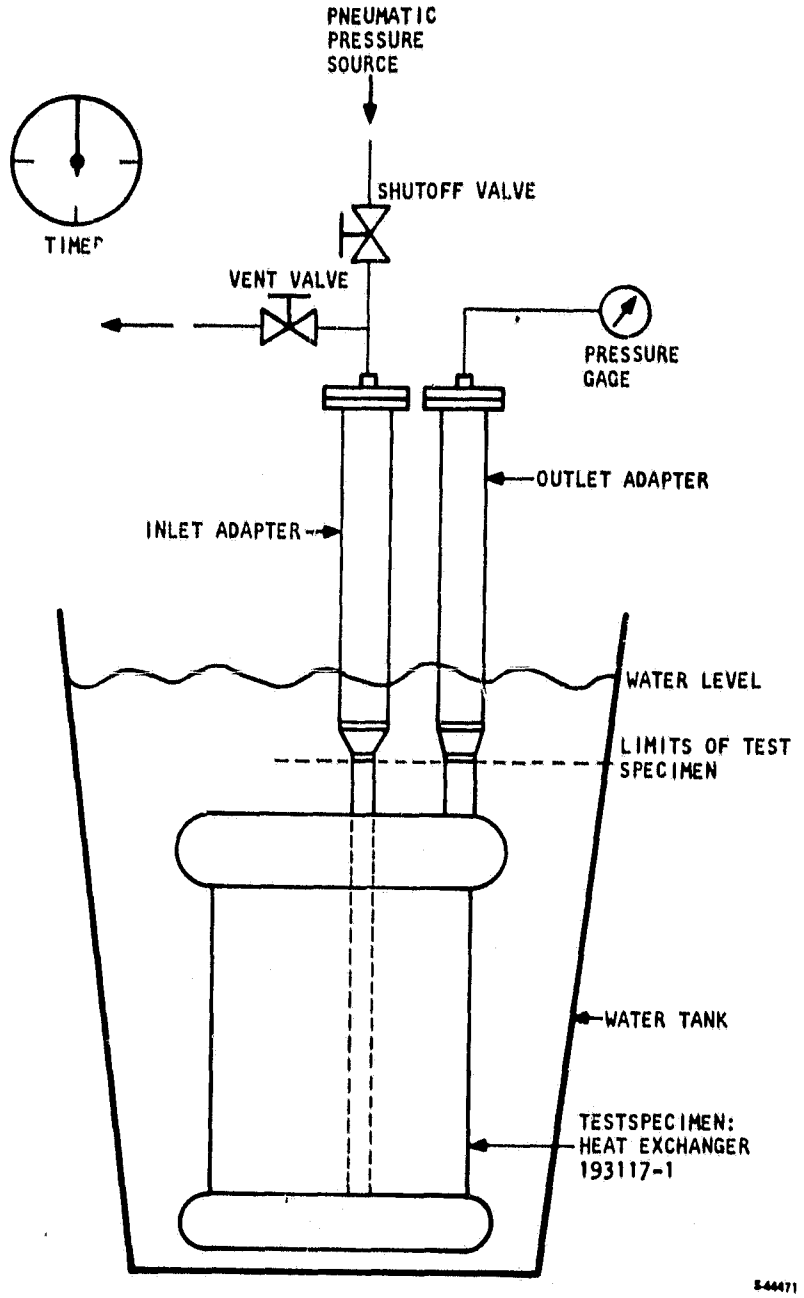

Figure 5-1. ABSR Leakage Test Setup

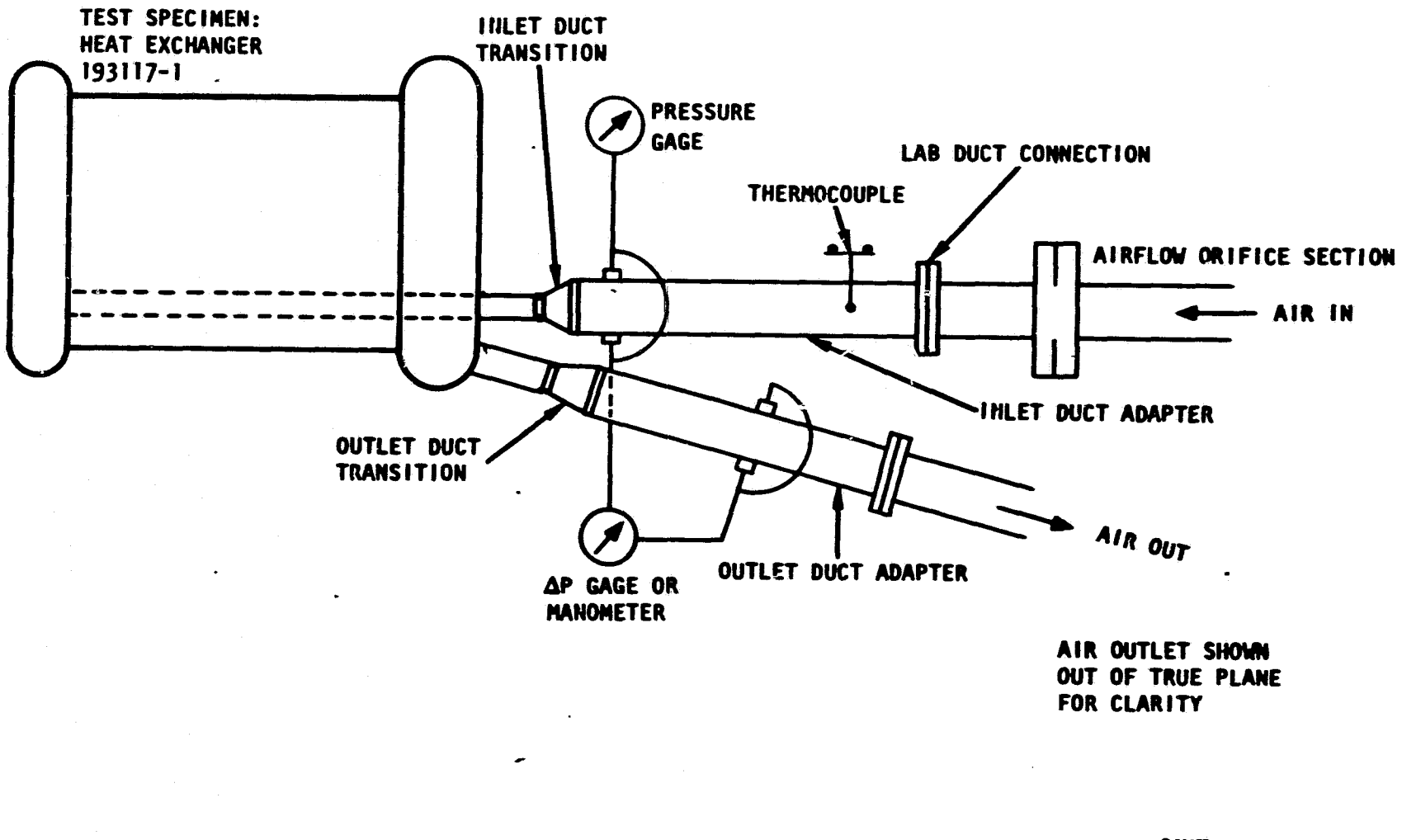

Figure 5-2. ABSR Pressure Drop Test Setup

TABLE 5-1

TEST RESULTS HEAT EXCHANGER S/N 1

FORM 61330A
AIRESEARCH MFG. CO.

HEAT TRANSFER LAB DATA SHEET

Page 1 of 1

EWO 3400-250561-03-0598 DATE 9/13/80 TEST PURPOSE AIR BRAYTON SOLAR RECEIVER – HEAT EXCHANGER, ISOTHERMAL PRESSURE DROP

P/N 194316/193117 BAROM 29.93 "Hg

S/N 1 TEMP 71.0°F TEST PERS. DON HARDING

	← HEAT EXCHANGER →								← ORIFICE DATA →							
	INLET PRESS PSIG	INLET TEMP °F	ΔP PSI	σ	σΔP PSI				STATIC PRESS "Hg A	ΔP "H2O	TEMP. °F	PIPE INCH	ORIF. SIDE INCH	σΔP "H2O	FLOW Lb/MIN	
NO.	1	2	3	4	5	6	7	8	9	10	11	12	13	14	15	REMARKS
1	0.69	72.2	0.659	1.026	0.674				32.0	12.0	71.0	8.0	.720	12.55	13.6	$\sigma = \frac{P_{AVE}}{P_{STD}} = \frac{P_{IN}}{P_{STD}}$
2	1.06	72.0	0.877	1.018	0.918				33.0	19.0	70.9	8.0	2.0	20.5	17.6	
3	1.82	71.8	1.46	1.009	1.598				35.0	34.5	70.7	8.0	2.0	36.09	23.4	
4	2.81	71.4	2.268	1.199	2.72				39.0	47.0	70.5	8.0	2.0	59.95	30.2	$\sigma = 0.084 (P_{IN} + P_{OUT})$
5	3.57	71.2	2.87	1.245	3.57				41.0	57.8	70.4	8.0	2.0	72.52	33.8	
6			2.90												34.2	$P_{STD} = 14.7$ PSIA
7																
8																P_{IN}, P_{OUT} → PSIA
9																
10																
11																
12			0.92 ←												34.2	← ESTIMATED THEORETICAL TOTAL PRESS. DROP FOR: $\dot{m} = 34.2$ LB/MIN, $P_{IN} = 36.7$ PSIA
13																
14																
15																
16																
17																
18																
19																
20																
21																

TABLE 5-2

TEST RESULTS HEAT EXCHANGER S/N 2

FORM 61830A
AiResearch Mfg. Co.

HEAT TRANSFER LAB DATA SHEET

Page 1 of 1

EWO 3400-25051-02-0397 DATE 11/22/80 TEST PURPOSE AIR BRAYTON SOLAR RECEIVER – HEAT EXCHANGER, ISOTHERMAL PRESSURE DROP

P/N 19431 6 / 19317 BAROM 29.9 "Hg

S/N 2 TEMP 67.0°F TEST PERS. EDMONDS

	← HEAT EXCHANGER →								← ORIFICE DATA →							
	INLET PRESS PSIG	INLET TEMP. °F	ΔP PSI	σ	σΔP PSI				STATIC PRESS "H2O	ΔP "H2O	TEMP °F	TYPE INCH.	ORIF. SIZE INCH	σΔP "H2O	FLOW LB/MIN	
NO.	1	2	3	4	5	6	7	8	9	10	11	12	13	14	15	REMARKS
1	0.64	627	0.532	1014	0.539				31.5	9.10	68.0	8.0	2.0	9.42	12.40	$\sigma = \frac{P_{AVE}}{P_{STD}} - \frac{P_{AVE}}{P_{STD}}$
2	0.90	626	0.756	1.020	0.771				32.5	12.90	67.8	8.0	2.0	13.78	14.50	
3	1.28	624	1.08	1.037	1.12				34.0	18.40	67.5	8.0	2.0	20.58	17.70	
4	2.00	621	1.67	1.065	1.78				36.0	27.70	67.2	8.0	2.0	32.62	22.20	$\sigma = 0.034\ (P_{IN} + P_{OUT})$
5	2.98	620	2.48	1.105	2.74				38.5	39.60	67.0	8.0	2.0	52.19	27.30	
6	3.50	66.7	2.88	1.126	3.24				40.5	45.90	66.7	8.0	2.0	60.57	30.0	$P_{STD} = 14.7$ PSIA
7			3.50												34.2	
8																P_{IN}, $P_{OUT} \rightarrow$ PSIA
9																
10																
11			0.92 ←												34.2	← ESTIMATED THEORETICAL
12																TOTAL PRESS. DROP
13																FOR:
14																$\dot{m} = 34.2$ LB/MIN
15																$P_{IN} = 36.7$ PSIA
16																
17																
18																
19																
20																
21																

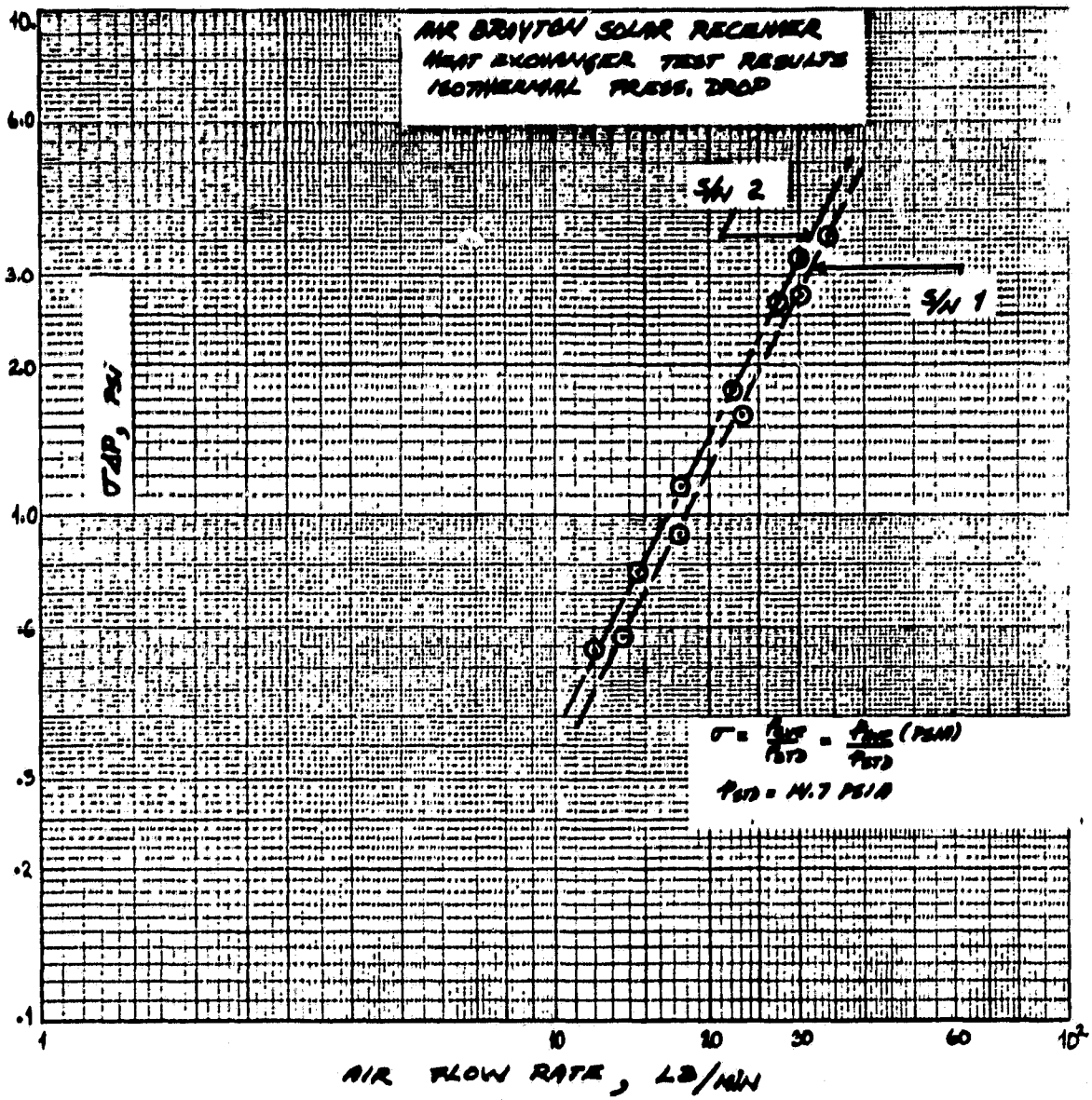

Figure 5-3. Isothermal Pressure Drop, Heat Exchangers S/N 1 and S/N 2.

APPENDIX A

AIR BRAYTON SOLAR RECEIVER

DETAIL DESIGN DRAWINGS

DETAIL DRAWINGS

Drawing No.	Name
193090	Core Assy
193091	Outer Shell
193105	Outer Case Assy
193117	Heat Exchanger
194316	Receiver Outline
194317	Receiver Assy

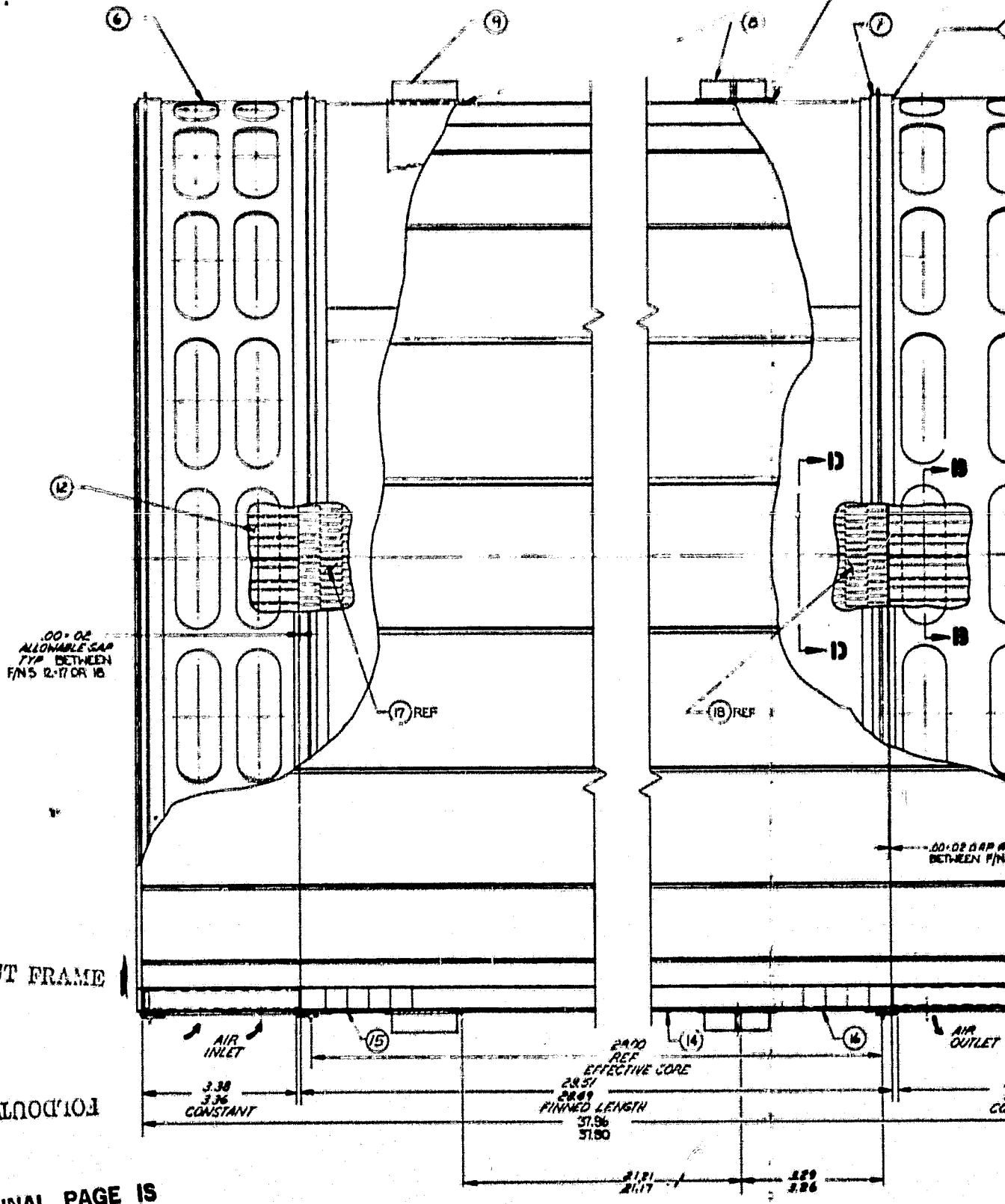

FOLDOUT FRAME

ORIGINAL PAGE IS
OF POOR QUALITY

ORIGINAL PAGE IS
OF POOR QUALITY

PRINTOUT FRAME 2

198090

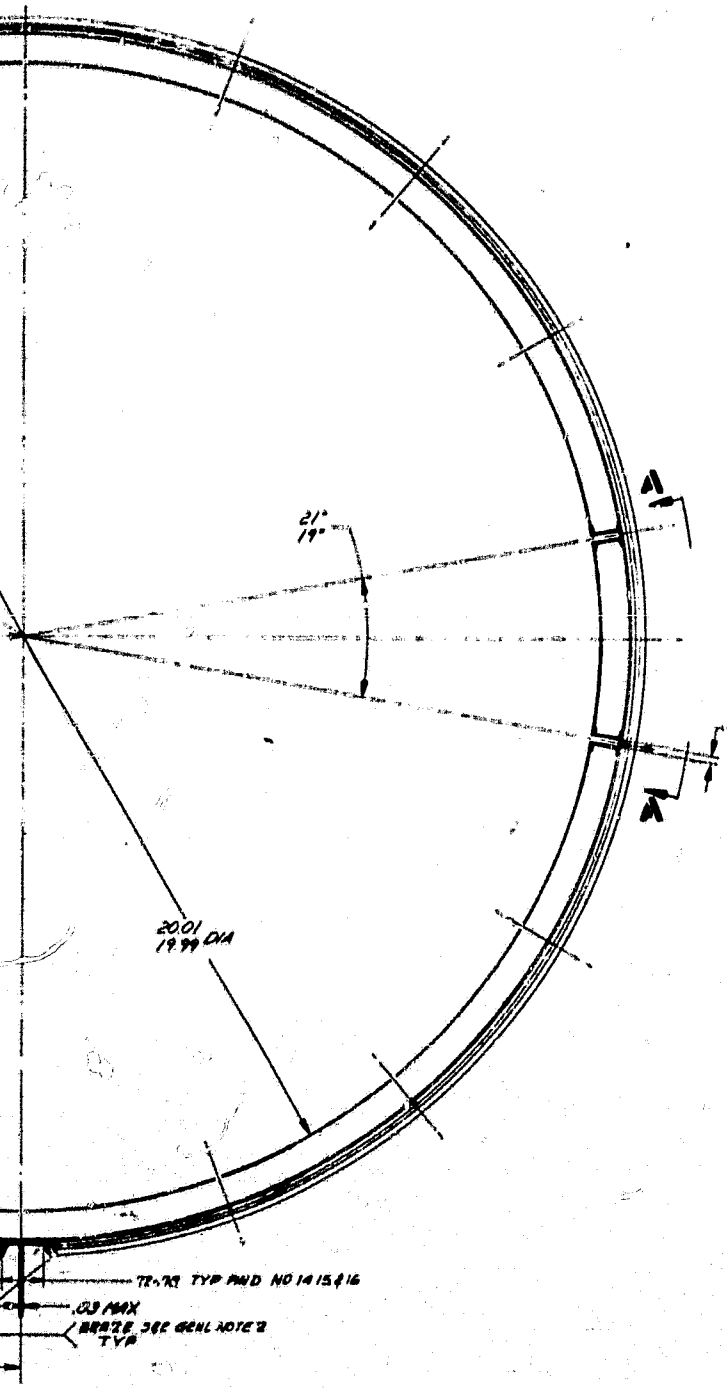

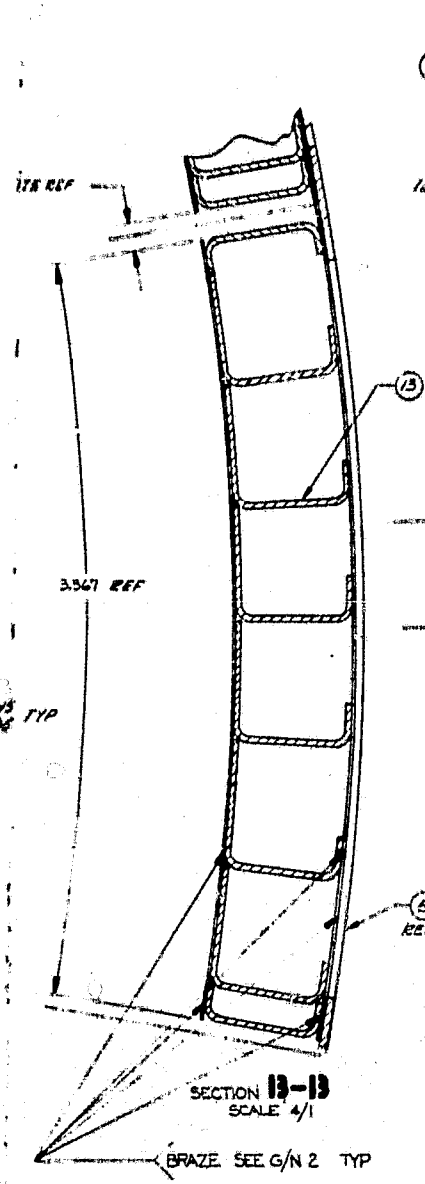

SECTION B-B
SCALE 4/1

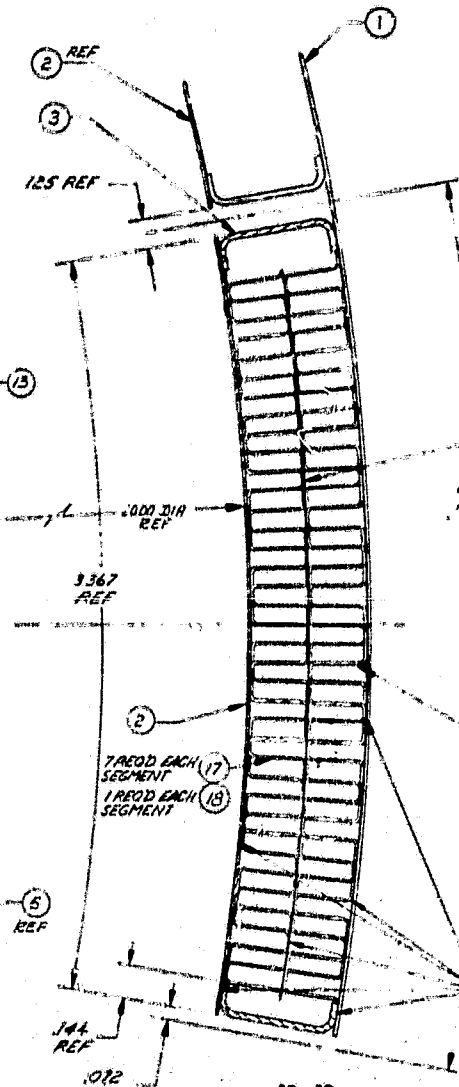

SECTION D-D
SCALE 4/1

FOLDOUT FRAME 3

SEE SEPARATE PA
AND GENERAL NO

ORIGINAL PAGE IS
OF POOR QUALITY

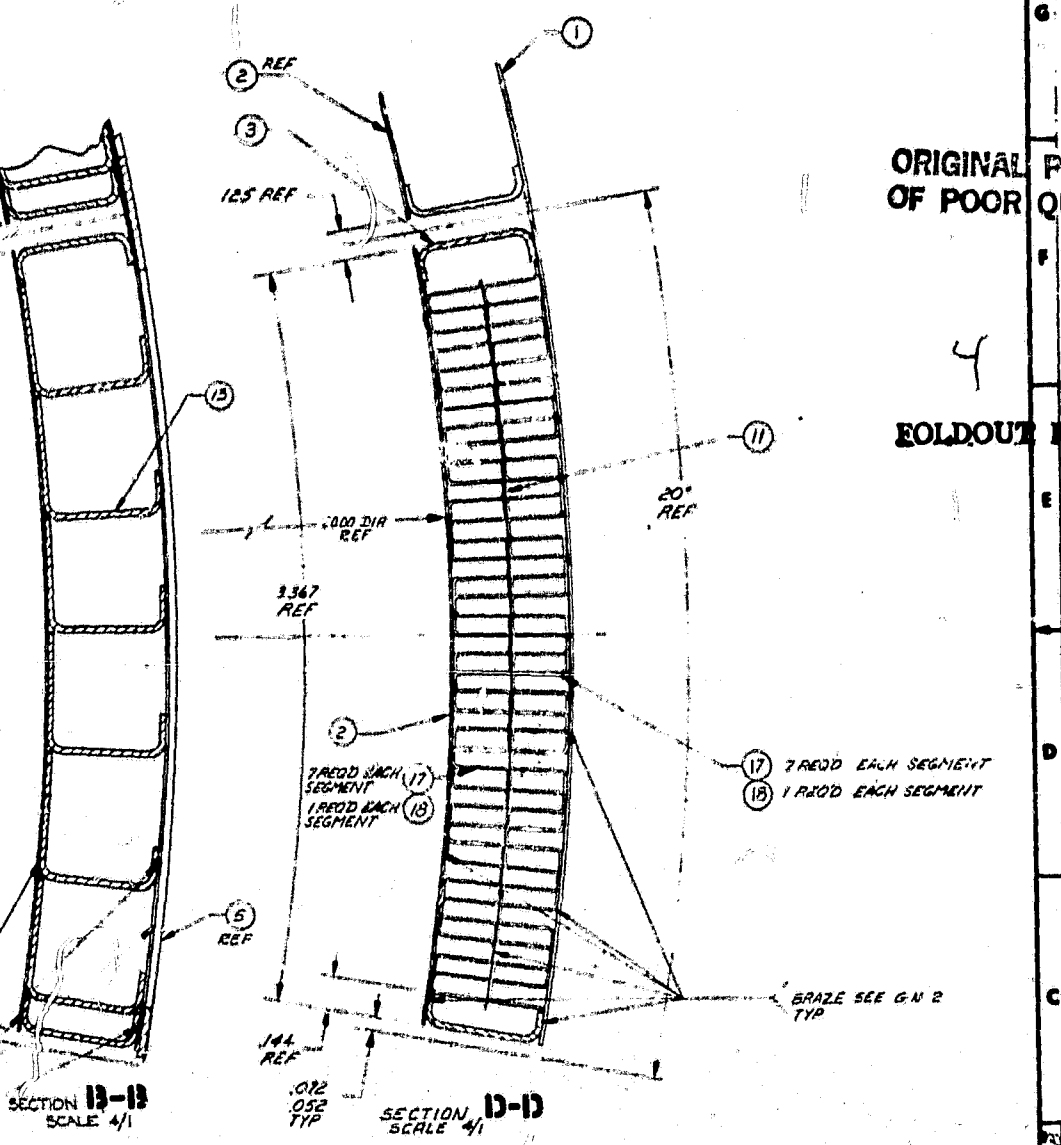

RAZE SEE G/N 2 TYP

ORIGINAL PAGE IS
OF POOR QUALITY

4

FOLDOUT FRAME

FOLDOUT FRAME 3

SEE SEPARATE PARTS LIST FOR REQUIRED ITEMS AND GENERAL NOTES

CORE ASS'Y, SOLAR RECEIVER PANEL

J 70210 193090

APPLICATION

3 2 1

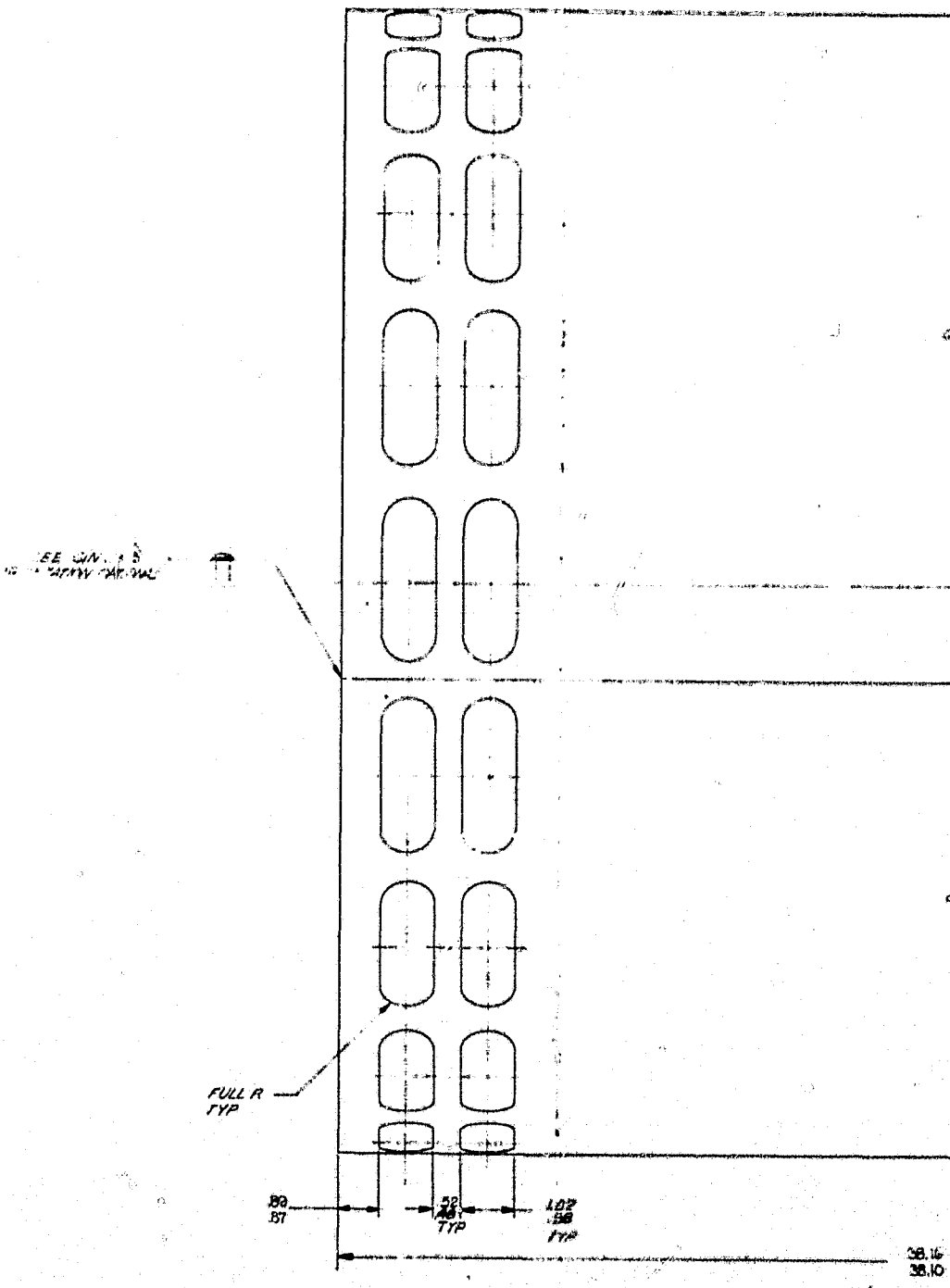

FOLDOUT FRAME

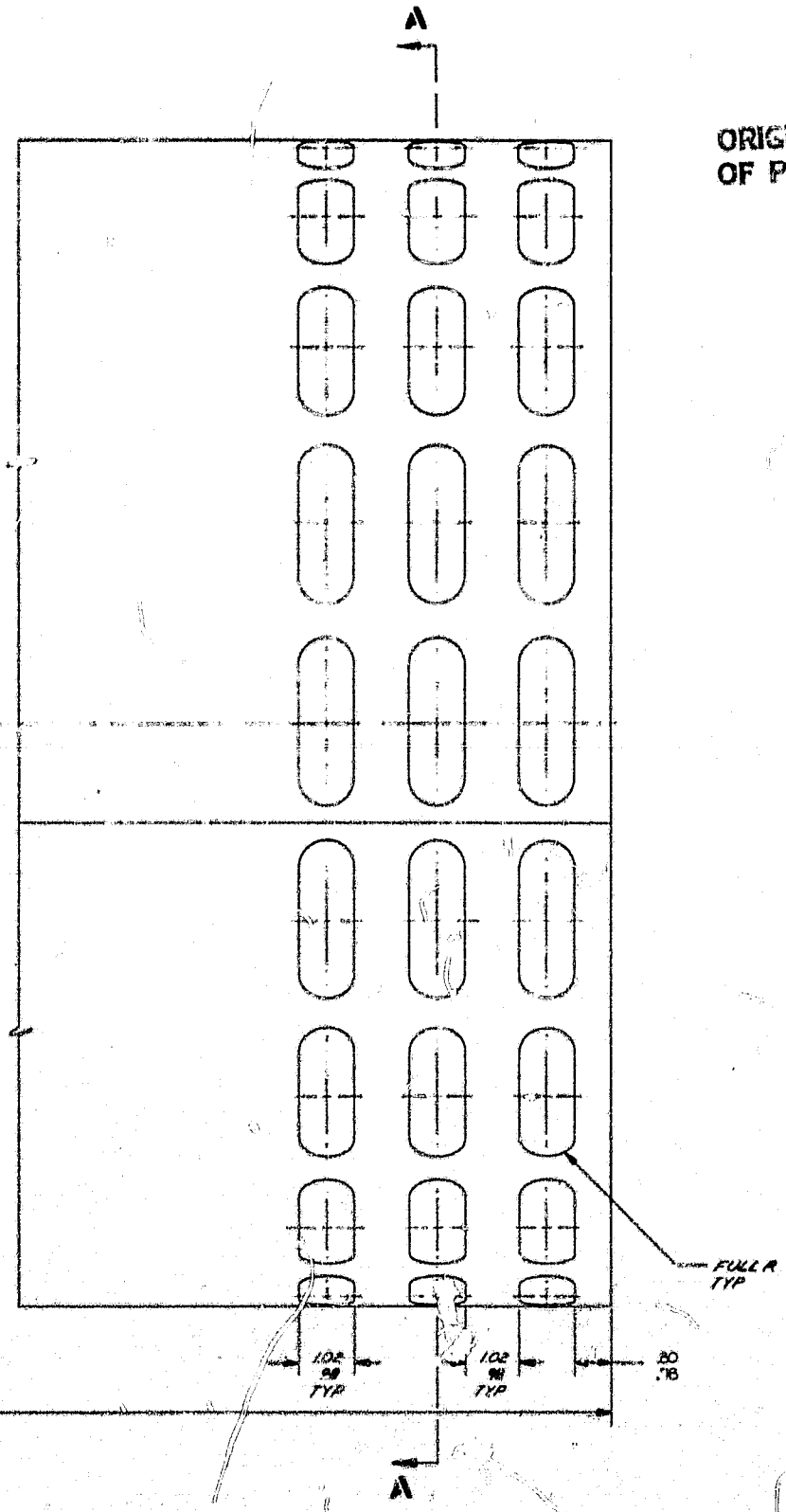

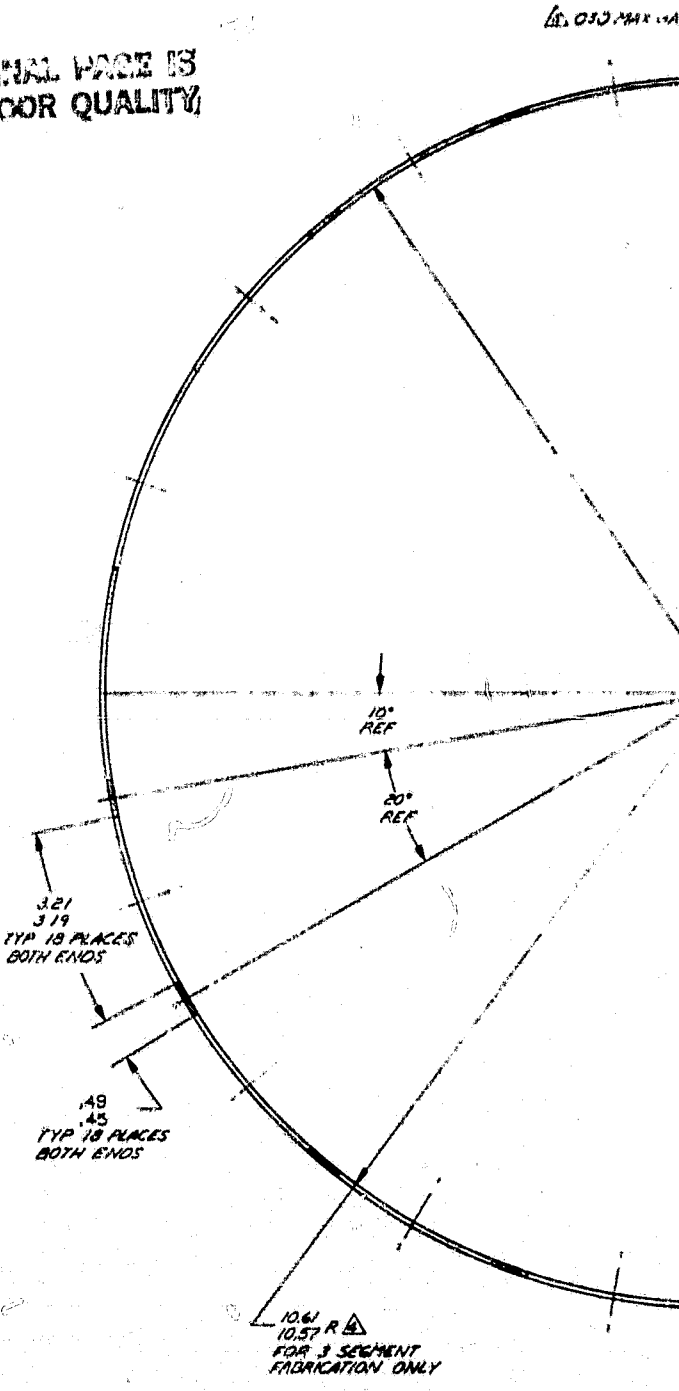

FOLDOUT FRAME 2

193091

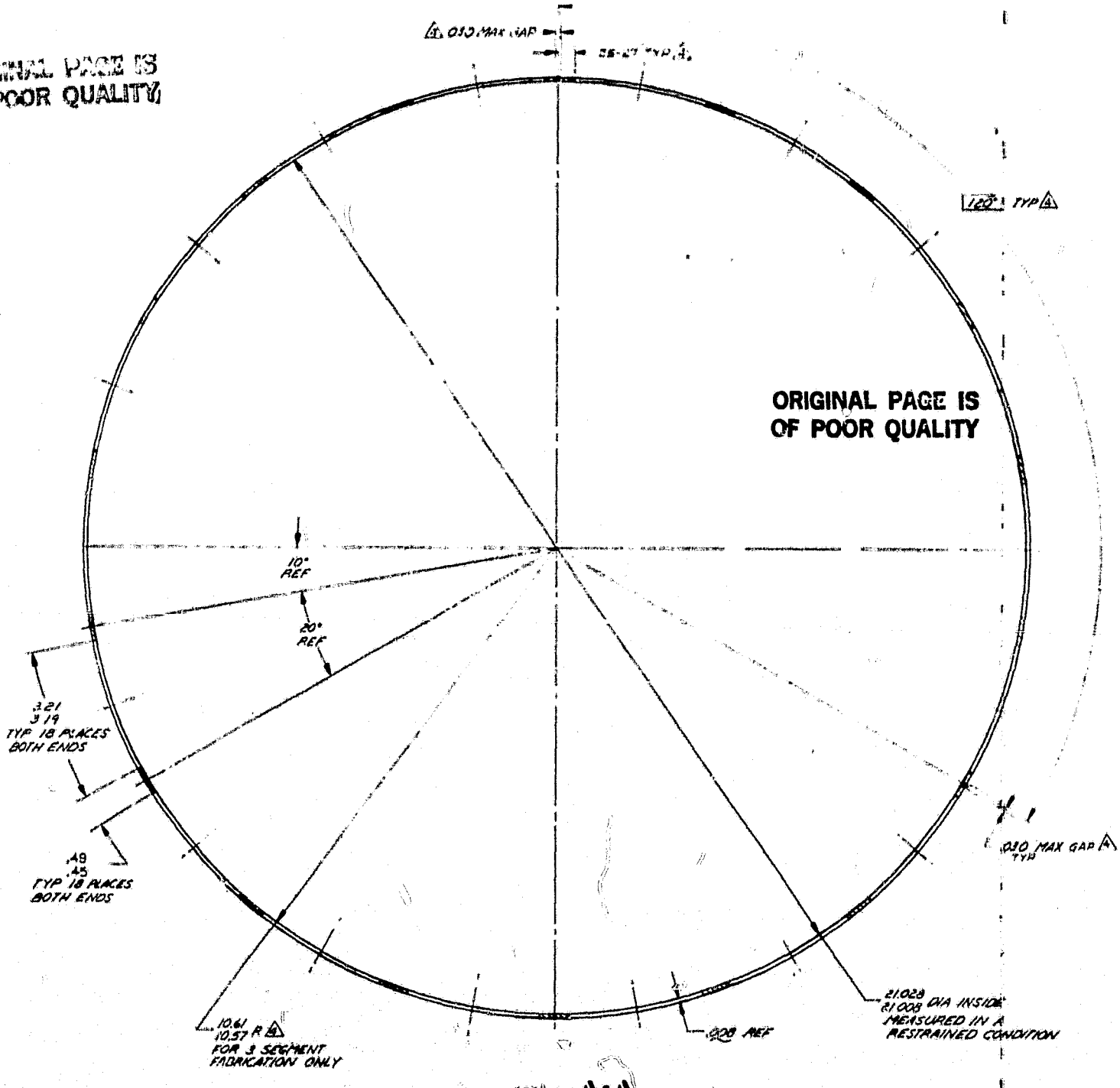

MAY BE FABRICATED INTO 3 EQUAL SEGMENTS TO DIM SHOWN
WELD SHALL BE MADE BY AUTOMATIC MACHINE INERT GAS TUNGSTEN ARC ONLY, AFTER WELD ROL PLANISH SEAM.
PART MAY BE FABRICATED FROM MORE THAN ONE PIECE AN BUTT WELD PER GAV 113.
WELD PER MBS19.

NOTES: UNLESS OTHERWISE SPECIFIED

8 7 6 5 4

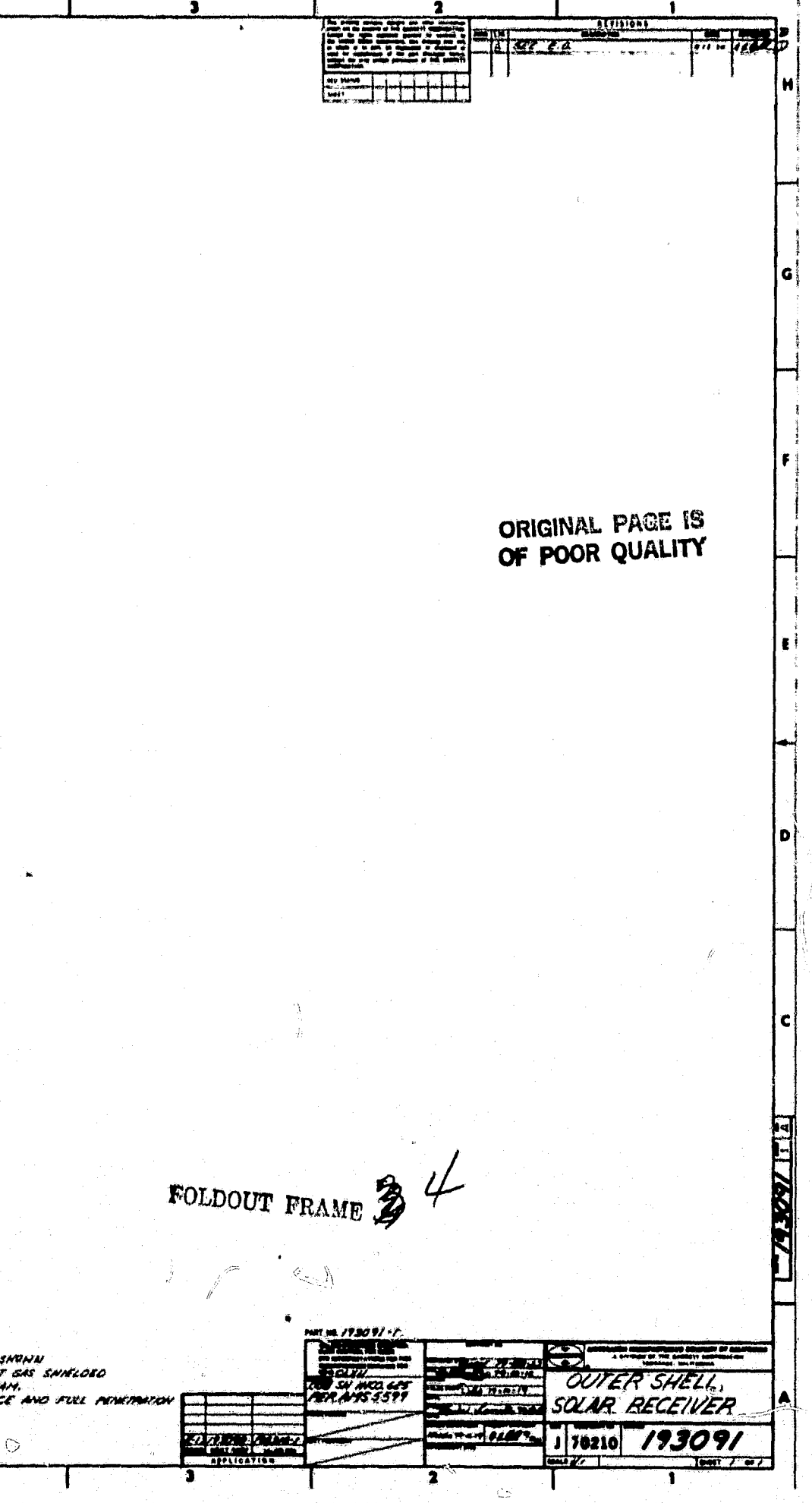

ORIGINAL PAGE IS
OF POOR QUALITY

FOLDOUT FRAME 3 4

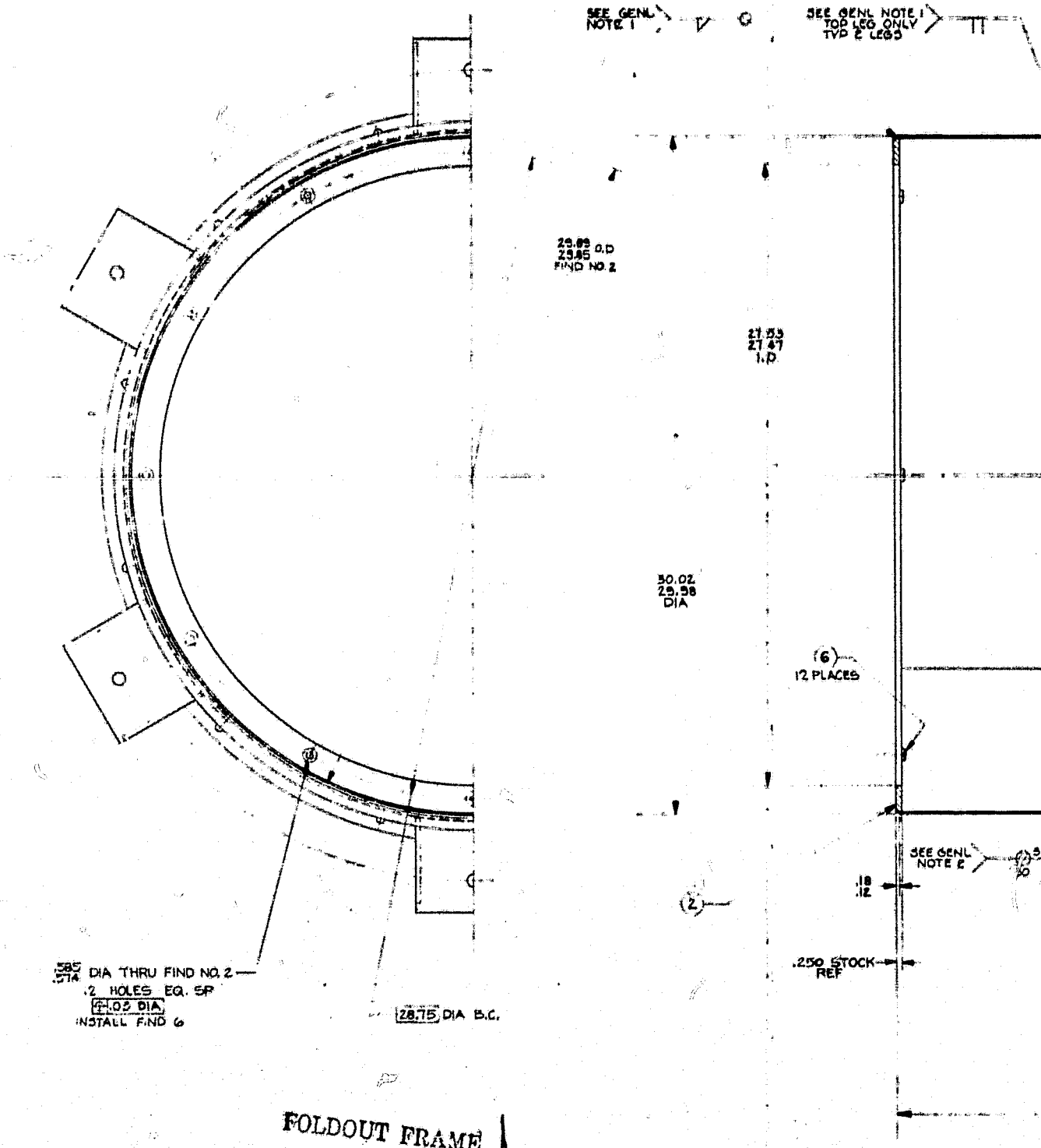

FOLDOUT FRAME

ORIGINAL PAGE IS
OF POOR QUALITY

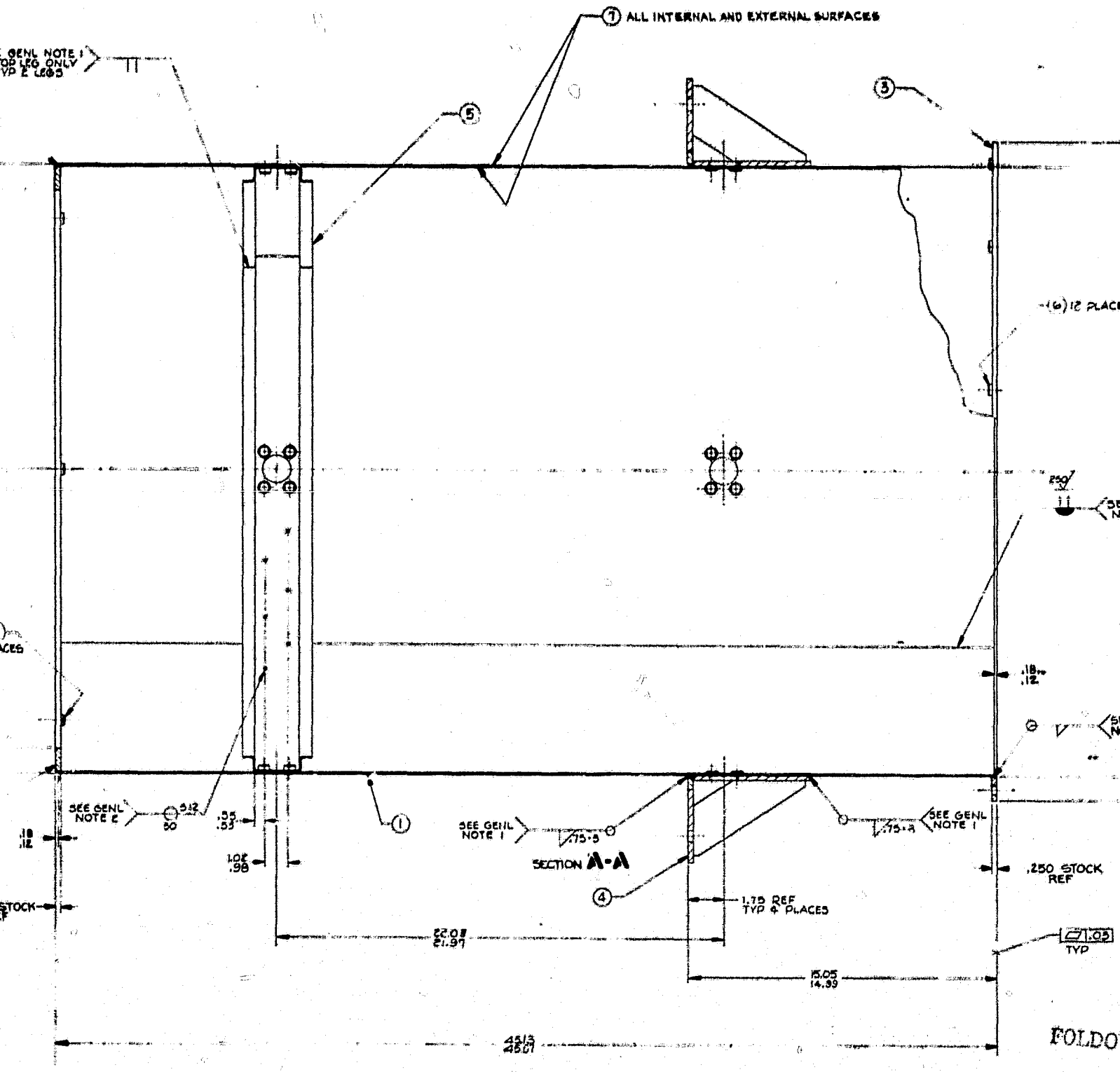

FOLDOUT FRAME 2

ORIGINAL PAGE IS
OF POOR QUALITY

URFACES

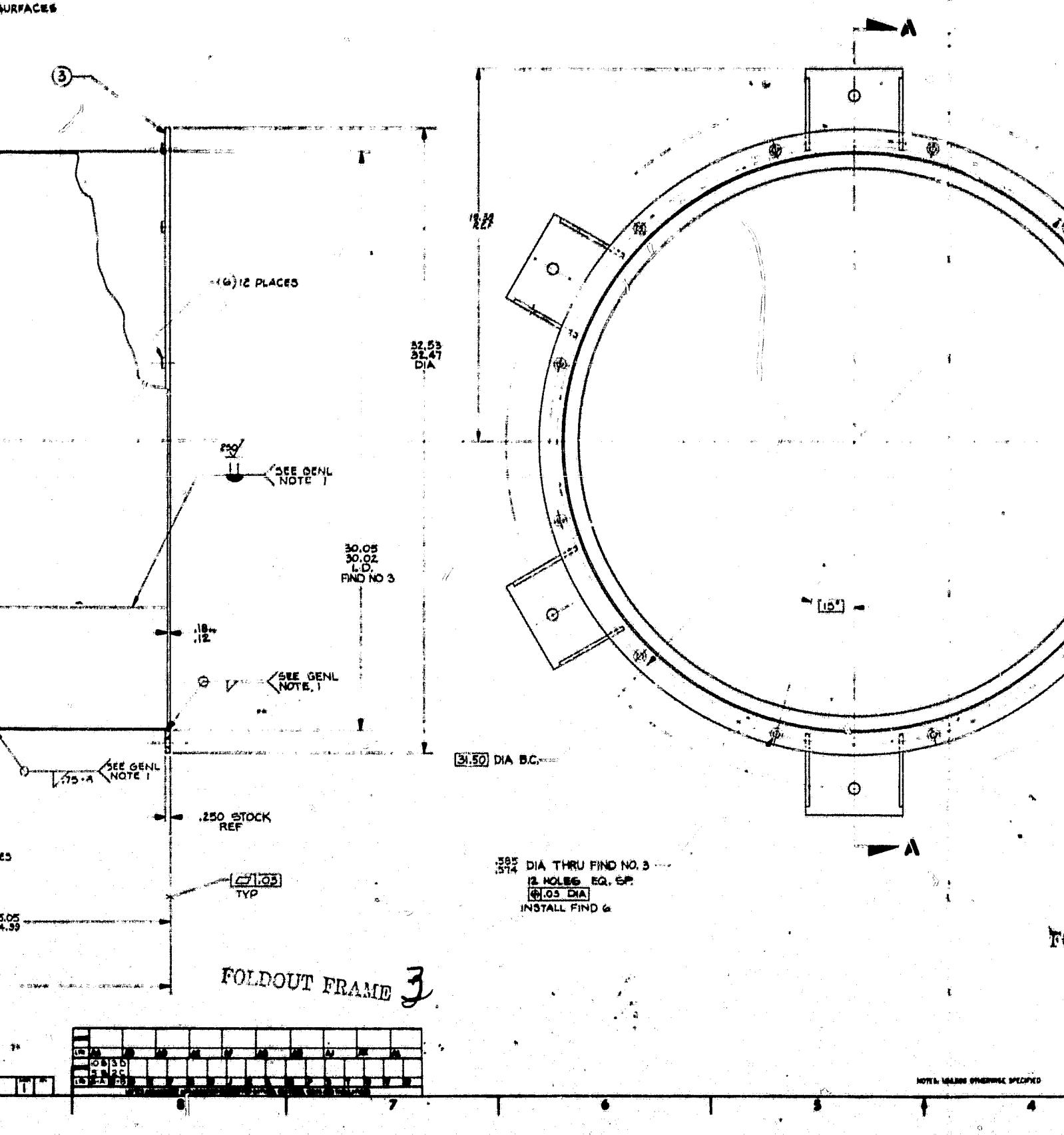

FOLDOUT FRAME 3

ORIGINAL PAGE IS
OF POOR QUALITY

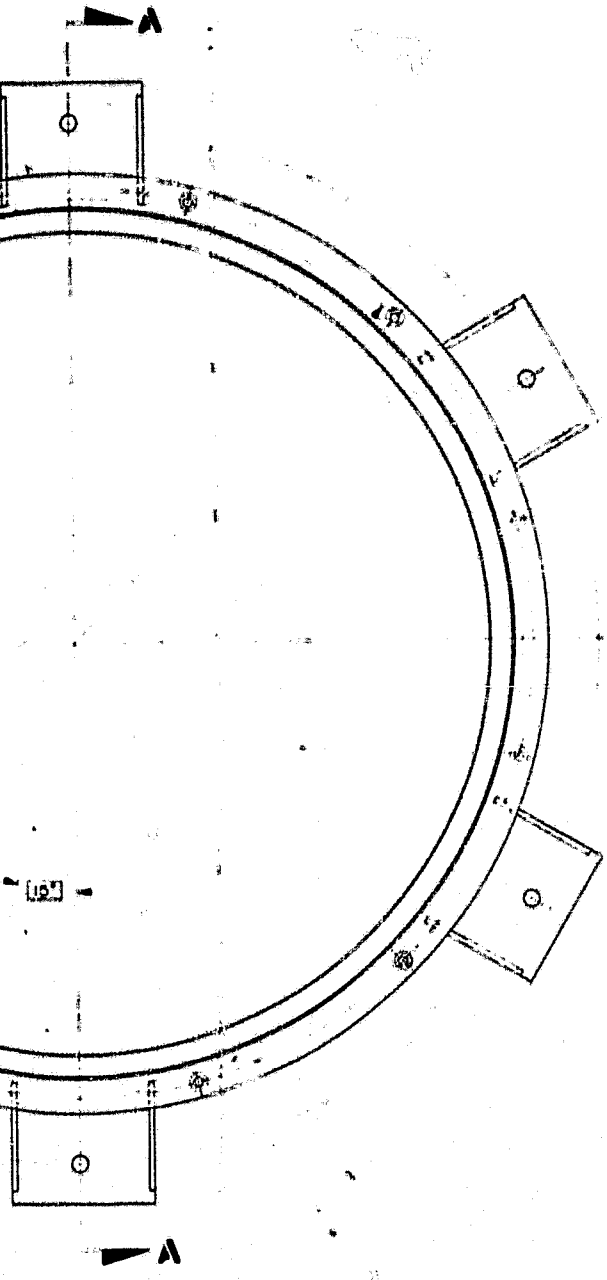

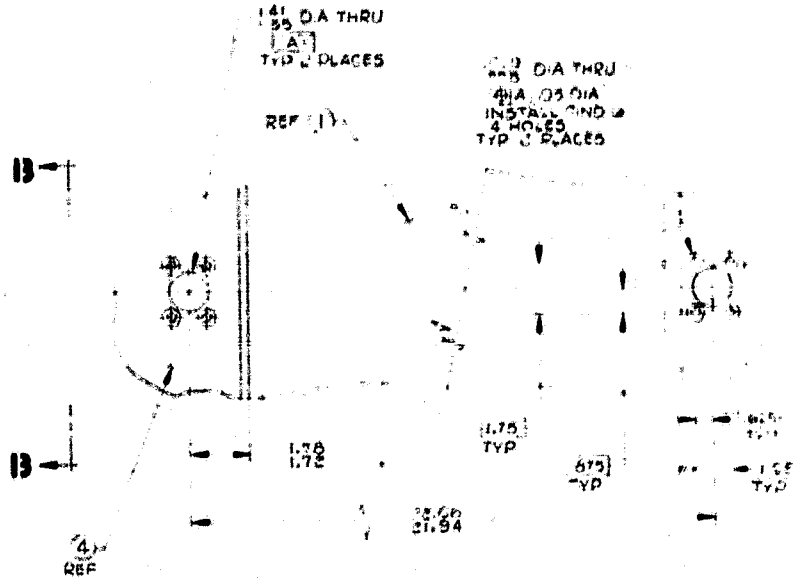

VIEW B - B
TYP 4 PLACES
APPROX 90° APART

FOLDOUT FRAME 2 4

SEE SEPARATE PARTS LIST FOR
REQUIRED ITEMS AND GENERAL NOTES

CASE ASSEMBLY
SOLAR RELIEF

J 70210 193105

FOLDOUT FRAME

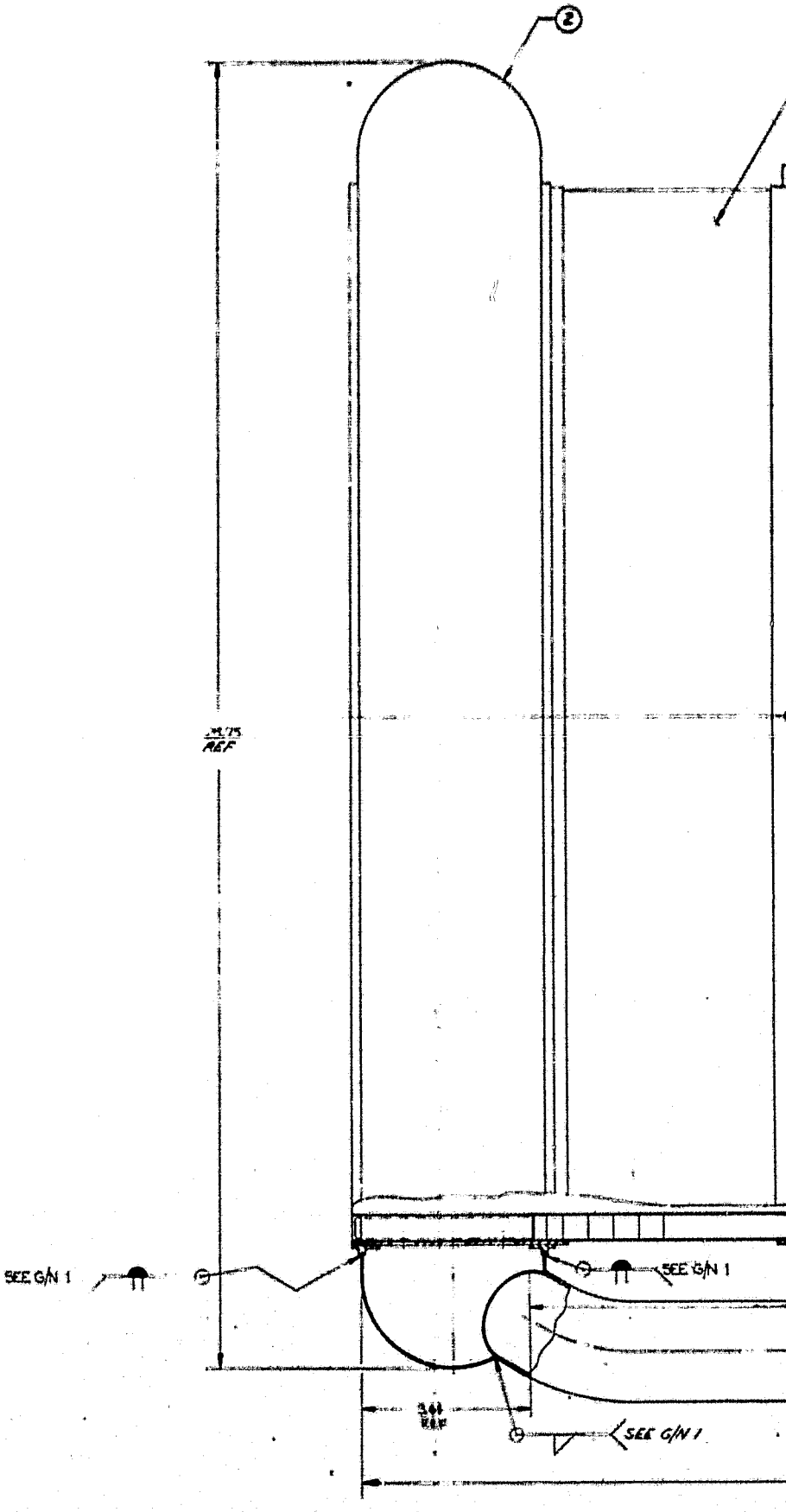

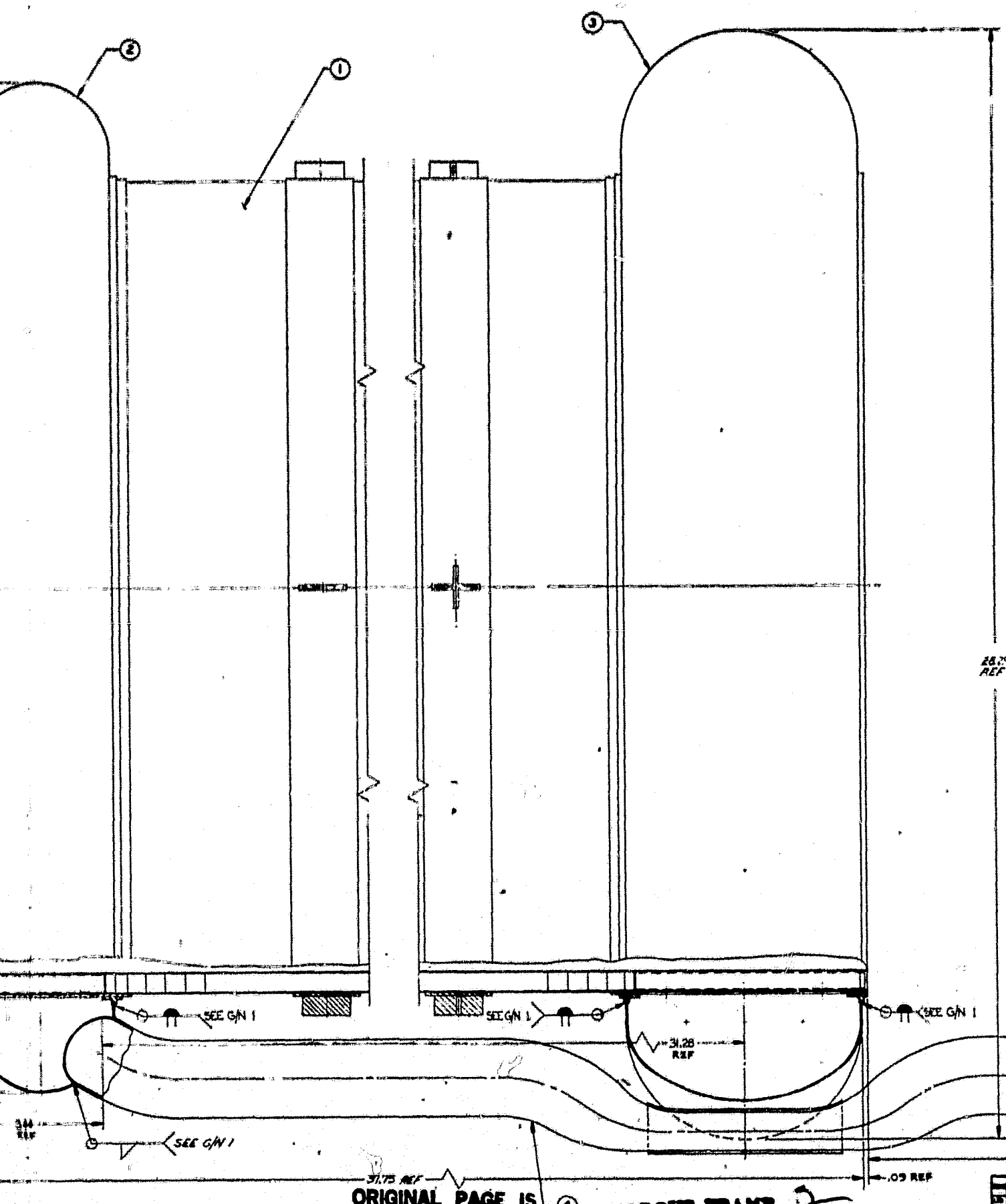

ORIGINAL PAGE IS OF POOR QUALITY

FOLDOUT FRAME

FOLD

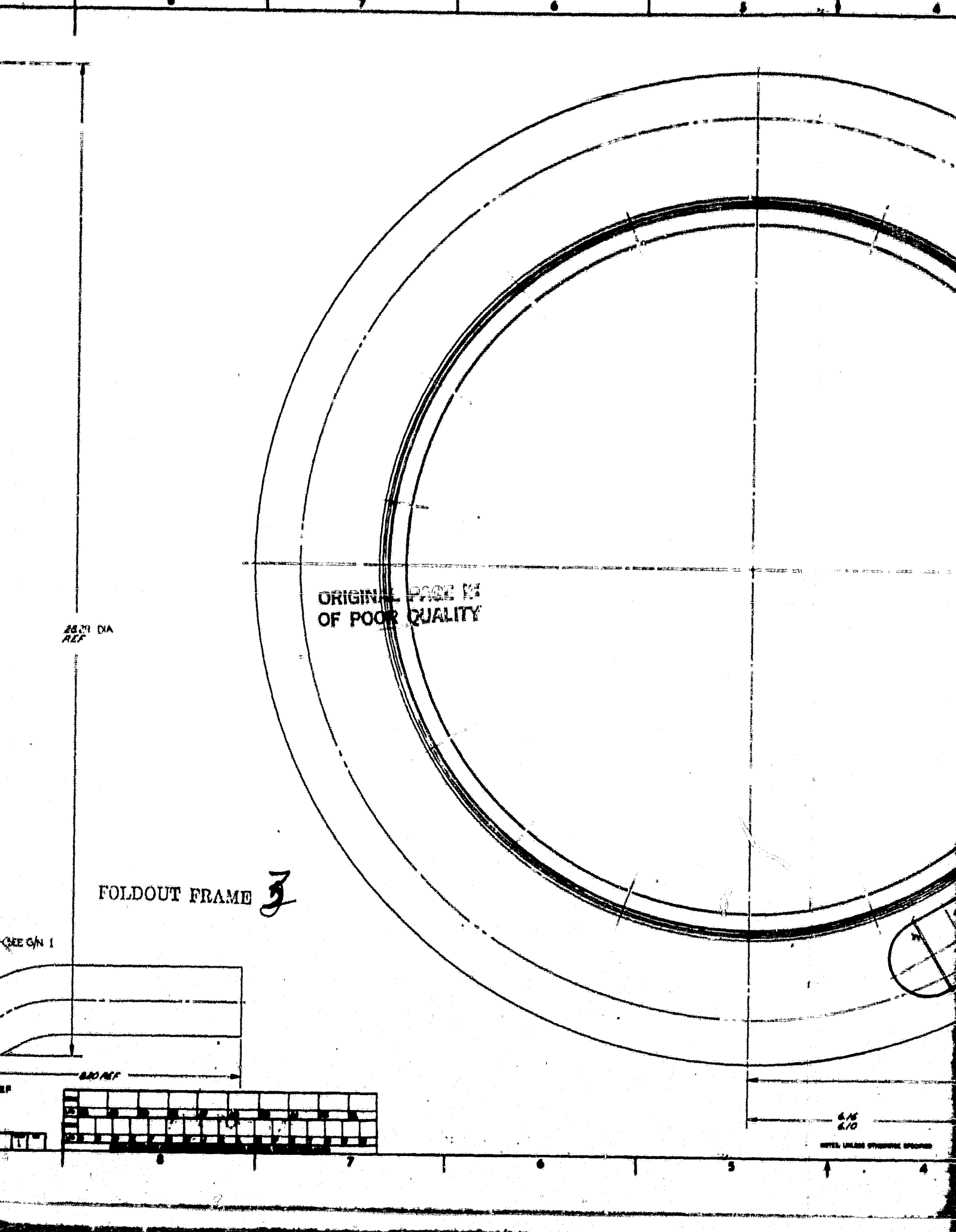
ORIGINAL PAGE IS
OF POOR QUALITY
FOLDOUT FRAME 3
SEE G/N 1
8
7
6
5
4

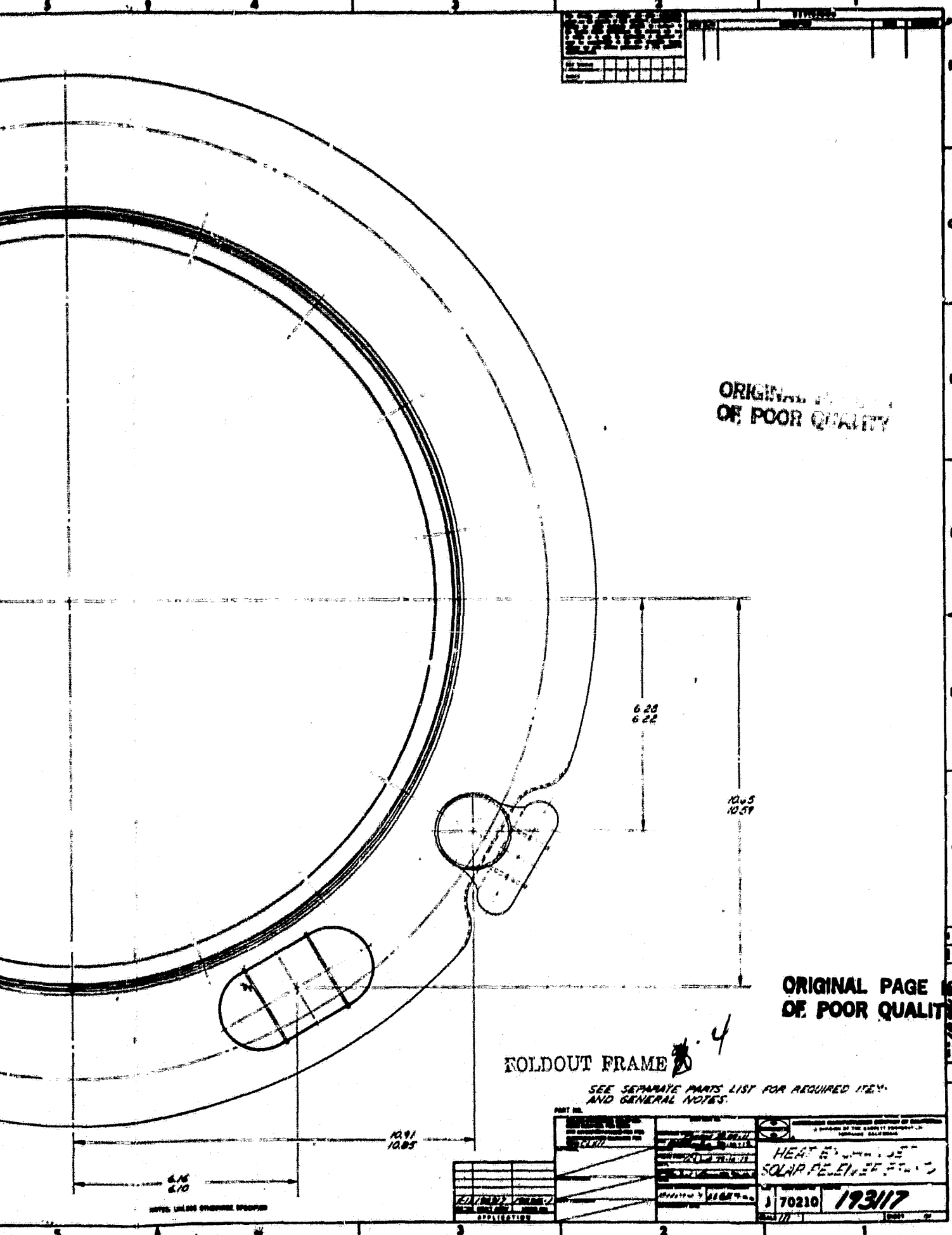

ORIGINAL PAGE IS
OF POOR QUALITY

ORIGINAL PAGE IS
OF POOR QUALITY

FOLDOUT FRAME 4

SEE SEPARATE PARTS LIST FOR REQUIRED ITEMS AND GENERAL NOTES.

HEAT EXCHANGER
SOLAR RECEIVER PANEL

J 70210 193117

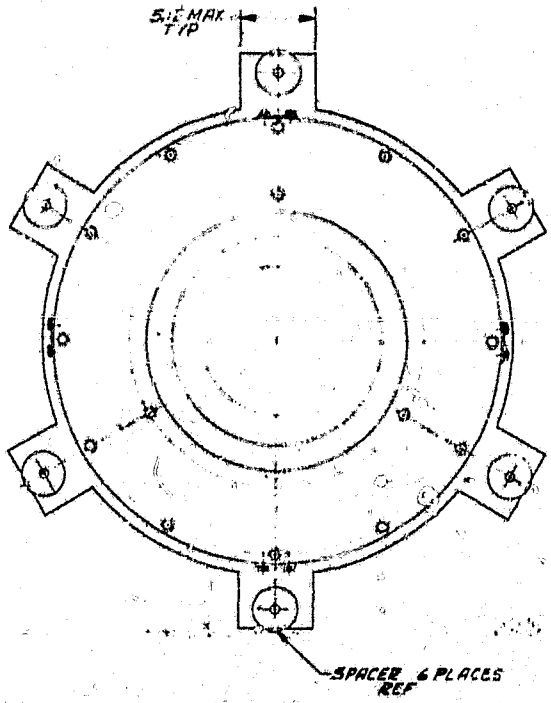

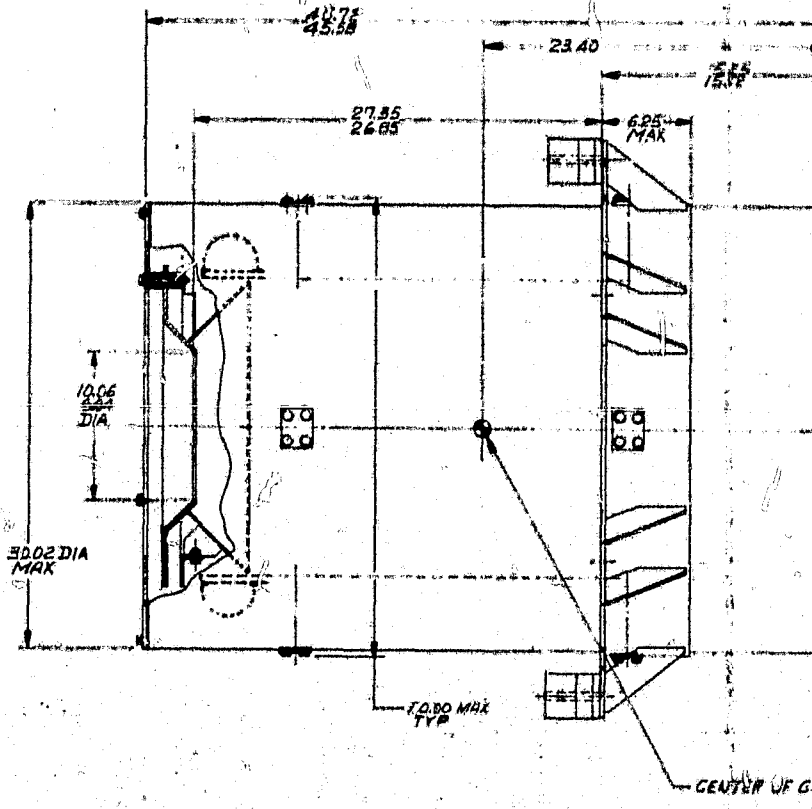

FOLDOUT FRAME

2. SHIPPING CLOSURES PROVIDED FOR ALL
REMOVE ONLY AT INSTALLATION.
1. DIMENSIONS ARE FOR INSTALLATION PU

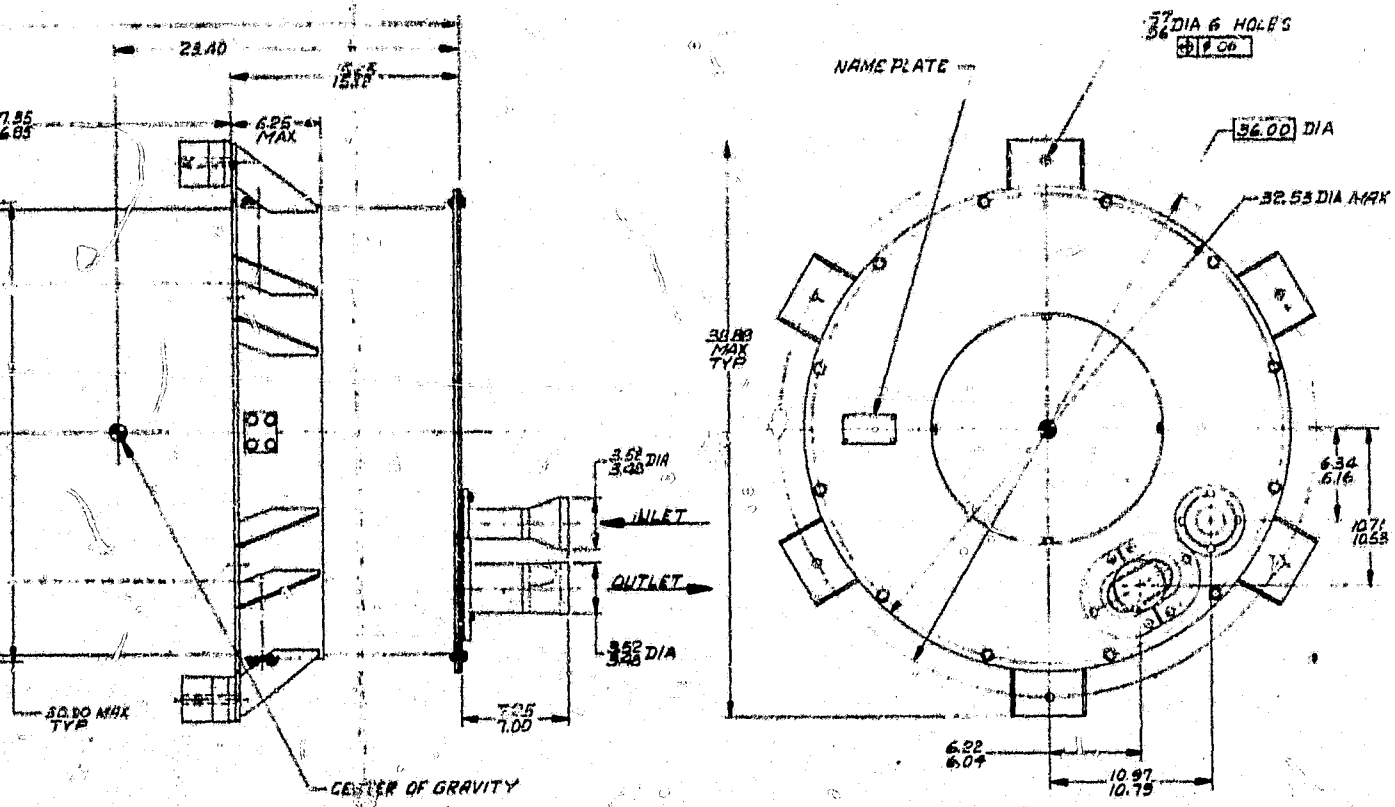

FOLDOUT FRAME 2

194316-1	194317-1	447 LBS	REMARKS
PART NO	ASSY NO.	CALC. WT	

2. SHIPPING CLOSURES PROVIDED FOR ALL OPENINGS, REMOVE ONLY AT INSTALLATION.
1. DIMENSIONS ARE FOR INSTALLATION PURPOSES ONLY.

SOLAR RECEIVER OUTLINE, BRAYTON HEAT SOURCE

E 70210 194316

194316

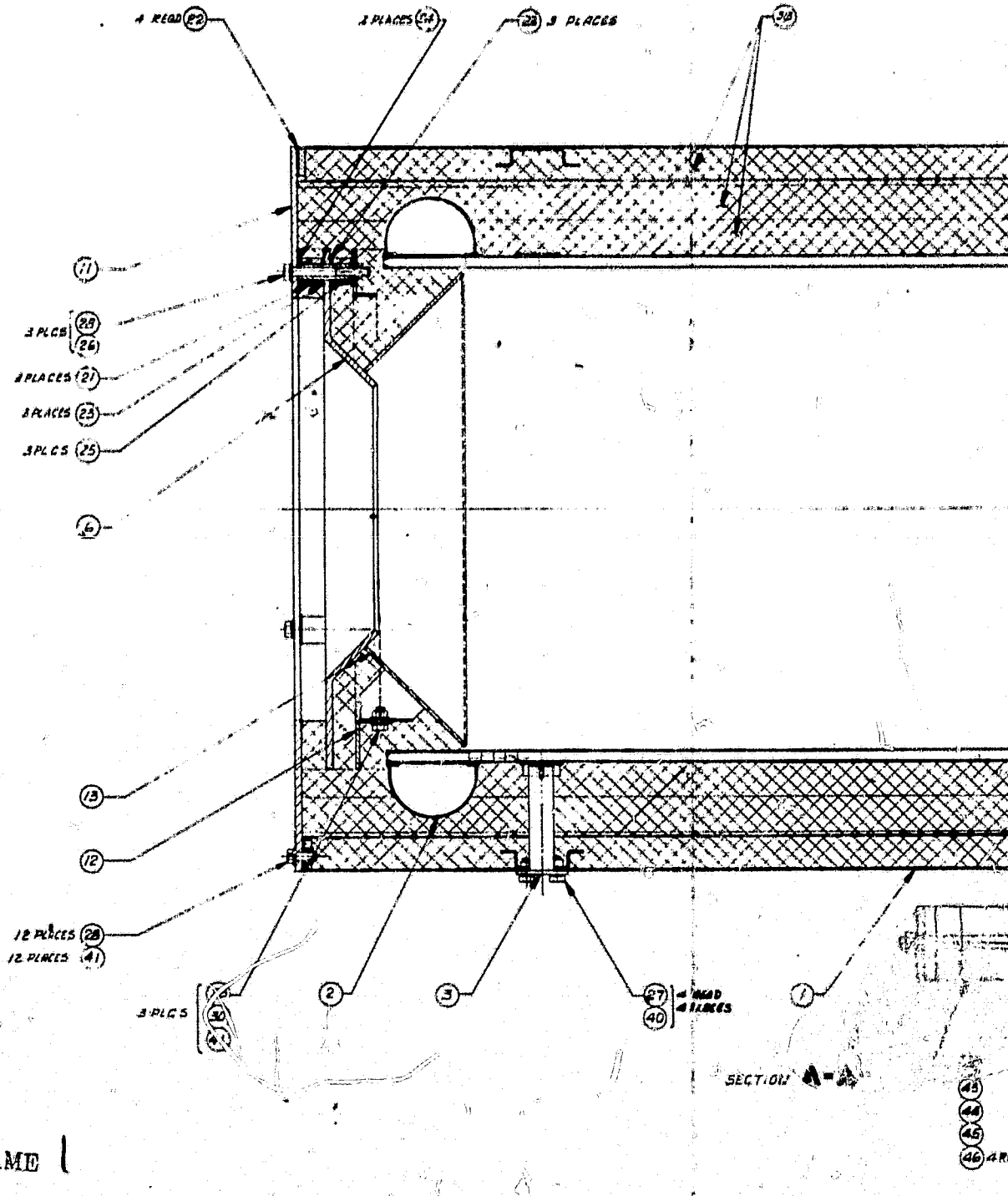

FOLDOUT FRAME

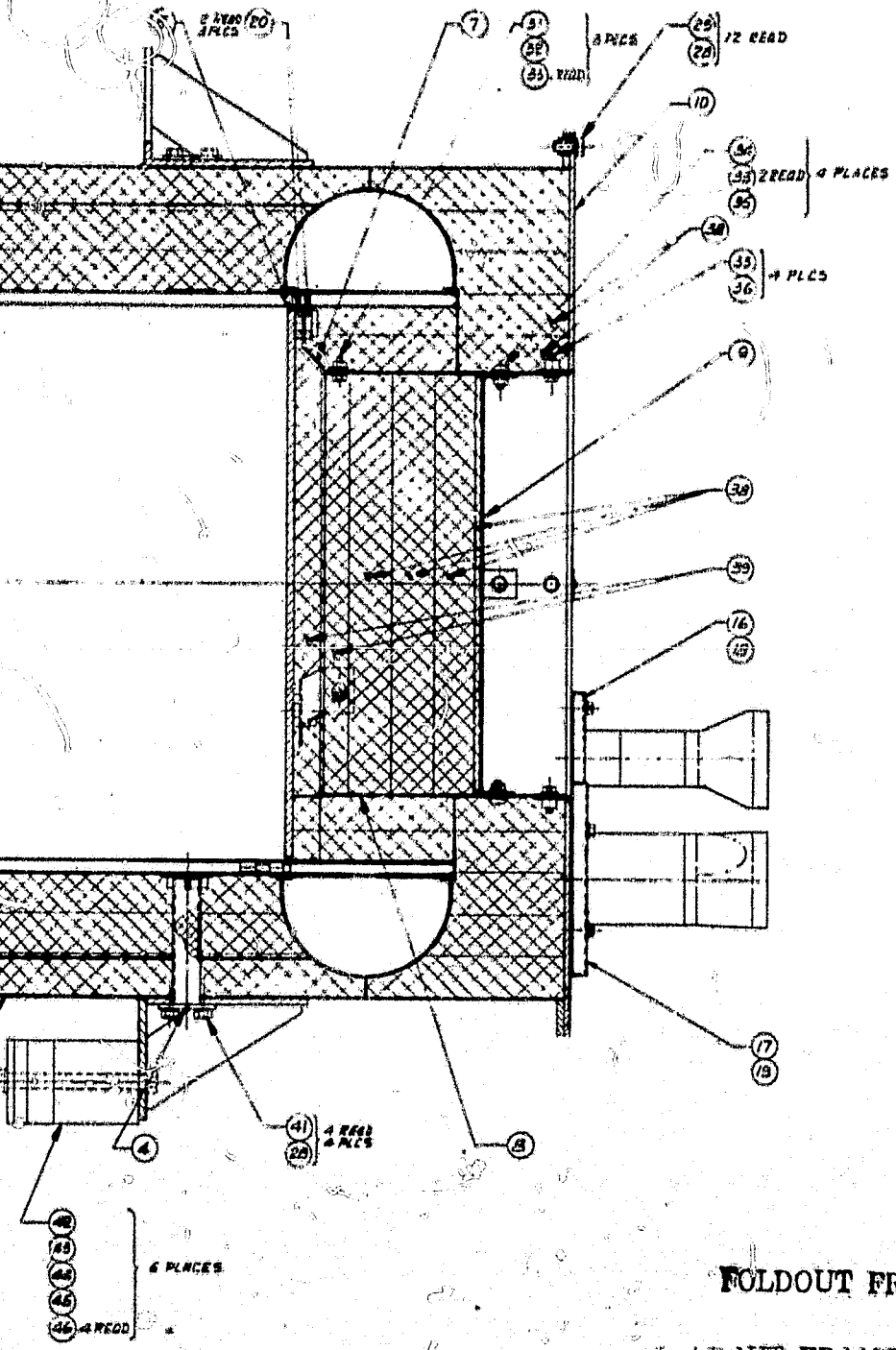

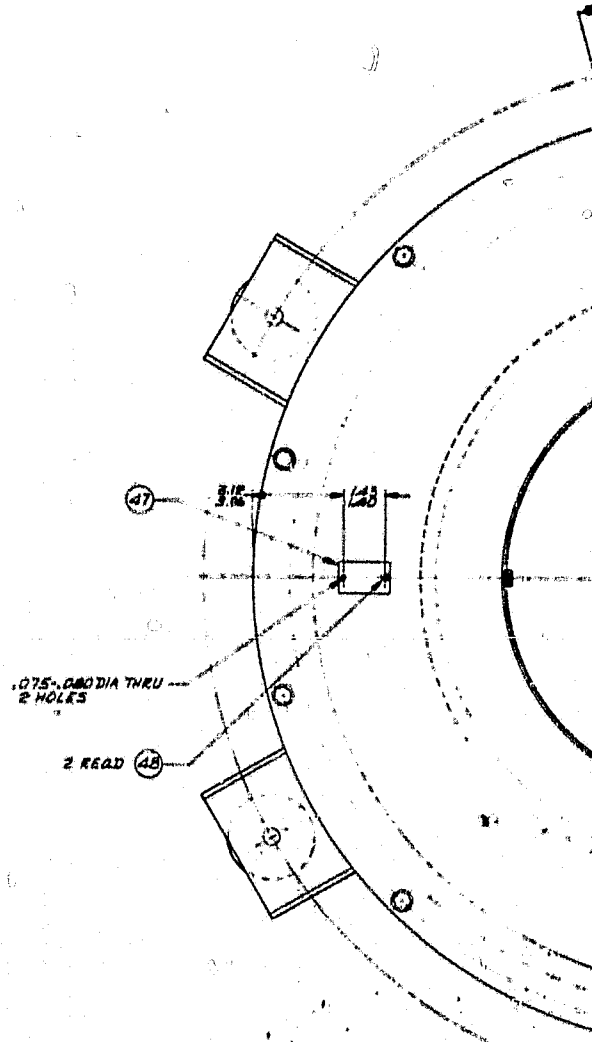

FOLDOUT FRAME 2

FOLDOUT FRAME

ORIGINAL PAGE IS
OF POOR QUALITY

104317

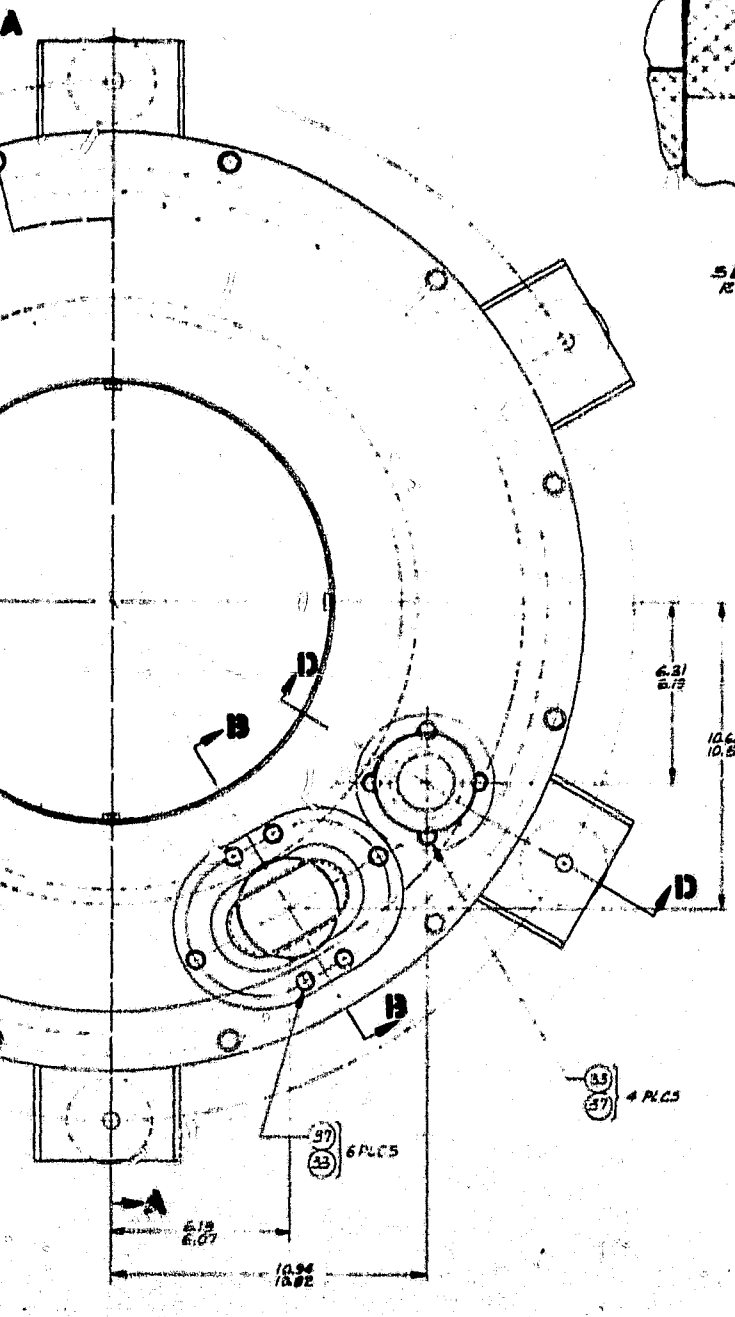

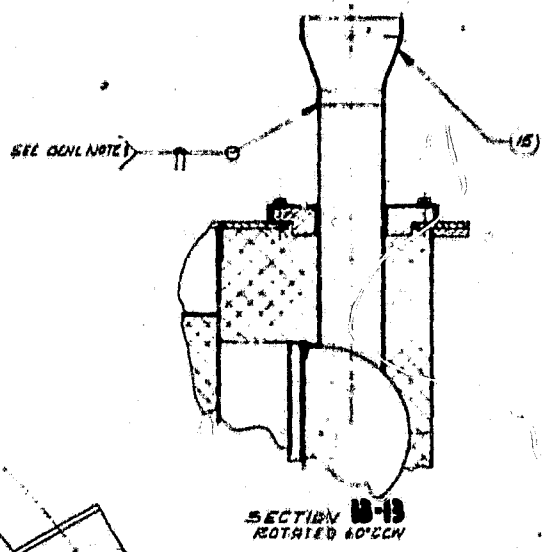

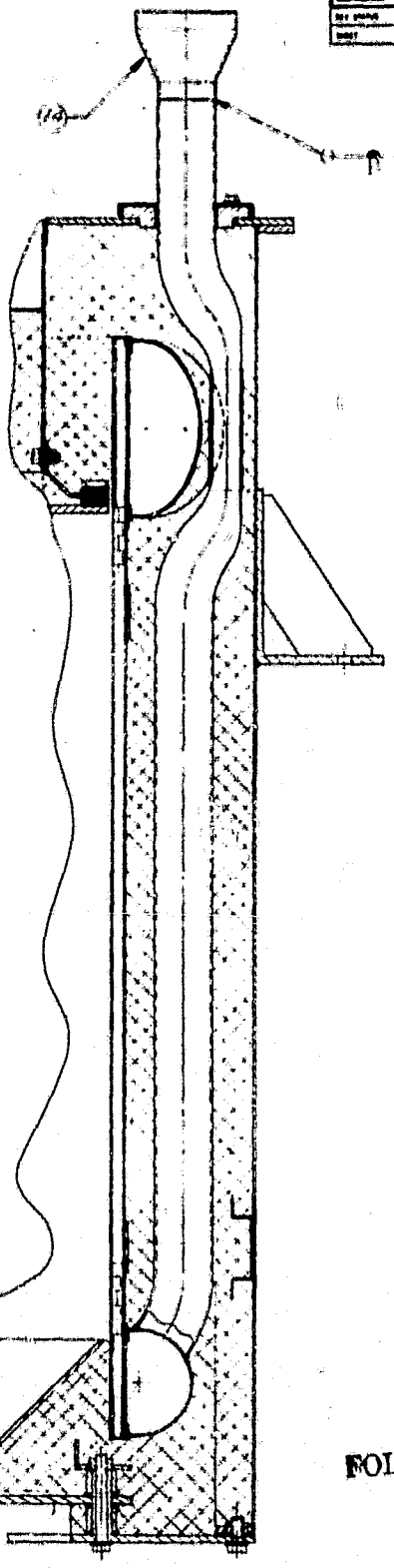

FOLDOUT

SEE SEPAR
ITEM

FOLDOUT FRAME 3

ORIGINAL PAGE IS
OF POOR QUALITY

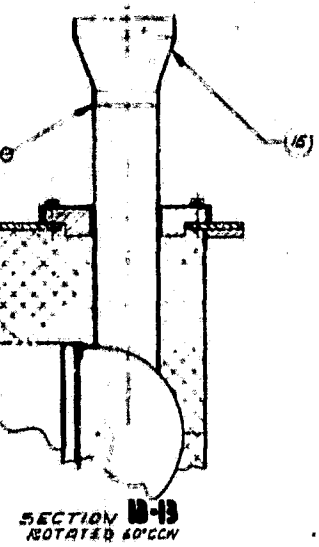

SECTION D-D
ROTATED 60° CCW

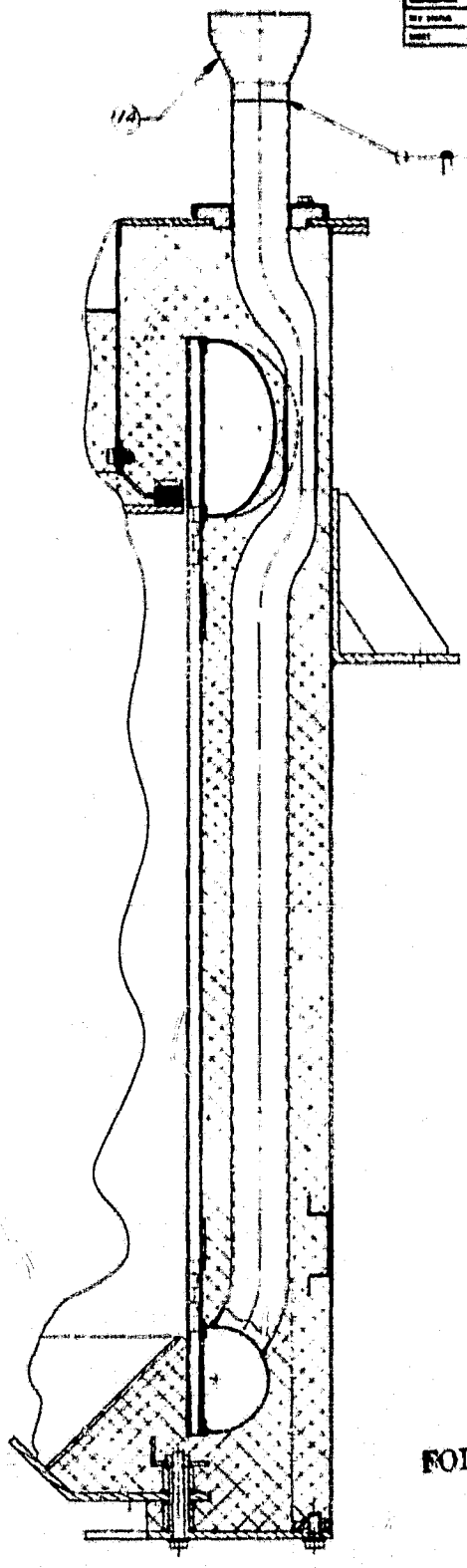

SECTION D-D
ROTATED 30° CCW

ORIGINAL PAGE IS OF POOR QUALITY

FOLDOUT FRAME 3 4

SEE SEPARATE PARTS LIST FOR REQ. PED ITEMS AND GENERAL NOTES

SOLAR RECEIVER ASSEMBLY
BRAYTON HEAT RECEIVER

J 70210 194317

194317